Universitat Politècnica de Catalunya
Programa de Doctorat en Enginyeria Civil

Departament de Matemàtica Aplicada III

Efficient models for building acoustics: combining deterministic and statistical methods

by

Cristina Díaz-Cereceda

PhD dissertation
Advisors: Jordi Poblet-Puig and Antonio Rodríguez-Ferran
Barcelona, November 2013

A mi familia de siempre,
i a la que he trobat pel camí.

Abstract

Efficient models for building acoustics: combining deterministic and statistical methods

Cristina Díaz-Cereceda

Advisors: Jordi Poblet-Puig and Antonio Rodríguez-Ferran

Modelling vibroacoustic problems in the field of building design is a challenging problem due to the large size of the domains and the wide frequency range required by regulations. Standard numerical techniques, for instance finite element methods (FEM), fail when trying to reach the highest frequencies. The required element size is too small compared to the problem dimensions and the computational cost becomes unaffordable for such an everyday calculation.

Statistical energy analysis (SEA) is a framework of analysis for vibroacoustic problems, based on the wave behaviour at high frequencies. It works directly with averaged magnitudes, which is in fact what regulations require, and its computational cost is very low. However, this simplified approach presents several limitations when dealing with real-life structures. Experiments or other complementary data are often required to complete the definition of the SEA model.

This thesis deals with the modelling of building acoustic problems with a reasonable computational cost. In this sense, two main research lines have been followed.

In the first part of the thesis, the potential of numerical simulations for extending the SEA applicability is analysed. In particular, three main points are addressed: first, a systematic methodology for the estimation of coupling loss factors from numerical simulations is developed. These factors are estimated from small deterministic simulations, and then applied for solving larger problems with SEA. Then, an SEA-like model for non-conservative couplings is presented, and a strategy for obtaining conservative and non-conservative coupling loss factors from numerical simulations is developed. Finally, a methodology for identifying SEA subsystems with modal analysis is proposed. This technique consists in performing a cluster analysis based on the problem eigenmodes. It allows detecting optimal SEA subdivisions for complex domains, even when two subsystems coexist in the same region of the geometry.

In the second part of the thesis, the sound transmission through double walls is analysed from different points of view, as a representative example of the complexities

of vibroacoustic simulations. First, a compilation of classical approaches to this problem is presented. Then, the finite layer method is proposed as a new way of discretising the pressure field in the cavity inside double walls, specially when it is partially filled with an absorbing material. This method combines a FEM-like discretisation in the direction perpendicular to the wall with trigonometric functions in the two in-plane directions. This approach has less computational cost than FEM but allows the enforcement of continuity and equilibrium between fluid layers. It is compared with experimental data and also with other prediction models in order to check the influence of commonly assumed simplifications.

Finally, a combination of deterministic and statistical methods is presented as a possible solution for dealing with vibroacoustic problems consisting of double walls and other elements. The global analysis is performed with SEA, and numerical simulations of small parts of the problem are used to obtain the required parameters. Combining these techniques, a realistic simulation of the vibroacoustic problem can be performed with a reasonable computational cost.

Acknowledgments

I would like to use these lines to thank all the people that, direct or indirectly, have contributed to the development of this thesis.

First of all I would like to thank my advisers: Antonio Rodríguez-Ferran and Jordi Poblet-Puig for providing me with an endless supply of help, inspiration and good advices, and for showing me that any task can be used as an opportunity to learn something.

I would like to thank Harm Akes for giving me the opportunity to spend a period at the University of Sheffield, full of interesting discussions and contagious enthusiasm.

I would like to show my gratitude to all the members of the tribunal for their willingness to participate in this thesis defence, and for their time and dedication.

I would like to thank Antonio Huerta and the rest of members of the Laboratori de Càlcul Numèric for these four years. In particular, I would like to thank Imma for her help with the *administrative stuff*, David for the assistance with the *computer issues* and the *lunch team* and *cake team*, for being a constant source of fresh air. I want to mention especially the 'E' girls of the team, for being such good friends: Eva, Esther and of course Elena. No sé què hauria fet sense tu!

D'altra banda, vull agrair a totes les persones que han sigut la meva família barcelonina, i que m'han fet conservar el seny durant aquests quatre anys: la genteta del dinar del mes, les *perracas i perracos*, els meus companys de pis (als diferents pisos), les nenes de mates, i molts altres més. És impossible no somriure cada dia estant rodejada de tots vosaltres.

Sólo tengo palabras de agradecimiento para aquellas personas que han creído en mí y que me han dado la oportunidad de crecer académicamente hasta llegar a este punto. En particular, Trini y Grané, aunque ha habido muchos más.

También quiero dedicar unas palabras especiales a mis padres, por haber sabido dejarme volar sin perderme de vista, y por confiar en mí y apoyarme en esta loca empresa (y en las que vendrán). También quiero agradecer a mis cuatro abuelos su fe y apoyo incondicional, a mi nueva familia de Briviesca por su cariño y su disposición para ayudar en lo que haga falta, y a Miriam, Ona y Viti por estar siempre ahí.

Mis últimas líneas son para Viku, el mejor compañero de viaje posible y cuya enorme paciencia sólo es equiparable a su gran corazón. Gracias por no dejarme perder la cordura ni la locura y por enseñarme que disfrutar del camino es tan o más importante que llegar a tiempo.

Contents

List of symbols and acronyms

Latin symbols

A	Absorbing area in a room
$\mathbf{A}$	Modal analysis matrix of the excited plate
$\mathbf{A_C}$	Fluid-structure coupling matrix for plate A
A_0	Reference absorption area
$\mathbf{a}$	Vector of modal contributions for the displacements of plate A
a_r	Modal contributions to the displacement of the excited plate
B	Bending stiffness
$\mathbf{B}$	Modal analysis matrix of the unexcited plate
$\mathbf{B_C}$	Fluid-structure coupling matrix for plate B
$\mathbf{b}$	Vector of modal contributions for the displacements of plate B
b_r	Modal contributions to the displacement of the unexcited plate
C	Damping coefficient of a dashpot
$\mathbf{C}$	Modal analysis matrix of the cavity, Chapter 5 FLM discretisation matrix of the cavity, Chapter 6
$\mathbf{C_A}$	Fluid-structure coupling matrix for the cavity, contributions of plate A
$\mathbf{C_B}$	Fluid-structure coupling matrix for the cavity, contributions of plate B
$\mathbf{C_{ii}}$	FLM discretisation matrix of the cavity i
$\mathbf{C_{ij}}$	Fluid-fluid FLM coupling matrix
c	Speed of sound in the air
c_{plate}	Bending wave velocity on a plate
D	Sound level difference between two rooms
D_{ij}	Vibration level difference
$d(a, b)$	Energy distance between a and b
E	Young's modulus
$\langle E_i \rangle$	Averaged energy of subsystem i (first configuration of excitation)
$\langle \widehat{E}_i \rangle$	Averaged energy of subsystem i (second configuration of excitation)
$\bar{E}_j$	Mean energy density in the domain for mode j
e_{ij}	Averaged energy density for mode j and cell i
$\tilde{e}_{ij}$	Normalised energy density for mode j and cell i

F	Excitation force
F_i	Force exerted on plate i
F_0	Force exerted by the tapping machine
f	Frequency
$\mathbf{f}$	Vector of the external forces
f_c	Frequency of coincidence between the plate and the air
f_{mam}	Mass-air-mass natural frequency
$\mathbf{g_k}$	Energy masss centre of cluster k
H	Thickness of the cavity
h	Thickness of the plate
I	Intensity
i	Imaginary unit
K	Spring stiffness
$\mathbf{K}$	Stiffness matrix
K_c	Complex stiffness of a connection
K_L	Stiffness per unit length of the line spring
K_θ	Rotation stiffness
k	Wavenumber in the air
k_i	Wavenumber in subsystem i
k_r	Modal wavenumber in the plate
k_s	Modal wavenumber in the cavity
L	Sound pressure level
L_{cav}	Sum of the lengths of the cavity edges
L_{edge}	Length of the edge
L_n	Normalised impact noise pressure level
$L_{n,w}$	Weighted normalised impact sound pressure level
L_x	Plate size, x direction
L_y	Plate size, y direction
$\mathbf{M}$	Mass matrix
M_i	Mass of leaf i
$M(x, y)$	Bending moment
$m(x, y)$	Distributed bending moment
N	Number of cells
$N_i(z)$, $N_j(z)$	Standard FEM interpolation function
N_k, N_l	Number of elements in cluster k, l
$\boldsymbol{n}$	Outward unit normal
n_c	Number of connections
n_i	Modal density of subsystem i
n_{modes}	Number of modes
n_L	Number of studs
n_{xy}	Number of interpolation functions in the xy plane
n_z	Number of nodes in the z direction
$p\,(\boldsymbol{x})$	Pressure field

$\mathbf{p}$	Vector of modal contributions for the pressure field, Chapter 5
	Vector of FLM contributions for the pressure field, Chapter 6
$\|p\|$	Amplitude of the pressure wave
$p^{\text{int}}(x, y)$	Pressure at the leaf-cavity interface
p_{js}	Pressure value at node j for the interpolation function $\Phi_s(x, y)$
$\langle p^2_{\text{rms}} \rangle$	Spatial root mean square value of pressure
p_s	Modal contributions to the pressure field
p_0	Reference pressure (usually 2×10^{-5} Pa)
$q(x, y)$	Force per unit surface
R	Sound reduction index
R_{rad}	Radiation resistance
R'_w	Weighted apparent sound reduction index
r	Reflection parameter
r_a	Relative error associated to quantity a
r_i	Reflection parameter in the near field
r_1, r_2	Relative error associated to the energy of subsystem 1, 2
S	Surface of the plate
S_{cav}	Surface of the cavity boundary
S_{room}	Surface of the room boundary
S_j^2	Variance of e_{ij} for mode j
t	Transmission parameter
t_i	Transmission parameter in the near field
$u(x, y)$	Displacement field of the plate
u_A, u_B	Displacement field in plate A, B
V	Potential
V_{cav}	Volume of the cavity
V_{room}	Volume of the room
v	Test function
$v(x, y)$	Vibration velocity of the plate
v_i	Velocity at the connecting point of leaf i
v_p	Velocity of the leaf at the excitation point
v_{zi}	Vibration field in span i
v_0	Velocity of leaf 1 far from the connection
v_n	Normal velocity at the fluid-fluid interface
$\langle v^2_{\text{rms}} \rangle$	Spatial root mean square value of velocity
$w(x, y)$	Rotational speed
$\boldsymbol{x} = (x, y, z)$	Vector of spatial coordinates
$\mathbf{x_i}$	Energy vector of cell i
Y_c	Point mobility of the connection
Y_c^L	Line mobility of the connection
Y_i	Point mobility of plate i
Y_i^L	Line mobility of plate i
Z	Impedance

Z_I	Input impedance
Z_i	Specific impedance of material layer i
Z_T	Terminal impedance
Z_0	Characteristic impedance of the air

Greek symbols

α	Absorption coefficient
β	Filling ratio in the cavity
Γ_D	Dirichlet boundary
γ_{ij}	Non-conservative coupling loss factor between subsystems i and j
δ	Thickness ratio between two plates
ϵ_r	Coefficient in the formulation of Xin *et al.* for the positive going wave
η	Loss factor
η_{ii}	Internal loss factor of subsystem i
η_{ij}	Conservative coupling loss factor between subsystems i and j
ζ_r	Coefficient in the formulation of Xin *et al.* for the negative going wave
θ	Rotation angle (Part I) and orientation angle of the pressure wave (Part II)
λ_{cav}	Wavelength in the air cavity
λ_{plate}	Wavelength in the plate
ν	Poisson's ratio
Π^{in}	Incident power
Π^{rad}	Radiated power
Π_i^{diss}	Power dissipated at subsystem i
Π_i^{in}	External power entering subsystem i
Π_{ij}	Power transmitted from subsystem i to subsystem j
Π_{ij}^{diss}	Power dissipated at the connection
$\Pi_{ij}^{(i)}$	Power exchanged between the connection and subsystem i (first configuration of excitation)
$\widehat{\Pi}_{ij}^{(i)}$	Power exchanged between the connection and subsystem i (second configuration of excitation)
ρ	Density
ρ_{air}	Density of the air
ρ_s	Mass per unit surface
σ	Flow resistivity for the absorbing material
σ_{rad}	Radiation efficiency
τ	Transmission coefficient
τ_{diff}	Transmission coefficient for diffuse sound incidence angle
$\Phi_s(x, y)$	Interpolation function for the FLM
φ	Incidence angle of the pressure wave

φ_{lim}	Limit value of the incidence angle
$\phi_r(x, y)$	Eigenfunctions of the simply supported plate
$\Psi(\boldsymbol{x})$	Velocity potential in the air cavity
$\psi_s(\boldsymbol{x})$	Eigenfunctions of the cavity
Ω_c	Acoustic domain
Ω_{xy}	Solid domain (plate)
ω	Angular frequency
ω_0	First eigenfrequency

Acronyms

CCLF	Conservative coupling loss factor
CLF	Coupling loss factor
dof	Degrees of freedom
FEM	Finite element method
FLM	Finite layer method
FSM	Finite strip method
mir	Mutual inertia ratio
MIR	Maximum mutual inertia ratio
NCLF	Non-conservative coupling loss factor
SEA	Statistical energy analysis
TL	Transmission loss
WFEM	Waveguide finite element method

Introduction

Motivation

Social concern about acoustic pollution has increased in recent years, leading to the emergence of associations dedicated to combating this phenomenon all over the world, such as the Spanish association of lawyers *Juristas Contra el Ruido* (2013), the French *Comité des victimes de la pollution et du bruit* (2013) or the American *Citizens Coalition Against Noise Pollution* (2013). For this reason, the problem of noise transmission has become a topic of growing interest in many fields.

For the particular case of building design, the maximum noise levels allowed in rooms are defined by regulations. Two types of noise sources are considered: noise caused by impacts in the structure (impact noise) or by acoustic sources in other rooms or outside the building (airborne noise). The trend of these regulations is to become more and more restrictive over time. For instance, in April 2009 the Spanish building regulations *Código Técnico de la Edificación* (technical building code) CTE (2009) were updated and the real noise perceived between dwellings was reduced from the old 88 dB (based on the basic standard for construction *Norma Básica de la Edificación* NBE-CA (1988)) to 65 dB.

Moreover, the best parameters for structural design are often in confrontation with the optimum parameters in acoustic design. For instance, continuous floor elements are useful for bearing wind or seismic loads, but they also transmit sound energy in the form of structure-borne vibration.

Due to all these reasons, reliable models for vibroacoustic problems are required, in order to predict the noise insulation through different structural configurations. With these models the most influencing parameters in the noise transmission can be determined and a correct acoustic design can be performed.

Building acoustics: regulations

The maximum allowable noise levels (either airborne or impact noise) in rooms are defined in the Spanish regulation CTE (2009). In that document, some acceptable configurations of structures are suggested in order to minimise the noise levels in rooms. If the configuration is not one of those suggested, a test must be performed *in situ* in order to verify the insulation level of the building.

Several parameters are defined by building acoustic regulations in order to establish the insulating effect of building structures for airborne noise. They all consider variables averaged both in space (a single value defining a wall or a room) and time.

The **sound level difference** $D = L_1 - L_2$ between two rooms separated by a partition is the difference between the sound pressure level

$$L = 10 \log_{10} \frac{\langle p_{\text{rms}}^2 \rangle}{p_0^2} \tag{I.1}$$

in the sending room and the receiving room. $\langle p_{\text{rms}}^2 \rangle$ is the spatial root mean square value of the pressure in the room and $p_0 = 2 \cdot 10^{-5}$ Pa is the threshold of audible pressure. The sound level difference depends on the room characteristics as much as on the wall properties. That is why the **sound reduction index** R (also known as transmission loss TL in some countries) is defined, see ISO 140-3 (1995). It is computed as the logarithmic ratio between the incident acoustic power in the structure and the transmitted acoustic power

$$R = 10 \log_{10} \frac{\Pi^{\text{in}}}{\Pi^{\text{rad}}}. \tag{I.2}$$

The impact noise is usually quantified with the **normalised impact sound pressure level** L_n. This parameter is defined by the ISO 140-6 (1998) as the sound pressure measured in the receiving room when the tested floor is excited by the normalised tapping machine, Fig. I.1, corrected with a factor that takes into account the acoustic absorption of the room

$$L_{\text{n}} = 10 \log_{10} \left(\frac{\Pi^{\text{rad}}}{p_0^2} \frac{4 \rho_{\text{air}} c}{A_0} \right), \tag{I.3}$$

where ρ_{air} is the air density, c is the sound speed in the air and A_0 is the reference absorption area ($10\,\text{m}^2$ for dwellings).

The **vibration level difference** D_{ij}, defined by Hopkins (2007), is a magnitude similar to the sound level difference, but related to vibrations instead of sound. It is

Fig. I.1: Tapping machine. Source: www.sp.se, retrieved on 2013-08-01

used to measure the vibration transmission between two structures through joints

$$D_{ij} = 10 \log_{10} \frac{\langle E_i \rangle}{\langle E_j \rangle}, \tag{I.4}$$

where $\langle E_i \rangle$ and $\langle E_j \rangle$ are the averaged energies of structures i and j respectively.

All these variables are frequency-dependent. They are usually averaged in third octave bands. Moreover, there are other magnitudes such as the weighted apparent sound reduction index R'_w, ISO 717-1 (1997), or the weighted normalised impact sound pressure level $L_{n,w}$, ISO 717-2 (1997), which provide a single value defining the insulating effect of a structure against the airborne and the impact noise respectively. These values are computed by comparison of the corresponding frequency-dependent curve with a reference curve, that typically includes frequencies from 100 to 3150 Hz, see example of Fig. I.2. The single number obtained is used in regulations to classify a structure as fit or unfit.

Main challenges

Modelling vibroacoustic problems in the field of building design has some particular features:

- The first aspect is the frequency range of interest. Magnitudes like R'_w or $L_{n,w}$ require computations between 100 and 3150 Hz, and sometimes this range is extended to 50-5000 Hz, ISO 717-1 (1997).

- The second feature is the size of the problem: typically several meters or even tens of meters.

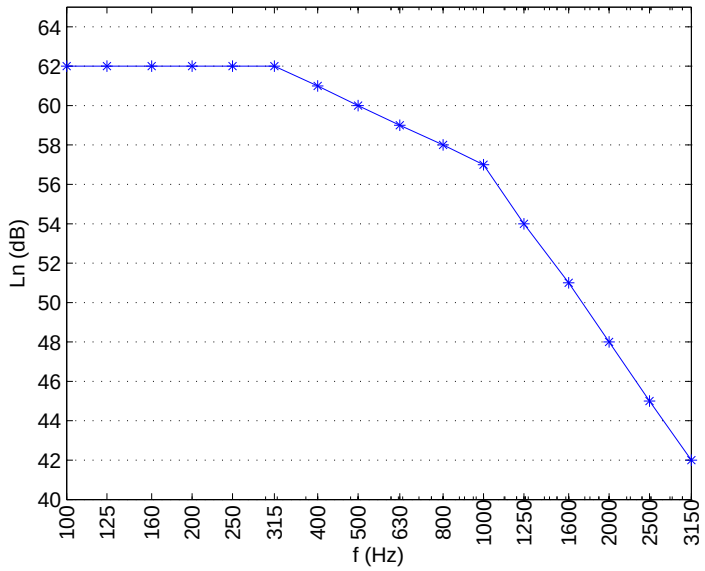

Fig. I.2: Reference curve for the impact noise, ISO 717-2 (1997)

- The third characteristic of the problem is the fluid-structure coupling: acoustic waves excite structures and these, in turn, cause new acoustic waves. This coupling implies different wavelengths in the problem at a certain frequency.

The combination of these special features causes the standard numerical techniques (for instance finite element methods) to fail when trying to reach the highest frequencies required by regulations. The element size required is too small for the problem dimensions and the computational cost becomes unaffordable for such an everyday problem, see Zienkiewicz (2000).

Alternative modelling techniques are used to avoid these problems: wave-based approximations, two-dimensional or even one-dimensional simplifications. However, they miss some information of the real problem.

Another widely used technique is statistical energy analysis (SEA), see Lyon (1975) and Craik (1996): this is a framework of analysis based on the averaged powers flowing between rooms and structures. This type of analysis is based on the wave behaviour at high frequencies and works directly with averaged magnitudes, which is in fact what regulations take into account. Its computational cost is very low. However, it presents several limitations for modelling complex configurations. Usually experimental data or numerical simulations are required to address these

deficiencies.

Therefore, there is a need for efficient and reliable strategies to model the sound transmission through any type of building structure. They should be able to deal with complex geometries and materials for the whole frequency range of interest and with a reasonable computational cost.

Overview

This thesis deals with the efficient modelling of real-life building acoustic problems. In this sense, two main research lines have been followed. On the one hand, the potential of numerical (deterministic) simulations to get relevant information for statistical energy analysis is assessed. On the other hand, efficient numerical methods are presented for modelling deterministically simple vibroacoustic problems. These two main topics are combined in order to deal with complex problems efficiently.

This thesis is divided in two parts. The fist one deals with the potential of combining numerical simulations with statistical energy analysis in order to model real vibroacoustic problems with a reasonable computational cost. This part is structured as follows:

- In Chapter 1 an introduction to statistical energy analysis is provided, detailing the main challenges and limitations of this framework of analysis.
- In Chapter 2 a study on the optimal procedure for obtaining SEA coupling loss factors numerically is presented. These factors are obtained from small deterministic simulations and then applied to solve larger problems with SEA.
- In Chapter 3 an SEA-like approach accounting for non-conservative couplings is developed, and a methodology for obtaining the associated parameters from small numerical simulations is presented.
- In Chapter 4 a new strategy for decomposing a vibroacoustic domain into SEA subsystems is proposed. It consists in performing a cluster analysis based on the problem eigenmodes, and allows the detection of different subsystems sharing the same physical region.

The second part of the thesis deals with the problem of sound transmission through double walls, as a representative example of the complexities of vibroacoustic sim-

ulations. In this part, comparisons of different models are shown, both reviewing classical methods and proposing new techniques. It is structured as follows:

- In Chapter 5 an introduction to double walls is done, as well as a review of existing models of their acoustic behaviour. In particular, four approaches to this problem, with different level of complexity, are presented in detail.
- In Chapter 6 the finite layer method is presented as a discretisation method for the pressure field in the cavity of a double wall, and compared with other methods and experimental data. This technique combines a FEM discretisation in the direction perpendicular to the wall with trigonometric functions in the two in-plane directions.
- In Chapter 7 an efficient approach for modelling the sound insulation of double walls is presented. It is based on statistical energy analysis, but uses deterministic simulations for obtaining SEA parameters.

At the end of the document, the main conclusions and contributions of the thesis are enumerated, as well as the related publications. They are followed by a list of the future research lines arising from this work.

Part I

Extending statistical energy analysis with numerical simulations

Chapter 1

Introduction: main challenges in statistical energy analysis

Statistical energy analysis (SEA) is an energy-based framework of analysis for vibroacoustic problems. It is typically used for modelling the transmission of sound and vibrations within closed domains such as buildings, vehicles, or industrial devices.

The first derivations of SEA appeared at two independent works, developed by Lyon and Maidanik (1962) and Smith (1962) respectively, and it is still widely used due to its low computational cost and simplicity, as shown by Crocker and Price (1969).

The first book compiling the basic theory of SEA and the procedure for applying it to dynamical systems was written by Lyon (1975). The main idea is that a complex vibroacoustic system can be divided into simpler subsystems, characterised by their modal densities and internal loss factors. The power fluxes between these subsystems can be expressed in terms of their averaged energies with the help of the coupling loss factors (CLFs). Knowing the power input to the system, a set of equations can be derived from the power balances of the subsystems, such that the only unknowns of the problem are their averaged energies.

These power flow equations are valid if the subsystems are reverberant, and therefore the pressure or vibration field in them can be considered to be diffuse. This is assumed to be true if the SEA subsystems satisfy a certain set of assumptions, known as the *SEA hypotheses*, which hold in most systems within the high frequency range,

see Hodges and Woodhouse (1986) and Lyon and DeJong (1995). These hypotheses are summarised in Table 1.1.

1. **Statistically independent excitation forces:** the external forces do not excite a particular mode. This is required for having uncorrelated modal vibrations.
2. **Equal probability of modes occurring in a certain frequency range:** all the modes within a certain subsystem and frequency range occur with the same probability. This also contributes to guarantee the diffuse field assumption.
3. **Equipartition of modal energy in a subsystem, and incoherent modal response between modes in the coupled subsystems:** the equipartition of modal energy means that every mode has equal energy. The incoherent modal response is the modal approach to the diffuse field assumption (no mode dominates the dynamics of the system), inherent to the statistical method.
4. **Weak (or light) coupling between subsystems:** the flow of exchanged energy is small compared with the internal dissipation of energy.

Table 1.1: SEA hypotheses

The SEA formulation is based on the power balances of the subsystems. For a particular subsystem i, this balance is expressed as

$$\Pi_i^{\text{in}} = \Pi_i^{\text{diss}} + \sum_{\substack{j=1 \\ j\neq i}}^{n} \Pi_{ij}, \qquad i = 1, \ldots, n, \tag{1.1}$$

where Π_i^{in} is the external power entering the subsystem, Π_i^{diss} is the power dissipated at the subsystem and Π_{ij} is the power exchanged between subsystems i and j. For the particular case of 2 subsystems, an illustrative sketch is shown in Fig. 1.1.

The power dissipated by subsystem i is

$$\Pi_i^{\text{diss}} = \omega \eta_{ii} \langle E_i \rangle, \qquad i = 1, \ldots, n, \tag{1.2}$$

where $\omega = 2\pi f$, f is the vibration frequency, and η_{ii} and $\langle E_i \rangle$ are the internal loss factor and the averaged energy of subsystem i respectively.

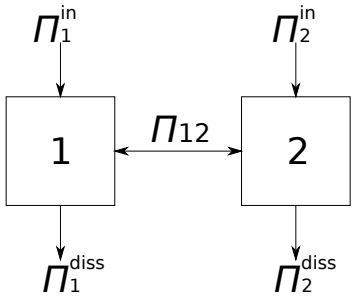

Fig. 1.1: Sketch of an SEA system consisting of two subsystems.

The key aspect of the SEA formulation is the assumption that the power Π_{ij} exchanged between subsystems i and j can be expressed in terms of their averaged energies as

$$\Pi_{ij} = \omega \left(\eta_{ij} \langle E_i \rangle - \eta_{ji} \langle E_j \rangle \right), \tag{1.3}$$

by means of the coupling loss factors η_{ij} and η_{ji}. These factors are assumed to satisfy the consistency relationship

$$\eta_{ij} n_i = \eta_{ji} n_j, \tag{1.4}$$

where n_i is the modal density (number of modes per Hz) of subsystem i. This is a reasonable assumption if the hypotheses of Table 1.1 are fulfilled, as discussed by Lyon (1975).

Therefore, for each subsystem, the power balance of Eq. (1.1) can be rewritten in terms of the energies of the subsystems as

$$\Pi_i^{\text{in}} = \omega \eta_{ii} \langle E_i \rangle + \omega \sum_{\substack{j=1 \\ j \neq i}}^{n} \left(\eta_{ij} \langle E_i \rangle - \eta_{ji} \langle E_j \rangle \right), \qquad i = 1, \ldots, n \tag{1.5}$$

and, joining the power balances of all the subsystems, one gets:

$$\omega \begin{bmatrix} \sum_{i=1}^{n} \eta_{1i} & -\eta_{21} & -\eta_{31} & \cdots & -\eta_{n1} \\ -\eta_{12} & \sum_{i=1}^{n} \eta_{2i} & -\eta_{32} & \cdots & -\eta_{n2} \\ -\eta_{13} & -\eta_{23} & \sum_{i=1}^{n} \eta_{3i} & \cdots & -\eta_{n3} \\ \vdots & \vdots & \vdots & \ddots & \vdots \\ -\eta_{1n} & -\eta_{2n} & -\eta_{3n} & \cdots & \sum_{i=1}^{n} \eta_{ni} \end{bmatrix} \begin{Bmatrix} \langle E_1 \rangle \\ \langle E_2 \rangle \\ \langle E_3 \rangle \\ \vdots \\ \langle E_n \rangle \end{Bmatrix} = \begin{Bmatrix} \Pi_1^{\text{in}} \\ \Pi_2^{\text{in}} \\ \Pi_3^{\text{in}} \\ \vdots \\ \Pi_n^{\text{in}} \end{Bmatrix}. \tag{1.6}$$

This linear system is used to obtain the averaged value of the energy at each subsystem for a given configuration of incoming powers.

Modelling a vibroacoustic system with SEA involves the following steps:

1. Dividing the system into subsystems.
2. Obtaining the internal loss factor of each subsystem.
3. Obtaining the coupling loss factors between each pair of subsystems exchanging energy.
4. Solving the linear system (1.6) to obtain the averaged energies for every subsystem.
5. Computing the output of engineering interest from the averaged energies.

These steps are clear enough for simple geometries and connections, and not so clear for complex systems. The division into subsystems is usually straightforward if the domain consists only of thin plates and acoustic volumes. Moreover, the internal loss factors of homogeneous solids or resonant cavities can be obtained from their material properties. Finally, the coupling loss factors can be obtained with analytical expressions for simple connections between the subsystems. These expressions are often based on the wave approach as detailed by Craik (1996) and Cremer et al. (1973).

Solving vibroacoustic problems with SEA has many advantages, such as low computational cost, robustness in front of small parameter changes and working directly with the averaged energy, which is often required for computing the quantity of interest. However, its application to real-life systems has serious limitations. Fahy (1994) compiles the most important shortcomings of SEA, such as the impossibility of dealing with non-conservative connections or the need of considering indirect couplings in order to reproduce the power fluxes in certain systems.

Besides, SEA hypotheses (Table 1.1) are not always satisfied in real problems. Different authors have studied to what extent these requirements have to be met to get good results with SEA. Elmallawany (1978) and Woodhouse (1981) study the importance of SEA hypotheses by means of comparisons with empirical expressions. Keane and Price (1987) study the applicability of SEA for strong couplings (springs), and provide an SEA-like formulation for such a case.

More recently, Culla and Sestieri (2006) compare SEA with deterministic simulations in order to identify those hypotheses determinant for the accuracy of the results. In the examples of their work, the modal equipartition is the crucial hypothesis for the good performance of SEA. Le Bot and Cotoni (2010), in turn, provide a space of

possible material and geometrical parameters such that SEA hypotheses are fulfilled, for different examples.

Another difficulty when using SEA is the modelling of vibroacoustic domains with heterogeneities, complex geometries or alternations of solid and fluid domains with small dimensions, such as masonry walls or honeycomb panels. In these cases, the division into subsystems may not be straightforward and there are no analytical expressions for the internal or coupling loss factors.

Different authors have worked to overcome these limitations. Some of them use experiments to obtain the missing information needed to perform a complete SEA analysis. For instance, Cuschieri and Sun (1994) use experiments to determine the dissipation and coupling loss factors (even for subsystems that are not in contact). Hopkins (2002) studies the particular case of the experimental estimation of coupling loss factors for low modal densities and overlaps.

Other authors use numerical simulations to analyse the system behaviour and obtain extra information. Some of them focus on the modal properties of the system: Maxit and Guyader (2003) present the SmEdA formulation, a reformulation of SEA taking modal energy distribution into account. They propose the use of the finite element method (FEM) to calculate modal information in the cases of complex subsystems. Finnveden (2004) computes the group velocity and modal density required for the analysis also with the help of FEM. Mace (2005) deals with the concept of proper SEA and quasi-SEA systems, studying the dependence of the direct and indirect CLFs on the modal properties of the system. Gagliardini et al. (2005), in their virtual SEA strategy, compute the energy transfer matrices with FEM for many frequencies and excitations and use this information to optimise the decomposition of the problem into SEA subsystems and estimate coupling loss factors.

Numerical simulations can also be directly combined with SEA leading to a coupled model. That is the case of the approach proposed by Shorter and Langley (2005), based on adding finite element discretisations to SEA at those parts of the domain where a detailed description is required. Cotoni et al. (2007) validate this technique with the help of experiments.

Besides the experiments and numerical simulations, other techniques are combined with SEA in order to overcome some of its limitations. Manning (1994) uses general mobility functions to formulate SEA parameters. Renji et al. (2001) propose a formulation accounting for both resonant and non-resonant transmission, with new

coupling loss factors. Guasch and Aragonès (2011) propose an algorithm based on graph theory to obtain the dominant energy transmission paths in an SEA model, and Barbagallo (2013) combines variational principles with SEA for modelling multilayered structures.

In summary, statistical energy analysis is a very powerful technique for dealing with vibroacoustic problems at high frequencies. Many authors have worked in the last decades to study and extend the applicability range of SEA. However, there are still many open problems and questions to be answered. In this part of the thesis, the potential of numerical simulations for extending the SEA applicability is analysed. In particular, three main points are addressed:

- The estimation of coupling loss factors for complex conservative connections, Chapter 2.
- The modelling of non-conservative couplings, Chapter 3.
- The subsystem identification, Chapter 4.

Simple numerical simulations are used to obtain the required information for dealing with real-life vibroacoustic problems with SEA.

Chapter 2

Conservative couplings: estimation of coupling loss factors[1]

A study on the optimal procedure for obtaining SEA coupling loss factors (CLF) numerically is presented. The energies of an SEA system with two subsystems (one excited, the other one unexcited) are obtained from deterministic numerical simulations. Three different ways of isolating the CLF are explored: from the power balance of the excited subsystem (first approach) or the unexcited subsystem (second approach) and from the power transmitted through the connection (third approach). An error propagation analysis shows that the first approach is unreliable and that the second approach is the best option. As application examples, the CLF between some typical building structures is computed. These examples also illustrate the potential of the estimated CLFs to solve larger problems with SEA.

2.1 Preliminaries

Due to its averaged nature, SEA is not designed to take into account small details of the problem geometry or heterogeneities. For complex systems, the parameters required in the SEA formulation, such as the coupling loss factors, cannot be calculated analytically. One option for obtaining these parameters is to identify them from labo-

[1]Chapter based on reference: Díaz-Cereceda et al. (2013a)

ratory measurements as De Langhe and Sas (1996) or Semprini and Barbaresi (2008) do.

Another option is to estimate these parameters with deterministic formulations and numerical methods. Some authors like Simmons (1991), Steel and Craik (1994) or Fredö (1997) use finite element methods (FEM) to obtain the energy fluxes in the problem and then estimate SEA parameters from them. Their interest is focused in dynamic problems with no acoustic interaction and they do not apply the obtained parameters for solving larger problems.

Maxit and Guyader (2001) estimate the coupling loss factors from modal parameters of the SEA subsystems. They use modal analysis to obtain these parameters by means of simplifying the problem with the help of substructuring. This approach is therefore limited to domains where, for every pair of subsystems in contact, one of them has a clearly stiffer behaviour than the other. However, it cannot deal with problems where the subsystems are not in direct contact but connected by a third element, such as double walls. Maxit and Guyader apply their approach to obtain coupling loss factors between beams and plates with common edges and Totaro et al. (2009) use the same approach to compute coupling loss factors between structures and cavities.

Finally, Thite and Mace (2007) deal with the idea of obtaining robust estimators of these parameters from the deterministic results. They explore the usefulness of Monte Carlo simulations for obtaining robust enough values of the coupling loss factors to be used later in different types of problems.

In this chapter, a technique for obtaining the coupling loss factors between two subsystems is proposed. This technique is based on deterministic simulations and is independent of the device connecting the subsystems. The goal is to apply the obtained factors for solving larger vibroacoustic problems with SEA.

2.2 Coupling loss factor calculation

The technique for computing the CLF between two subsystems is based on the sound transmission between them when only one of the subsystems is excited. For any connecting device between them, the SEA formulation is

$$\left\{ \begin{array}{c} \Pi_1^{\text{in}} \\ 0 \end{array} \right\} = \omega \left[\begin{array}{cc} \eta_{11} + \eta_{12} & -\eta_{21} \\ -\eta_{12} & \eta_{21} + \eta_{22} \end{array} \right] \left\{ \begin{array}{c} \langle E_1 \rangle \\ \langle E_2 \rangle \end{array} \right\}. \tag{2.1}$$

The standard procedure in SEA would be to compute the averaged energies of the subsystems with Eq. (2.1). The input power is usually known, for a given excitation. In building acoustics, the internal loss factor can be computed with analytical expressions available in the literature for most types of subsystems, see Craik (1996). However, the analytical expression for the coupling loss factor is only available for simple connections.

Here, the SEA formulation for a system consisting of two subsystems is used to estimate the coupling loss factor. The averaged energies are obtained from the numerical simulation of the same vibroacoustic problem and Eqs. (2.1) and (1.4) are used to compute η_{12}. Since the energy values are frequency-dependent, the CLF will also depend on the frequency, and therefore the result of the computation will not be a single value but a CLF law in terms of the frequency.

Three different ways are explored for computing the coupling loss factor. Two of them are based on the SEA formulation for the 2-subsystem case, Eq. (2.1). The third one is based on the power exchange at the connection, Eq. (1.3). They are:

First expression: CLF is isolated from the first equation in system (2.1) (power balance of subsystem 1) as

$$\eta_{12} = \frac{\Pi_1^{\text{in}}/\omega - \eta_{11}\langle E_1\rangle}{\langle E_1\rangle - \frac{n_1}{n_2}\langle E_2\rangle}. \tag{2.2}$$

Second expression: CLF is isolated from the second equation in system (2.1) (power balance of subsystem 2) as

$$\eta_{12} = \frac{\eta_{22}\langle E_2\rangle}{\langle E_1\rangle - \frac{n_1}{n_2}\langle E_2\rangle}. \tag{2.3}$$

Third expression: CLF is isolated from the expression (1.3) of the power transmitted through the connection as

$$\eta_{12} = \frac{\Pi_{12}}{\omega\left(\langle E_1\rangle - \frac{n_1}{n_2}\langle E_2\rangle\right)}. \tag{2.4}$$

2.3 Error propagation analysis

The three techniques described in Section 2.2 involve operations between approximated quantities. Both the energies of the subsystems and the incoming and exchanged powers are computed from numerical simulations. Therefore, an analysis of

the error propagation (see Henrici (1964) or Higham (1996)) is required in order to check the reliability of the three expressions proposed to compute the CLF.

The relative error of a certain approximation $\bar{x}$ with respect to the exact value x can be computed as

$$r_x = \frac{x - \bar{x}}{x}. \tag{2.5}$$

For the sake of simplicity, the following assumptions are made:

- $\langle E_1 \rangle \gg \langle E_2 \rangle$. This is the weak coupling hypothesis of Table 1.1, required by the SEA framework.
- $\eta_{11} = \eta_{22}$ and $n_1 = n_2$. In all the examples both subsystems have the same properties, in particular the same internal loss factor and modal density. This assumption is not necessary but simplifies the expressions and facilitates the understanding of the error propagation.
- The internal loss factors η_{ii} are known with a high accuracy and, therefore, their error is negligible.

If these simplifications are incorporated to Eq. (2.2), the value of the relative error of η_{12} computed with the **first expression** is

$$\begin{aligned} r_{\eta_{12}} \simeq (r_{\Pi_1^{\text{in}}} - r_1) \frac{\left(\Pi_1^{\text{in}}\right)}{\omega \langle E_1 \rangle \left(\frac{\Pi_1^{\text{in}}}{\omega \langle E_1 \rangle} - \eta_{11}\right)} = (r_{\Pi_1^{\text{in}}} - r_1) \left(1 + \frac{\langle E_1 \rangle \eta_{11}}{\frac{\Pi_1^{\text{in}}}{\omega} - \eta_{11} \langle E_1 \rangle}\right) = \\ = (r_{\Pi_1^{\text{in}}} - r_1) \left(1 + \frac{\langle E_1 \rangle}{\langle E_2 \rangle}\right) = \left(1 + \frac{\langle E_1 \rangle}{\langle E_2 \rangle}\right) r_{\Pi_1^{\text{in}}} - \left(1 + \frac{\langle E_1 \rangle}{\langle E_2 \rangle}\right) r_1, \end{aligned} \tag{2.6}$$

where r_1 and $r_{\Pi_1^{\text{in}}}$ are the relative errors associated to the computation of $\langle E_1 \rangle$ and Π_1^{in} respectively.

The assumption of weak coupling leads to the conclusion that $|r_{\eta_{12}}| \gg |r_{\Pi_1^{\text{in}}} - r_1|$. The relative error of the CLF computed with this approach is larger than those of the energy and incoming power of subsystem 1. There is an amplifying factor of the error caused by the subtraction of two very similar values, Π_1^{in}/ω and $\eta_{11} \langle E_1 \rangle$, that makes this way of estimating the CLF unreliable.

The error committed in the computation of the CLF obtained with the **second expression** (2.3) is

$$r_{\eta_{12}} = \frac{r_2 - r_1}{1 - r_1} \simeq r_2 - r_1 \tag{2.7}$$

where r_2 is the relative error in the calculation of $\langle E_2 \rangle$. The error in the CLF is of the same order of the errors in the calculation of the energies.

In a similar way, the value of the error committed with the **third expression** (2.4) is

$$r_{\eta_{12}} \simeq r_{\Pi_{12}} - r_1, \tag{2.8}$$

where $r_{\Pi_{12}}$ is the relative error associated to the computation of Π_{12}. As in Eq. (2.7), the error in the CLF is of the order of the errors of the computed quantities, with no amplifying factor.

The relative error of the three expressions can be computed as a linear combination of the relative errors of the energies and powers. In Equations (2.7) and (2.8) the combination coefficients are equal to one, but in Eq. (2.6) they are much larger than one. The main conclusion is that subtractions of very similar quantities should be avoided in the computation of the CLF. Instead, expressions in which the power exchanged in the connection or the energy of the unexcited subsystem appear in the numerator provide better results.

Two considerations must be done regarding these results. The first one is their dependence on the weak coupling between the subsystems. If the coupling is strong, the first expression (2.2) performs much better in terms of the error propagation, because the two quantities in the subtraction are not similar any more. However, the weak coupling is a hypothesis of SEA and, therefore, strong couplings lead to unreliable results with the three expressions.

The second consideration is related to the estimation of the CLF from experimental values. In that case, the experimental error may be a systematic error, and the values of $r_{\Pi_1^{\text{in}}}$ and r_1 may have the same sign and be of the same order. In that case, even if the coefficients that multiply the energy and power errors in Eq. (2.6) are much greater than one, the value of the two terms may be similar and therefore, they could compensate and provide a low value of the CLF error. This is one possible reason for the good results achieved by Campolina et al. (2012), when they estimate the coupling loss factor from experimental measurements. However, it is better to use the second expression, since it provides a more robust way for computing the CLF. In fact, this expression is equivalent to those resulting from the formulations of Fredö (1997) and Simmons (1991) and the CLF expression derived in the Power Injection Method, see De Langhe and Sas (1996). The third expression is also reliable, but it requires obtaining another value: the transmitted power.

2.4 Applications in building acoustics

The three techniques described in Section 2.2 for estimating the CLF are validated here for some mechanical examples whose analytical expression is provided in the literature. Also, the traditional treatment of double walls with SEA is analysed here, comparing it with the CLF estimations derived from numerical simulations of this vibroacoustic problem.

2.4.1 Coupling loss factor for mechanical connections

In this section, some structural configurations with a known analytical expression of the CLF are studied. All the examples consist of walls or floors. They have been modelled as thin plates, connected by mechanical devices. More details on the deterministic model are provided in Appendix A.

The mechanical and geometric properties of the plates are summarised in Tables 2.1 and 2.2 respectively. The external excitation of the system is always a force of 1 N, applied on plate 1 at every Hz. Therefore $\Pi_j^{\text{in}} = 0$ for $j > 1$. The excitation is applied in twenty different (random) points and the resulting energies and powers are averaged as described in Appendix A.

The CLF calculations obtained for each Hz are also averaged in third octave bands before plotting the result.

Variable	**Symbol**	**Value**
Young's modulus	E	$2.5 \times 10^9\,\text{N m}^{-2}$
Density	ρ	$692.3\,\text{kg m}^{-3}$
Poisson's ratio	ν	0.3
Loss factor	η	3%

Table 2.1: Mechanical properties of the GN plasterboard plates.

Variable	**Symbol**	**Value**
Plate size, x direction	L_x	2.4 m
Plate size, y direction	L_y	2.4 m
Thickness	h	13 mm

Table 2.2: Geometric properties of the GN plasterboard plates.

2.4.1.1 Double wall with connecting point springs

The first example reproduces the case of a double wall without considering the effect of the air in the cavity. It consists of two parallel simply supported leaves connected with nine translational springs, equally distributed along the leaves as shown in Fig. 2.1. These springs represent the effect of studs connected by point screws to the leaves. The stiffness of each spring is $K = 8 \cdot 10^5 \text{ N m}^{-1}$.

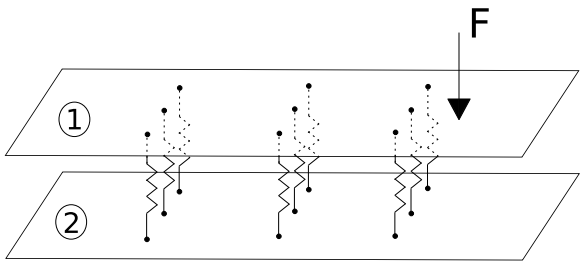

Fig. 2.1: Distribution of the nine springs.

The CLF estimations have been compared with an analytical expression typically used in SEA by Hopkins (2007) or Craik (1996), obtained by analogy with an electrical circuit and valid when each connection acts independently of the others

$$\eta_{12} = \frac{n_c \text{Re}\{Y_2\}}{\omega M_1 |Y_1 + Y_2 + Y_s|^2}. \tag{2.9}$$

In Eq. (2.9),

$$Y_i = \frac{1}{8\sqrt{B_i \rho_{si}}} \qquad i = 1,\, 2 \tag{2.10}$$

is the point mobility of each leaf, M_1 is the mass of leaf 1,

$$Y_s = \frac{\mathrm{i}\omega}{K} \tag{2.11}$$

is the mobility of the spring, $\mathrm{i} = \sqrt{-1}$ is the imaginary unit, $B_i = Eh^3/12(1-\nu^2)$ is the bending stiffness of plate i, ρ_{si} its mass per unit surface, and $n_c = 9$ is the number of springs used.

In Fig. 2.2 the three methods described in Section 2.2 for computing the CLF are compared with the analytical expression.

For this simple problem, the numerical estimations of the CLF provide good results for the second and third expressions. However, results derived from the first

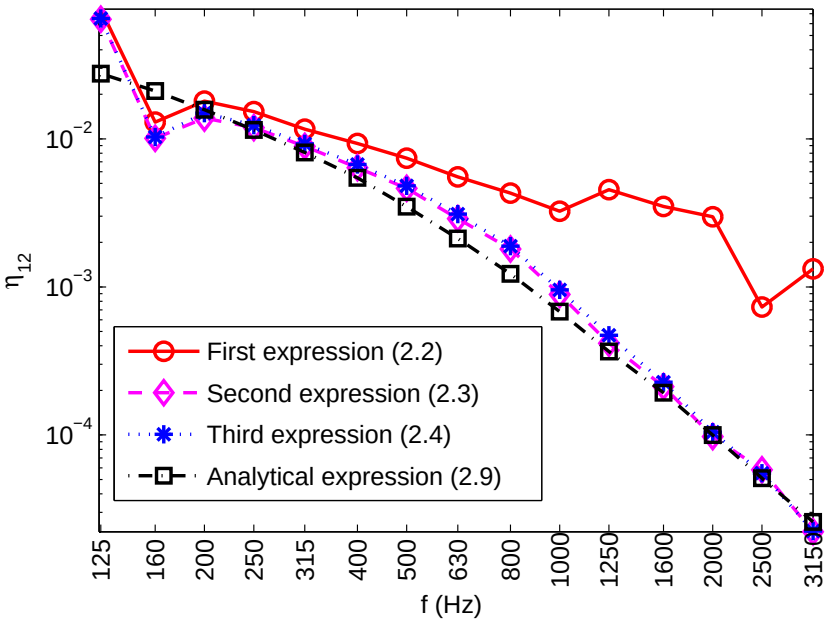

Fig. 2.2: Comparison of the coupling loss factor η_{12} for nine spring connections.

expression (2.2) are wrong. This behaviour is explained with the analysis of error propagation shown in Section 2.3, and confirms the unreliability of this expression for obtaining the CLF, specially when the coupling between the leaves is very weak. This is illustrated in Fig. 2.3, where the evolution of the ratio $\langle E_1 \rangle / \langle E_2 \rangle$ with the frequency is shown.

The figure shows that, the larger the frequency, the larger the amplifying factor. This is coherent with the weaker behaviour of the coupling when the frequency increases, and explains the large error of the first expression, specially at the highest frequencies.

The differences at low frequencies are reasonable, since most of the SEA hypotheses are not satisfied at those frequencies and therefore the SEA-based expressions are no longer valid. That is why frequencies lower than 125 Hz are not shown in the figures.

2.4.1.2 Rotational joint

The second example consists of two adjacent floors with a rotational joint in the common edge, see Fig. 2.4. It reproduces the effect of elastic joints through a long

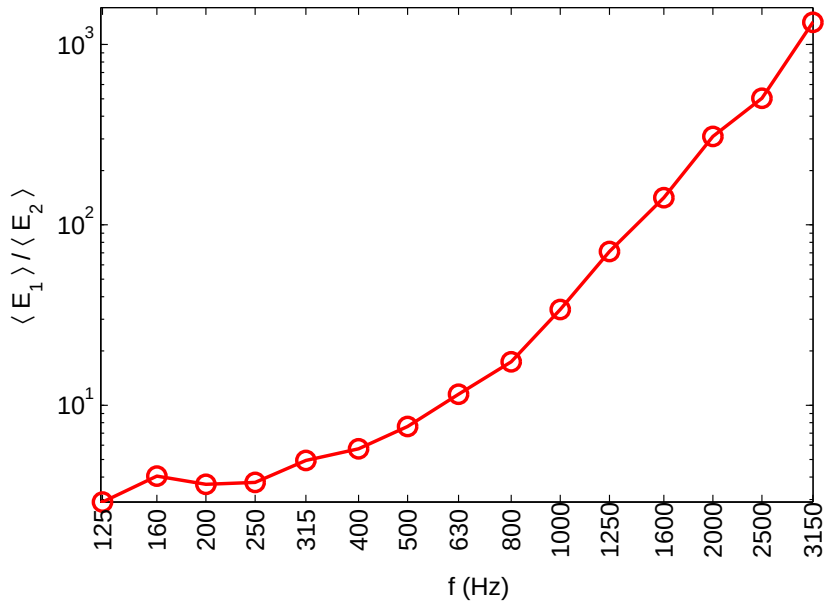

Fig. 2.3: Evolution of the error amplification factor with the frequency.

floor. The rotation stiffness of the joint is $K_\theta = 10^3$ N m/rad m. It relates the plate rotations θ and bending moments m on both sides of the joint as $m_1 = m_2 = K_\theta\,(\theta_1 - \theta_2)$. For more details on this model, see Díaz-Cereceda et al. (2011).

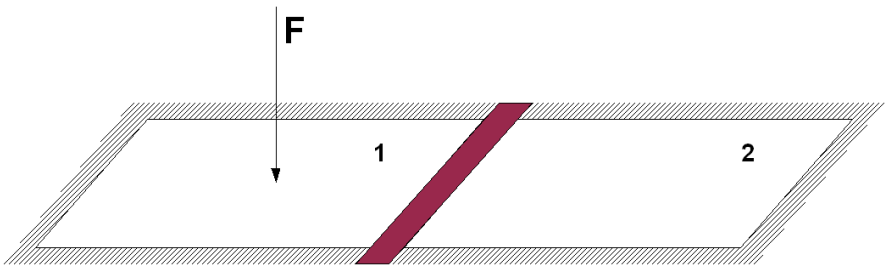

Fig. 2.4: Sketch of the rotational joint.

The CLF estimated from the numerical solution is compared with an analytical expression obtained with the wave approach, see Cremer et al. (1973). It is based on the orthogonality between the joint and the waves propagating in the floor. The vibration field in the excited floor span (subsystem 1) is assumed to consist of incident waves, reflected waves in the far field (propagating) and reflected waves in the near

field (evanescent). The vibration field in the span with no external excitation consists of transmitted waves, both in the near and the far field. The expressions of the vibration fields in spans 1 and 2 (v_{z1} and v_{z2}) are

$$\begin{aligned} v_{z1} &= v_z \left(\exp\left(-\mathrm{i}k_1 y\right) + r\exp\left(\mathrm{i}k_1 y\right) + r_i \exp\left(k_1 y\right)\right) \\ v_{z2} &= v_z \left(t\exp\left(-\mathrm{i}k_2 y\right) + t_i \exp\left(-k_2 y\right)\right) \end{aligned} \tag{2.12}$$

where k_1 and k_2 are the wavenumbers in spans 1 and 2 respectively, r and t are the reflection and transmission parameters, r_i and t_i their equivalents in the near field and y is the direction of the wave propagation.

In order to find r, t, r_i and t_i the boundary conditions at the contact line of both spans are applied

$$v_{z1} = 0; \quad v_{z2} = 0; \quad m_1 = m_2 = K_\theta \left(\theta_1 - \theta_2\right). \tag{2.13}$$

Assuming that the wavenumbers and bending stiffnesses are the same for both spans $k_1 = k_2 = k_s$ and $B_1 = B_2 = B$, the following linear system holds:

$$\begin{bmatrix} 1 & 1 & 0 & 0 \\ 0 & 0 & 1 & 1 \\ -1 & 1 & 1 & -1 \\ \mathrm{i} & 1 & \mathrm{i} - \frac{Bk_s}{K_\theta} & 1 + \frac{Bk_s}{K_\theta} \end{bmatrix} \begin{Bmatrix} r \\ r_i \\ t \\ t_i \end{Bmatrix} = \begin{Bmatrix} -1 \\ 0 \\ 1 \\ \mathrm{i} \end{Bmatrix}. \tag{2.14}$$

From this system, the value of r is obtained and therefore the transmission coefficient can be computed as $\tau_{12} = 1 - |r|^2$. The CLF is obtained with the expression for two plates sharing one edge

$$\eta_{12} = \frac{2c_{\text{plate}} L_{\text{edge}} \tau_{12}}{\pi \omega S} \tag{2.15}$$

where $c_{\text{plate}} = \sqrt{\omega^2 B/\rho_s}$ is the propagation velocity of the waves in the plates, L_{edge} is the length of the common edge and S is the surface of one plate.

In Fig. 2.5 the comparison between the three estimation methods described in Section 2.2 and this analytical approximation is shown.

Again the errors with the first expression (2.2) are unacceptable, while the other techniques present the same trend as the analytical one. However, there are some differences between the results obtained with the second and third expressions. A possible explanation for this discrepancy is that the computation of the power transmitted at the joint is less trustable than that of the example of Section 2.4.1.1. In this

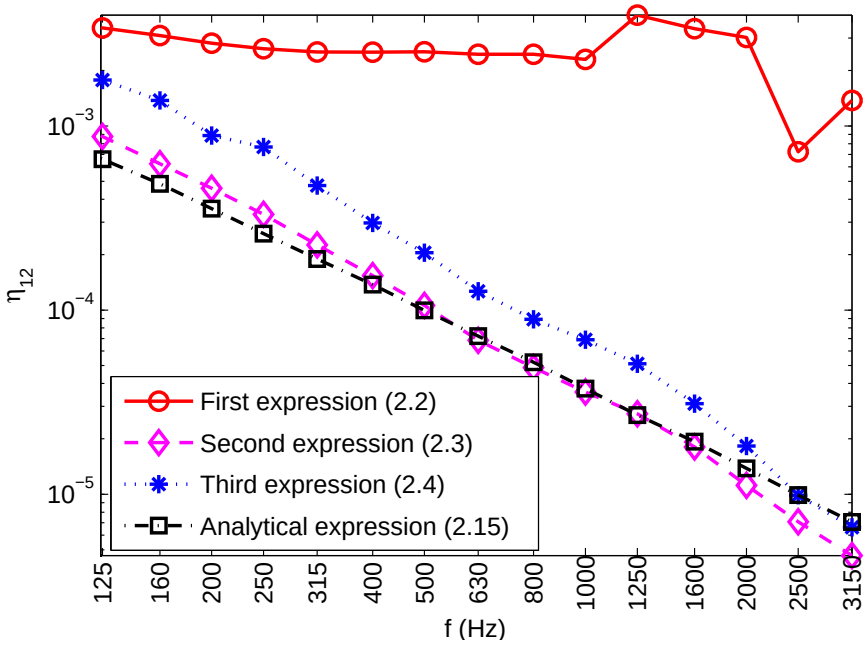

Fig. 2.5: Comparison of the coupling loss factor η_{12} for the rotational joint.

case, the power must be computed along a line and is also affected by the boundary conditions of the plate (the joint is located at an edge of the span). Therefore, the estimation of the CLF from the power at the connection (third expression) is less accurate than in the previous example.

2.4.1.3 Application for long floors

With the CLF estimations for the rotational joint, a new configuration is simulated: the propagation of vibrations through a long floor consisting of four simply supported plates linked together with elastic joints as shown in Fig. 2.6.

The goal is to check whether the CLF obtained in Section 2.4.1.2 for the rotational joint can be used in the SEA simulation of a structure consisting of more than two subsystems, i.e. more than two floor spans. This is an example of the potential of the technique proposed in this chapter: obtaining the coupling loss factor between two subsystems with a deterministic computation and applying it for solving larger problems with SEA.

In order to perform the full statistical energy analysis, the only information needed, in addition to the coupling loss factor, are the internal loss factors of the

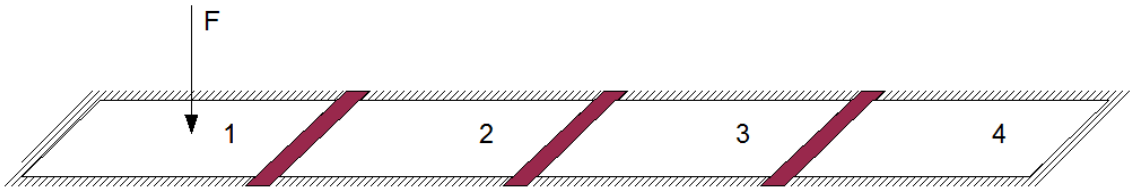

Fig. 2.6: Sketch of the four plates linked with rotational joints.

subsystems and the input power. The internal loss factor is the same for all the subsystems and is defined in Table 2.1 ($\eta_{ii} = \eta$). The input power is computed as $\Pi_1^{\text{in}} = \frac{1}{2}|F_1|^2 \text{Re}\{1/Y_1\}$ because the velocity field is not known *a priori*. F_1 is the force applied to subsystem 1.

Using the CLF η_{12}^{num} obtained in Section 2.4.1.2 for every joint and assuming that all the connections and subsystems are equal ($\eta_{ij} = \eta_{12}^{\text{num}} \quad \forall\, i \neq j$), the energies of every subsystem are obtained from the global SEA system

$$\begin{Bmatrix} \Pi_1^{\text{in}} \\ 0 \\ 0 \\ 0 \end{Bmatrix} = \omega \begin{bmatrix} \eta + \eta_{12}^{\text{num}} & -\eta_{12}^{\text{num}} & 0 & 0 \\ -\eta_{12}^{\text{num}} & \eta + 2\eta_{12}^{\text{num}} & -\eta_{12}^{\text{num}} & 0 \\ 0 & -\eta_{12}^{\text{num}} & \eta + 2\eta_{12}^{\text{num}} & -\eta_{12}^{\text{num}} \\ 0 & 0 & -\eta_{12}^{\text{num}} & \eta + \eta_{12}^{\text{num}} \end{bmatrix} \begin{Bmatrix} \langle E_1 \rangle \\ \langle E_2 \rangle \\ \langle E_3 \rangle \\ \langle E_4 \rangle \end{Bmatrix}. \quad (2.16)$$

The vibration level difference between the first and the fourth floor spans

$$D_{14} = 10 \log \frac{\langle E_1 \rangle}{\langle E_4 \rangle} \quad (2.17)$$

obtained with SEA is compared in Fig. 2.7 with the numerical solution obtained for the deterministic analysis of the four plates. The results obtained with SEA are computed using the two best CLF laws estimated in the 2-subsystem case: the second and third expressions (Eqs. (2.3) and (2.4) respectively). The trend of D_{14} is well captured with SEA, for both laws of the CLF. For the SEA computation, a tridiagonal 4×4 problem is solved at each frequency, while the linear systems to be solved in the numerical computation are block-tridiagonal and their size ranges from 624 degrees-of-freedom (dof) for the lowest frequency to 968 dof for the highest frequency.

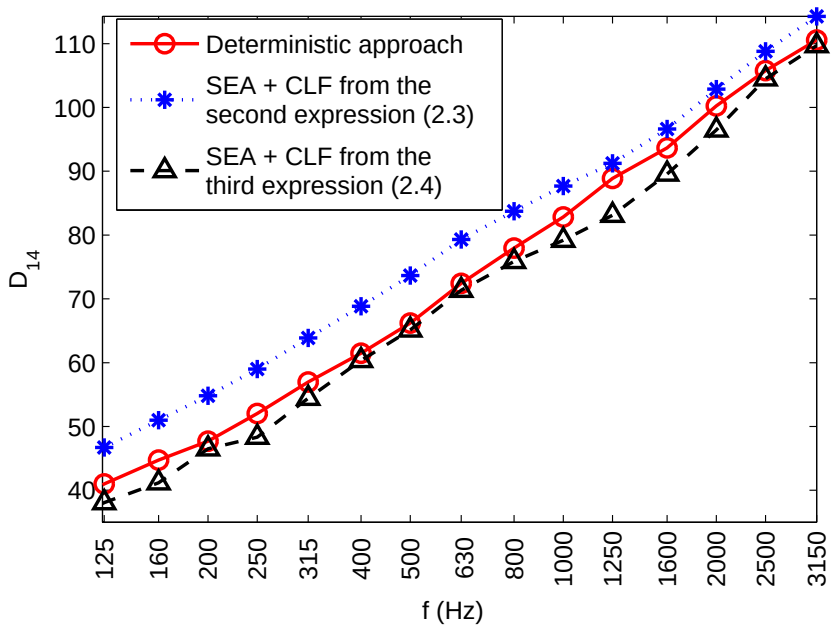

Fig. 2.7: Comparison of the vibration level difference D_{14} for a floor consisting of four spans.

2.4.2 Coupling loss factor in double walls

The isolating effect of the air cavity located between the two leaves of a double wall is analysed here. This example has been chosen because it is a representative vibroacoustic problem and also because the SEA treatment of double walls is a challenge: the air cavity may be treated as an SEA subsystem or just as a connection between subsystems, see Hopkins (2007).

The use of statistical energy analysis for modelling double walls is analysed by Brekke (1981), Craik and Smith (2000) and Craik (2003). Brekke concludes, with the help of experiments, that the effect of the air stiffness should be taken into account, as well as the resonant transmission, for lower frequencies. On the other hand, Craik focuses on the search of accurate expressions for the indirect coupling loss factor between the rooms and the cavity.

Here, the coupling loss factor between the two leaves of the double wall is computed numerically and compared with analytical expressions available in the literature. The numerical calculation is done using modal analysis to discretise both the leaves and the cavity. More details on this approach can be found in Section 5.2.3

(Part II). The excitation is an impact on one of the leaves. Twenty different positions of the excitation are used, and the resulting energies are computed and averaged as described in Appendix A.

The properties of the leaves are described in Table 2.1 and the cavity thickness is $H = 70$ mm. Therefore, the mass-air-mass natural frequency for the two leaves and the cavity is $f_{\text{mam}} = 106.5$ Hz. Moreover, the absorption coefficient at the cavity contour is assumed to be $\alpha = 0\%$. This is a reasonable assumption, since the area of the cavity contour is much lower than the rest of areas involved in the problem, and therefore the dissipation at the cavity is negligible compared to the energy transmissions. If the cavity was filled with absorbing material, the behaviour would be very different and the cavity should be treated as a non-conservative connection between the two leaves. This topic is addressed in Chapter 3.

Different SEA references such as Craik (1996) or Hopkins (2007) do not coincide in the optimal way to deal with double walls in SEA. Neither the identification of subsystems nor the coupling loss factor expressions are clear.

A very common option is to consider the cavity as an SEA subsystem as shown by Craik (1996) (see Fig. 2.8), and obtain its own modal density

$$n_i = \frac{4\pi f^2 V_{\text{cav}}}{c^3} + \frac{2\pi f S_{\text{cav}}}{4c^2} + \frac{L_{\text{cav}}}{8c} \tag{2.18}$$

and internal loss factor

$$\eta_{ii} = \frac{c\alpha S_{\text{cav}}}{8\pi f V_{\text{cav}}}, \tag{2.19}$$

where c is the sound speed in the air, V_{cav} is the cavity volume, S_{cav} is the surface of the cavity boundary (the sum of the areas of all the faces surrounding the cavity except the contact surfaces with the leaves) whose absorbing factor is α and L_{cav} is the sum of the lengths of the twelve cavity edges. In the examples of this work, $\eta_{ii} = 0$.

Then, the coupling loss factors between the cavity and the leaves are obtained as

$$\eta_{ij} = \frac{\rho_{\text{air}} c \sigma_{\text{rad}} f_c}{4\pi f^2 \rho_s}, \tag{2.20}$$

where f_c is the coincidence frequency between the leaf and the air and σ_{rad} is the radiation efficiency of the leaf. The radiation efficiency is computed with the expressions defined by Maidanik (1962) with a small modification: the critical frequency treatment is applied for all the frequencies in a range of $f_c \pm 5$ Hz.

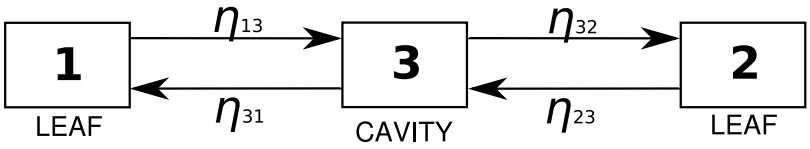

Fig. 2.8: SEA sketch of a double wall with the cavity considered as a subsystem.

For this case, an equivalent coupling loss factor between the leaves is obtained in order to compare it with the other techniques. This is possible because the absorption coefficient at the cavity is null and, therefore, the cavity only transmits energy, without dissipating it.

Considering the cavity as subsystem 3, the global SEA-system is

$$\left\{ \begin{array}{c} \Pi_1^{\text{in}} \\ 0 \\ 0 \end{array} \right\} = \omega \left[\begin{array}{ccc} \eta_{11}+\eta_{13} & -\eta_{31} & 0 \\ -\eta_{13} & \eta_{33}+\eta_{31}+\eta_{32} & -\eta_{23} \\ 0 & -\eta_{32} & \eta_{22}+\eta_{23} \end{array} \right] \left\{ \begin{array}{c} \langle E_1 \rangle \\ \langle E_3 \rangle \\ \langle E_2 \rangle \end{array} \right\}. \tag{2.21}$$

Assuming that the two leaves are identical ($\eta_{13} = \eta_{23}$, $\eta_{31} = \eta_{32}$ and $\eta_{11} = \eta_{22}$) and imposing $\eta_{33} = 0$, the system becomes

$$\left\{ \begin{array}{c} \Pi_1^{\text{in}} \\ 0 \\ 0 \end{array} \right\} = \omega \left[\begin{array}{ccc} \eta_{11}+\eta_{13} & -\eta_{31} & 0 \\ -\eta_{13} & 2\eta_{31} & -\eta_{13} \\ 0 & -\eta_{31} & \eta_{11}+\eta_{13} \end{array} \right] \left\{ \begin{array}{c} \langle E_1 \rangle \\ \langle E_3 \rangle \\ \langle E_2 \rangle \end{array} \right\}. \tag{2.22}$$

Isolating $\langle E_3 \rangle$ from the second equation and replacing it in the other two, the system can be reduced to

$$\left\{ \begin{array}{c} \Pi_1^{\text{in}} \\ 0 \end{array} \right\} = \omega \left[\begin{array}{cc} \eta_{11}+\eta_{13}/2 & -\eta_{13}/2 \\ -\eta_{13}/2 & \eta_{11}+\eta_{13}/2 \end{array} \right] \left\{ \begin{array}{c} \langle E_1 \rangle \\ \langle E_2 \rangle \end{array} \right\} \tag{2.23}$$

and, therefore, the equivalent coupling loss factor is

$$\eta_{12}^{\text{equi}} = \frac{\eta_{13}}{2}. \tag{2.24}$$

Another option is to consider the air cavity as a connection between the two subsystems (leaves) as shown in Fig. 2.9; in particular as a spring with stiffness $K_{\text{air}} = \rho_{\text{air}} c^2 S/H$. This approach takes into account the non-resonant transmission caused by the stiffness of the air. The coupling loss factor is computed with the electrical circuit analogy, as done by Hopkins (2007), using Eq. (2.9) with $n_c = 1$.

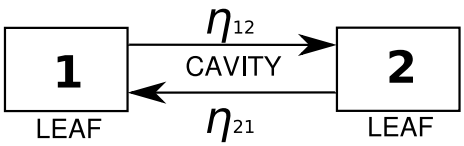

Fig. 2.9: SEA sketch of a double wall with the cavity considered as a connection.

In this work, the coupling loss factor between the two leaves of a double wall is obtained solving the vibroacoustic problem with modal analysis and isolating the CLF with the second expression (2.3). This CLF law is compared with the two analytical approaches in Fig. 2.10. The dimensions of the leaves are the same as in Table 2.2.

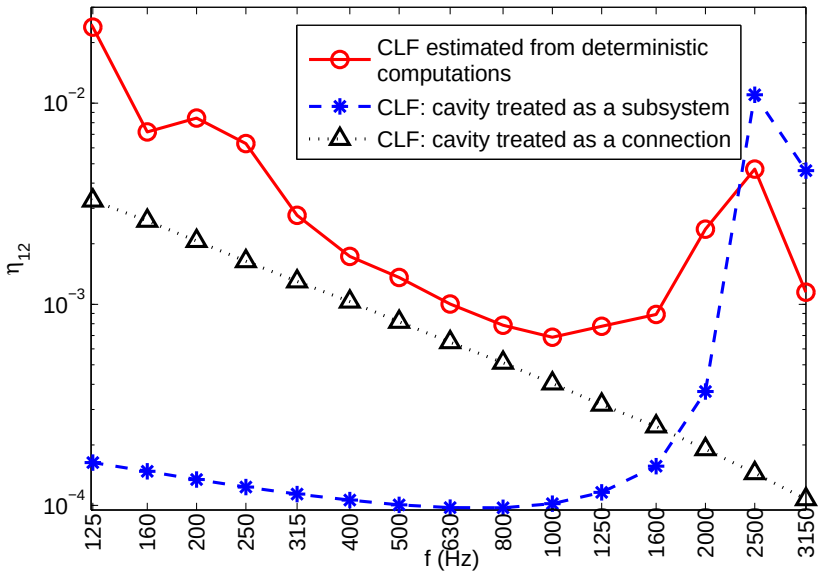

Fig. 2.10: Comparison of the coupling loss factor η_{12} for the cavity inside double walls. Separated effects.

Leaving the low-frequency discrepancies aside, Fig. 2.10 shows that the numerical estimation of the CLF is a good way of taking into account all the physical phenomena occurring in the wall. It shows, as suggested by Brekke (1981), two main features: on the one hand, the importance of the equivalent stiffness of the air, specially at mid frequencies; on the other hand, the coincidence phenomenon that takes place at 2500 Hz in this double wall. This phenomenon is only considered by SEA when the cavity is treated as a subsystem. In fact, SEA overestimates a little the transmission at that

frequency. This may be due to the simplifications involved in the expressions of the radiation efficiency. Therefore, both analytical expressions miss part of the physical information. However, if the analytical expressions are to be used, a complete SEA model is recommended, considering both transmission paths in order to reproduce the real behaviour. The cavity must be considered both as a connecting device and as a subsystem (see Fig. 2.11).

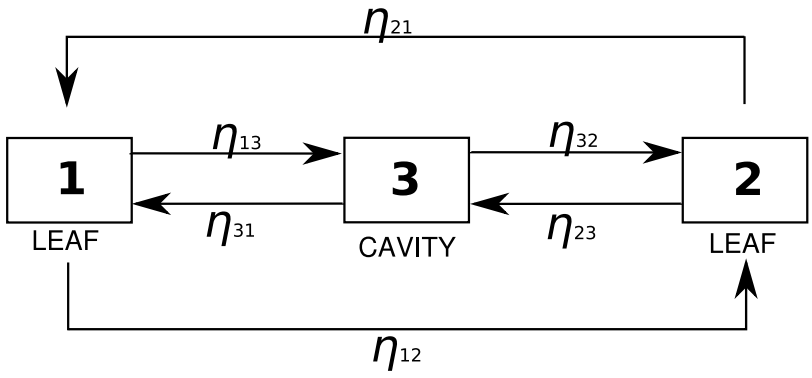

Fig. 2.11: SEA sketch for the combination of the two techniques.

In Fig. 2.12 the coupling loss factor obtained numerically is compared with the CLF resulting from adding the coupling loss factor between the two leaves computed with the electrical analogy and the equivalent coupling loss factor between the leaves described in Eq. (2.24). The need of considering both behaviours together along the whole frequency range becomes evident.

2.5 Concluding remarks

- The main idea developed in this chapter is that small deterministic simulations can be used to estimate SEA coupling loss factors. These factors can be further used to solve larger problems with SEA.

- The way of computing the CLF once the deterministic problem is solved is very important for performing a good estimation. The quantities from which the CLF is computed already have a certain error, and therefore a study of the error propagation is required. Expressions where two similar quantities are subtracted must be avoided.

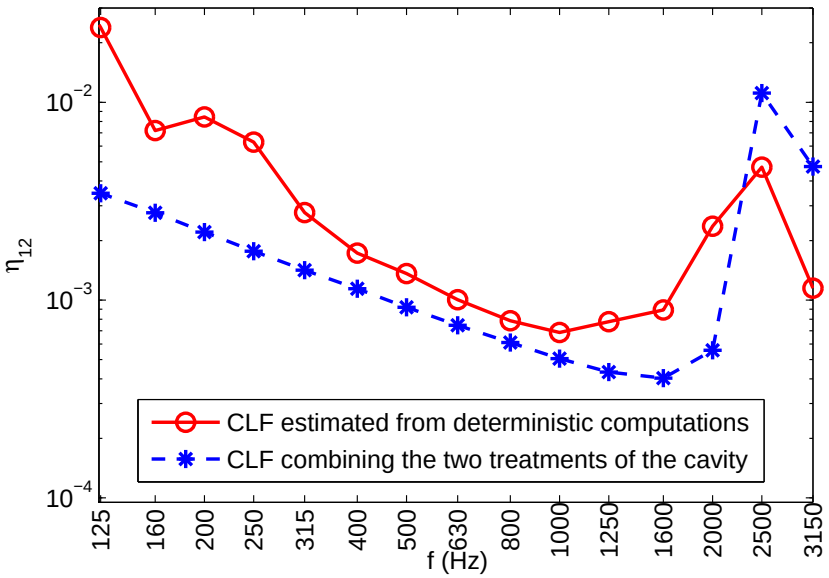

Fig. 2.12: Comparison of the coupling loss factor η_{12} for the cavity in double walls. Combined effects.

- For vibroacoustic problems, such as the case of double walls, a numerical estimation allows to take into account both the resonant and the non-resonant transmission. It also allows to detect that the two analytical approaches, associated to the treatment of the cavity as a subsystem or as a connection respectively, only provide a good model of the real behaviour if they are added.

Chapter 3

Non-conservative couplings[2]

Accounting for dissipative (non-conservative) couplings with statistical energy analysis is an open issue. In this chapter, an equivalent circuit analogy is used to relate the power dissipation at a coupling with the energies of the subsystems. The coupling is characterised by means of two factors: the conservative coupling loss factor (CCLF) and the non-conservative coupling loss factor (NCLF), related to the transmitted and dissipated energy respectively. A methodology for obtaining these parameters from small numerical simulations is presented, and validated with a simple example that can be approached analytically. This technique is applied in Chapter 7 for modelling the sound transmission through double walls filled with absorbing material.

3.1 Preliminaries

As discussed by Fahy (1994), dealing with non-conservative couplings is one of the major challenges of SEA. Some efforts have been done in considering this kind of connections with SEA by Chow and Pinnington (1987), Fredö (1996), Beshara and Keane (1996) and Sheng et al. (1998, 2004). They reach an SEA-like system that takes into account dissipative effects in the couplings.

In particular, Chow and Pinnington introduce an equivalent internal loss factor of the subsystems that models the losses in the connection. Fredö does not modify the internal loss factors of the subsystems or their coupling loss factors; he introduces

[2]Chapter based on references: Díaz-Cereceda et al. (2013b) and Díaz-Cereceda et al. (2013c)

radiation loss factors at the connection. Beshara and Keane also introduce a damping parameter in the connection instead of modifying the internal or coupling loss factors. Finally, Sheng et al. provide a formulation in which the effect of the non-conservative coupling is considered with an equivalent internal loss factor for the subsystems (like Chow and Pinnington) and a new coupling loss factor that accounts for transmission and damping and the same time.

The two last works are restricted to mechanical problems, and are not further applied for vibroacoustic cases, or absorbing materials. Besides, the possibility of extending any of these formulations for dealing with larger SEA systems, consisting of both conservative and non-conservative connections, is not discussed.

The technique developed here is aimed at describing an SEA-like approach for systems with non-conservative connections and a methodology to apply it for any vibroacoustic system consisting of both conservative and non-conservative couplings.

3.2 Non-conservative couplings with SEA

The SEA framework divides the problem domain into two types of elements: subsystems and connections.

An SEA subsystem is a part of the domain such that the energy associated to each of its modes is ideally the same. Every subsystem has its own modal density and an internal loss factor that characterises the fraction of energy dissipated in it.

SEA connections are those elements connecting the subsystems. They have a conservative behaviour, transmitting energy from one subsystem to the other without losses. They are characterised by a coupling loss factor that relates the power across the connection with the energies of the subsystems connected by it.

The effect of a point connection between two SEA subsystems may be studied with the equivalent circuit approach proposed by Olson (1943). This technique is used by Hopkins (2007) to compute the coupling loss factor of a spring connecting two leaves. In general, for any point device connecting two leaves, the global system may be represented as a circuit like that of Fig. 3.1, where Y_1 and Y_2 are the point mobilities of leaves 1 and 2 respectively and Y_c is the mobility of the connection.

The mechanical−electrical analogy is described in Table 3.1 and the assumptions of the analysis are:

- Leaf 1 has an external excitation and leaf 2 has none.

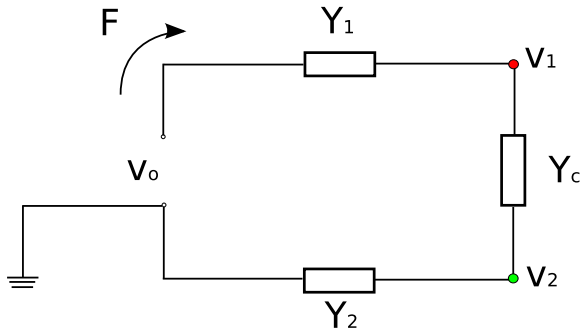

Fig. 3.1: Circuit equivalent to a double wall.

- v_0 is the propagating bending wave velocity of leaf 1 far from the point connection.
- Any point of the unexcited leaf that is far enough from the connection point has a negligible velocity compared to v_0.
- v_1 and v_2 are the velocities at the connecting point of leaves 1 and 2 respectively.

Mechanics	**Electrics**
Force F	Intensity I
Velocity v	Potential V
Admittance (point mobility Y)	Impedance Z

Table 3.1: Mechanical-electrical analogy.

By analogy with the electrical circuit, the excitation force can be expressed in terms of the velocities and point mobilities as

$$F = \frac{v_0}{Y_1 + Y_2 + Y_c} \tag{3.1}$$

and the velocities of the leaves at the connecting point can be expressed as $v_1 = (Y_2 + Y_c)F$ and $v_2 = Y_2 F$.

The power entering the connection (on the closest side to leaf 1) is, see Hopkins (2007),

$$\Pi_{12}^{(1)} = \frac{1}{2}\mathrm{Re}\{F v_1^*\} = \frac{1}{2}\frac{\mathrm{Re}\{Y_2 + Y_c\}|v_0|^2}{|Y_1 + Y_2 + Y_c|^2} \tag{3.2}$$

and the power leaving the connection (on the leaf 2 side) is

$$\Pi_{12}^{(2)} = \frac{1}{2}\mathrm{Re}\{F v_2^*\} = \frac{1}{2}\frac{\mathrm{Re}\{Y_2\}|v_0|^2}{|Y_1 + Y_2 + Y_c|^2}. \tag{3.3}$$

Therefore, the power dissipated at the connection is

$$\Pi_{12}^{\mathrm{diss}} = \Pi_{12}^{(1)} - \Pi_{12}^{(2)} = \frac{1}{2}\frac{\mathrm{Re}\{Y_c\}|v_0|^2}{|Y_1 + Y_2 + Y_c|^2}. \tag{3.4}$$

If the connection is conservative, the power leaving subsystem 1 enters subsystem 2 without losses, that is $\Pi_{12}^{\mathrm{diss}} = 0$ (Fig. 3.2): the connection mobility Y_c is purely imaginary. For the particular case where the connection is a spring, it is $Y_c = \mathrm{i}\omega/K$. In that case, $\mathrm{Re}\{Y_c\} = 0$ and therefore $\Pi_{12}^{\mathrm{diss}} = 0$: there is no dissipation at the conservative connection. The power entering the connection is the same as the power leaving it.

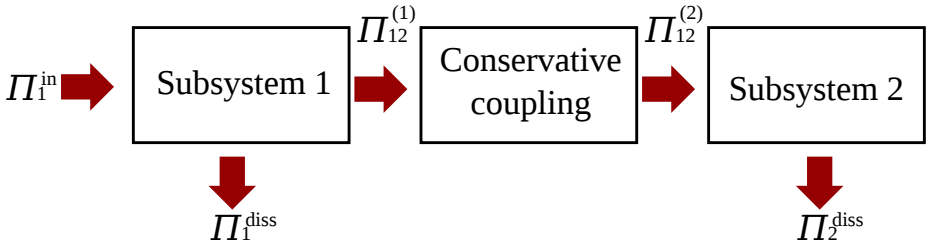

Fig. 3.2: Sketch of a conservative coupling.

If the coupling, on the contrary, has a dissipative behaviour, part of the power leaving subsystem 1 is transmitted to subsystem 2 and the rest is dissipated at the connection. The mobility Y_c in this case has a non-zero real part. For instance, in the particular case of a set of spring and dashpot shown in Fig. 3.3,

$$Y_c = \frac{1}{C + K/\mathrm{i}\omega}, \tag{3.5}$$

and therefore $\mathrm{Re}\{Y_c\} \neq 0$. Some power is dissipated at the connection (Fig. 3.4).

The power balances of the two leaves are

$$\Pi_1^{\mathrm{in}} = \Pi_1^{\mathrm{diss}} + \Pi_{12}^{(1)} \tag{3.6}$$

for the excited leaf and

$$\Pi_2^{\mathrm{diss}} = \Pi_{12}^{(2)} \tag{3.7}$$

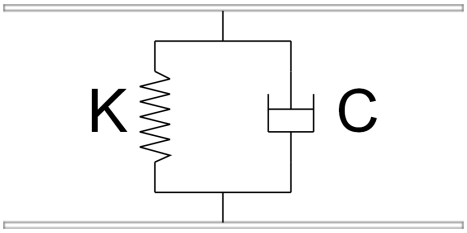

Fig. 3.3: Connection consisting of a spring and a dashpot.

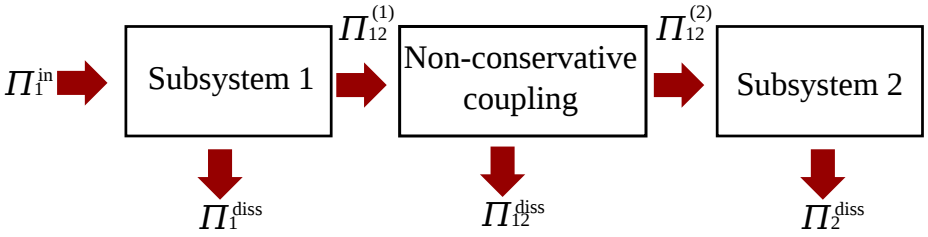

Fig. 3.4: Sketch of a non-conservative coupling.

for the unexcited one.

Assuming that $\langle E_1 \rangle = M_1 \langle v_{\text{rms}}^2 \rangle$, where $\langle v_{\text{rms}}^2 \rangle = |v_o|^2/2$, the power dissipated at the connection can be expressed as

$$\Pi_{12}^{\text{diss}} = \omega \gamma_{12} \langle E_1 \rangle \tag{3.8}$$

and the power transmitted to subsystem 2 as

$$\Pi_{12}^{(2)} = \omega \eta_{12} \langle E_1 \rangle. \tag{3.9}$$

Therefore, the power leaving the connection is $\Pi_{12}^{(1)} = \omega \left(\eta_{12} + \gamma_{12}\right) \langle E_1 \rangle$.

In Eqs. (3.8) and (3.9), two new parameters have been introduced. On the one hand, a factor governing the amount of power dissipated at the connection: the non-conservative coupling loss factor (NCLF)

$$\gamma_{ij} = \frac{\text{Re}\{Y_c\}}{\omega M_i |Y_i + Y_j + Y_c|^2}, \quad i \neq j. \tag{3.10}$$

On the other hand, a factor governing the amount of power reaching the unexcited leaf: the conservative coupling loss factor (CCLF)

$$\eta_{ij} = \frac{\text{Re}\{Y_j\}}{\omega M_i |Y_i + Y_j + Y_c|^2}, \quad i \neq j. \tag{3.11}$$

The power balances of Eqs. (3.6) and (3.7) can be rewritten in terms of the averaged energies for the non-conservative coupling as

$$\Pi_1^{\text{in}}/\omega = \eta_{11}\langle E_1\rangle + (\eta_{12}+\gamma_{12})\langle E_1\rangle \tag{3.12}$$

and

$$\eta_{22}\langle E_2\rangle = \eta_{12}\langle E_1\rangle. \tag{3.13}$$

Following the same procedure in a more general case, with excitations on both subsystems, the global system yields

$$\begin{aligned}\Pi_1^{\text{in}}/\omega &= \eta_{11}\langle E_1\rangle + (\eta_{12}+\gamma_{12})\langle E_1\rangle - \eta_{21}\langle E_2\rangle \\ \Pi_2^{\text{in}}/\omega &= \eta_{22}\langle E_2\rangle + (\eta_{21}+\gamma_{21})\langle E_2\rangle - \eta_{12}\langle E_1\rangle,\end{aligned} \tag{3.14}$$

which can be written in matrix form as

$$\omega \begin{bmatrix} \eta_{11}+\eta_{12}+\gamma_{12} & -\eta_{21} \\ -\eta_{12} & \eta_{22}+\eta_{21}+\gamma_{21} \end{bmatrix} \begin{Bmatrix} \langle E_1\rangle \\ \langle E_2\rangle \end{Bmatrix} = \begin{Bmatrix} \Pi_1^{\text{in}} \\ \Pi_2^{\text{in}} \end{Bmatrix}. \tag{3.15}$$

The effect of the non-conservative joint leads to an SEA-like system with two new factors in the diagonal: the non-conservative coupling loss factors γ_{12} and γ_{21}. If these factors are equal to zero, the conservative case is recovered. However, if the coupling dissipates energy, they are different from zero and factors η_{12} and η_{21} change with respect to the conservative case.

Eq. (3.15) provides similar relations between the connection losses and the energies of the subsystems as Sheng et al. (2004) do. However, the information included in the coefficients is different. Sheng et al. define a new equivalent internal loss factor instead of adding an extra term in the diagonal (defined here as NCLF). The advantage of defining the NCLF is that several non-conservative couplings of the same type can be concatenated easily without having to recompute any parameter. The equivalent internal loss factor defined by Sheng et al. needs to be recomputed when the subsystem is in contact with more than one non-conservative coupling..

Another remarkable difference with Sheng et al. is the nomenclature used for the loss factors. In their formulation, they incorporate the factor γ_{ij} within the equivalent internal loss factor. Therefore, they only have one coupling loss factor, which they call non-conservative coupling loss factor. In this thesis, however, a formulation with two coupling loss factors is developed, see Eq. (3.15). They have been called CCLF and NCLF because, if the dissipative component of the coupling is removed, the NCLF

becomes zero and the CCLF becomes the classical coupling loss factor. Therefore, the name of non-conservative coupling loss factor is used with a different meaning in the two works.

3.3 Estimation of the coupling loss factors

The expressions for η_{ij} and γ_{ij}, defined in Eqs. (3.10) and (3.11) respectively for a point connection, cannot be used for most of the real-life dissipative connections. Therefore, to model a large vibroacoustic problem with many subsystems and non-conservative connections, these parameters can be computed from the numerical simulation of smaller parts of the problem. Once these parameters are known, the global system can be solved with the SEA-like approach.

Parameters η_{ij} and γ_{ij} of a non-conservative coupling between two subsystems can be obtained from numerical simulations of the energy transmission between the two subsystems. These simulations should include the dissipative behaviour of the coupling. For a given excitation, both the input powers Π_i^{in} and the averaged energies of the leaves $\langle E_i \rangle$ can be computed solving the vibroacoustic problem numerically, as described in Appendix A. Assuming that η_{ii} is known for every subsystem, the rest of the SEA parameters can be isolated from the power balances of the system.

If the two subsystems have different properties (which is the most common case), the structure is not symmetric and there are four parameters to compute: η_{12}, η_{21}, γ_{12} and γ_{21}.

To obtain them all, the SEA formulation of two mutually independent problems is required, in a similar way as the approach used by Yan et al. (2000) for conservative connections. These two problems correspond to the system behaviour for two different excitations: one on subsystem 1 and the other on subsystem 2. For each different excitation, the averaged energies of the subsystems are computed numerically. If these energies are replaced in the SEA-like formulation of each problem (3.15), a 4×4 linear system can be solved to obtain the four parameters desired

$$\begin{pmatrix} \langle E_1 \rangle & -\langle E_2 \rangle & \langle E_1 \rangle & 0 \\ \langle \widehat{E}_1 \rangle & -\langle \widehat{E}_2 \rangle & \langle \widehat{E}_1 \rangle & 0 \\ -\langle E_1 \rangle & \langle E_2 \rangle & 0 & \langle E_2 \rangle \\ \langle -\widehat{E}_1 \rangle & \langle \widehat{E}_2 \rangle & 0 & \langle \widehat{E}_2 \rangle \end{pmatrix} \begin{Bmatrix} \eta_{12} \\ \eta_{21} \\ \gamma_{12} \\ \gamma_{21} \end{Bmatrix} = \begin{Bmatrix} \Pi_1^{\text{in}}/\omega - \eta_{11}\langle E_1 \rangle \\ -\eta_{11}\langle \widehat{E}_1 \rangle \\ -\eta_{22}\langle E_2 \rangle \\ \Pi_2^{\text{in}}/\omega - \eta_{22}\langle \widehat{E}_2 \rangle \end{Bmatrix}. \tag{3.16}$$

In system (3.16), $\langle E_i \rangle$ and $\langle \widehat{E}_i \rangle$ are the averaged energies of subsystem i for excitations applied to subsystems 1 and 2 respectively.

Analytical solution of the linear system (3.16) leads to

$$\eta_{12} = \frac{\mathit{\Pi}_2^{\text{in}} \langle E_2 \rangle}{\omega \left(\langle E_1 \rangle \langle \widehat{E}_2 \rangle - \langle E_2 \rangle \langle \widehat{E}_1 \rangle \right)} \tag{3.17}$$

and

$$\gamma_{12} = \frac{\mathit{\Pi}_1^{\text{in}} \langle \widehat{E}_2 \rangle - \mathit{\Pi}_2^{\text{in}} \langle E_2 \rangle}{\omega \left(\langle E_1 \rangle \langle \widehat{E}_2 \rangle - \langle E_2 \rangle \langle \widehat{E}_1 \rangle \right)} - \eta_{11} \tag{3.18}$$

(and similar expressions for η_{21} and γ_{21}). Eq. (3.17) is a robust way of computing the conservative coupling loss factor η_{12}. Eq. (3.18), on the other hand, is unreliable for $\gamma_{12} \ll \eta_{11}$, because it involves the subtraction of two similar numbers in such a case. Indeed, the subtraction of two similar quantities is a dangerous operation (as commented in Section 2.3), prone to amplify any errors in the numerical estimation of the energies and powers. More details on this particular are given in Section 3.4.

Due to the unreliability of Eq. (3.18) for $\gamma_{12} \ll \eta_{11}$, an alternative formulation is proposed. If the power exchanged between the subsystems and the connection is computed on both sides of the connection, it can be expressed in terms of the energies of the subsystems for the two types of excitations as

$$\begin{aligned} \mathit{\Pi}_{12}^{(1)}/\omega = &\quad (\eta_{12} + \gamma_{12}) \langle E_1 \rangle - \eta_{21} \langle E_2 \rangle \\ \mathit{\Pi}_{12}^{(2)}/\omega = &\quad \eta_{12} \langle E_1 \rangle - (\eta_{21} + \gamma_{21}) \langle E_2 \rangle \end{aligned} \tag{3.19}$$

and

$$\begin{aligned} \widehat{\mathit{\Pi}}_{12}^{(2)}/\omega = &\quad (\eta_{21} + \gamma_{21}) \langle \widehat{E}_2 \rangle - \eta_{12} \langle \widehat{E}_2 \rangle \\ \widehat{\mathit{\Pi}}_{12}^{(1)}/\omega = &\quad \eta_{21} \langle \widehat{E}_2 \rangle - (\eta_{12} + \gamma_{12}) \langle \widehat{E}_1 \rangle. \end{aligned} \tag{3.20}$$

Subtracting the two equations of each system and rearranging them, the following system results:

$$\begin{pmatrix} \langle E_1 \rangle & \langle E_2 \rangle \\ \langle \widehat{E}_1 \rangle & \langle \widehat{E}_2 \rangle \end{pmatrix} \begin{Bmatrix} \gamma_{12} \\ \gamma_{21} \end{Bmatrix} = \frac{1}{\omega} \begin{Bmatrix} \mathit{\Pi}_{12}^{(1)} - \mathit{\Pi}_{12}^{(2)} \\ \widehat{\mathit{\Pi}}_{12}^{(1)} - \widehat{\mathit{\Pi}}_{12}^{(2)} \end{Bmatrix}. \tag{3.21}$$

Analytical solution of the linear system (3.21) leads to

$$\gamma_{12} = \frac{\left(\mathit{\Pi}_{12}^{(1)} - \mathit{\Pi}_{12}^{(2)} \right) \langle \widehat{E}_2 \rangle - \left(\widehat{\mathit{\Pi}}_{12}^{(1)} - \widehat{\mathit{\Pi}}_{12}^{(2)} \right) \langle E_2 \rangle}{\omega \left(\langle E_1 \rangle \langle \widehat{E}_2 \rangle - \langle E_2 \rangle \langle \widehat{E}_1 \rangle \right)} \tag{3.22}$$

(and a similar expression for γ_{21}). As will be described in Section 3.4, Eq. (3.22) is only unreliable if the coupling transmission is much higher than the dissipation ($\mathit{\Pi}_{12}^{(2)} \gg \mathit{\Pi}_{12}^{(1)} - \mathit{\Pi}_{12}^{(2)}$). However, in that case the connection may be considered conservative and the classical SEA formulation should be used, assuming $\gamma_{12} = 0$. Therefore, Eq. (3.22) is more robust than Eq. (3.18) because its reliability does not depend on the properties of the subsystems. The main disadvantage of system (3.21) is the extra postprocessing effort required for computing $\mathit{\Pi}_{12}^{(i)}$ and $\widehat{\mathit{\Pi}}_{12}^{(i)}$ from the results of the numerical simulation. However, it is the most advisable way to compute γ_{12} and γ_{21}.

If the two leaves are identical, the problem is symmetric and then $\eta_{12} = \eta_{21}$ and $\gamma_{12} = \gamma_{21}$. For this case, only one simulation is required, and the systems to be solved are simpler.

3.4 Error propagation for the coupling loss factors

A study on the error propagation committed in the computation of the CCLF and the NCLF is shown here. For the sake of simplicity, the problem is assumed symmetric. Therefore, subsystems 1 and 2 are equal and $\gamma_{12} = \gamma_{21}$ and $\eta_{12} = \eta_{21}$.

In that case, only one simulation is required (exciting only one of the subsystems, in this case subsystem 1) and the expressions for the coupling loss factors derived from Eq. (3.16) are:

$$\eta_{12} = \frac{\mathit{\Pi}_1^{\text{in}} \langle E_2 \rangle}{\omega \left(\langle E_1 \rangle^2 - \langle E_2 \rangle^2 \right)} \tag{3.23}$$

and

$$\gamma_{12} = \frac{\mathit{\Pi}_1^{\text{in}}}{\omega \left(\langle E_1 \rangle + \langle E_2 \rangle \right)} - \eta_{11}. \tag{3.24}$$

The error committed when computing the coupling loss factors from numerical values of the powers and energies is analysed. The effect of the error propagation from those quantities estimated numerically is studied. Other magnitudes such as the frequency and the internal loss factors are assumed error-free.

The error committed computing η_{12} with Eq. (3.23) is

$$r_{\eta_{12}} = r_{\mathit{\Pi}_1^{\text{in}}} + r_2 - 2r_1 \left(\frac{\langle E_1 \rangle^2}{\langle E_1 \rangle^2 - \langle E_2 \rangle^2} \right) + 2r_2 \left(\frac{\langle E_2 \rangle^2}{\langle E_1 \rangle^2 - \langle E_2 \rangle^2} \right) \tag{3.25}$$

which, assuming that $\langle E_1 \rangle \gg \langle E_2 \rangle$, leads to

$$r_{\eta_{12}} =\simeq r_{\Pi_1^{\text{in}}} + r_2 - 2r_1, \tag{3.26}$$

where r_i is the error committed in the calculation of $\langle E_i \rangle$. The value of the error in the CLF is of the same order of the errors of the energies and power.

The error committed computing γ_{12} with Eq. (3.24) is

$$r_{\gamma_{12}} = \frac{\Pi_1^{\text{in}}}{\Pi_1^{\text{in}} - \eta_{11}\omega\left(\langle E_1 \rangle + \langle E_2 \rangle\right)} \left(r_{\Pi_1^{\text{in}}} - r_1 \frac{\langle E_1 \rangle}{\langle E_1 \rangle + \langle E_2 \rangle} - r_2 \frac{\langle E_2 \rangle}{\langle E_1 \rangle + \langle E_2 \rangle} \right). \tag{3.27}$$

Assuming that $\langle E_1 \rangle \gg \langle E_2 \rangle$, the error is

$$r_{\gamma_{12}} \simeq \frac{\Pi_1^{\text{in}}}{\Pi_1^{\text{in}} - \eta_{11}\omega\left(\langle E_1 \rangle + \langle E_2 \rangle\right)} \left(r_{\Pi_1^{\text{in}}} - r_1 \right). \tag{3.28}$$

In case η_{11} is greater than γ_{12} by orders of magnitude, the factor multiplying the errors $\Pi_1^{\text{in}} / \left[\Pi_1^{\text{in}} - \eta_{11}\omega\left(\langle E_1 \rangle + \langle E_2 \rangle\right)\right] \gg 1$, and therefore Eq. (3.24) amplifies the error committed in the computation of γ_{12}. This expression is not reliable for computing the non-conservative coupling loss factor in this case.

Instead, if the symmetric version of Eq. (3.21) is used

$$\gamma_{12} = \frac{\Pi_{12}^{(1)} - \Pi_{12}^{(2)}}{\omega\left(\langle E_1 \rangle - \langle E_2 \rangle\right)}, \tag{3.29}$$

the error committed is

$$r_{\gamma_{12}} = \frac{\Pi_{12}^{(1)}}{\Pi_{12}^{(1)} - \Pi_{12}^{(2)}} r_{\Pi_{12}^{(1)}} - \frac{\Pi_{12}^{(2)}}{\Pi_{12}^{(1)} - \Pi_{12}^{(2)}} r_{\Pi_{12}^{(2)}} - \frac{\langle E_1 \rangle}{\langle E_1 \rangle - \langle E_2 \rangle} r_1 - \frac{\langle E_2 \rangle}{\langle E_1 \rangle - \langle E_2 \rangle} r_2. \tag{3.30}$$

Assuming that $\langle E_1 \rangle \gg \langle E_2 \rangle$, the error becomes

$$r_{\gamma_{12}} \simeq \frac{\Pi_{12}^{(1)}}{\Pi_{12}^{(1)} - \Pi_{12}^{(2)}} r_{\Pi_{12}^{(1)}} - \frac{\Pi_{12}^{(2)}}{\Pi_{12}^{(1)} - \Pi_{12}^{(2)}} r_{\Pi_{12}^{(2)}} - r_1. \tag{3.31}$$

The error committed in the computation of γ_{12} with Eq. (3.29) is only amplified if $\Pi_{12}^{(2)} \gg \Pi_{12}^{(1)} - \Pi_{12}^{(2)}$. However, in that case, the dissipative behaviour of the connection can be neglected and the NCLF can be set as $\gamma_{12} = 0$.

3.5 Validation example

The technique proposed in Section 3.3 for the coupling loss factor estimation is applied here for a simple mechanical problem. In this particular case, the coupling loss factors

can be computed analytically with a simplified approach and compared with the numerical estimations.

The example consists of two leaves of plasterboard connected through a mechanical device. This device is represented as a spring with a complex stiffness, in order to model a connection that both transmits and dissipates energy. In this case, the point mobility associated to the connection is

$$Y_c = \frac{\mathrm{i}\omega}{K_c}, \tag{3.32}$$

where $K_c \in \mathbb{C}$ is the stiffness of the connecting device. Therefore, the coupling loss factors can be computed with Eqs. (3.10) and (3.11).

Eqs. (3.10) and (3.11) are based on all the hypotheses described in Section 3.2. The energy flux is supposed to go only in one direction and the force is assumed to be the same from the application point to the receiving leave. These hypotheses are reasonable for this example.

The numerical problem is solved as described in Appendix A, considering a complex value of the spring stiffness. The excitation is a point force applied on one of the leaves, averaged as described in the Appendix. The properties of the leaves have already been described in Table 2.1 and Table 2.2, and the stiffness of the connection is $K_c = 10^4\,(1 + 0.1\,\mathrm{i})$ N m^{-1}.

The comparison of the numerical estimations and the analytical expressions for the CCLF and the NCLF is shown on Figs. 3.5 and 3.6 respectively, averaged in third octave bands. Results for frequencies lower than 250 Hz are not shown because SEA hypotheses are not fulfilled there.

Fig. 3.5 shows a very good agreement between the two techniques for the CCLF. On Fig. 3.6 the NCLF is estimated both with Eq. (3.22) and Eq. (3.18). As the error propagation analysis suggested, Eq. (3.18) provides wrong results for the NCLF estimation because $\gamma_{12} \ll \eta_{11}$. In fact, some parts of the curve are not plotted because the computed NCLF is negative at those frequencies. The CCLF obtained with Eq. (3.17) is almost identical to the one computed with the analytical expression. This agreement is regarded as a validation of both the simplifying hypotheses of the analytical approach and the proposed numerical technique for estimating coupling loss factors.

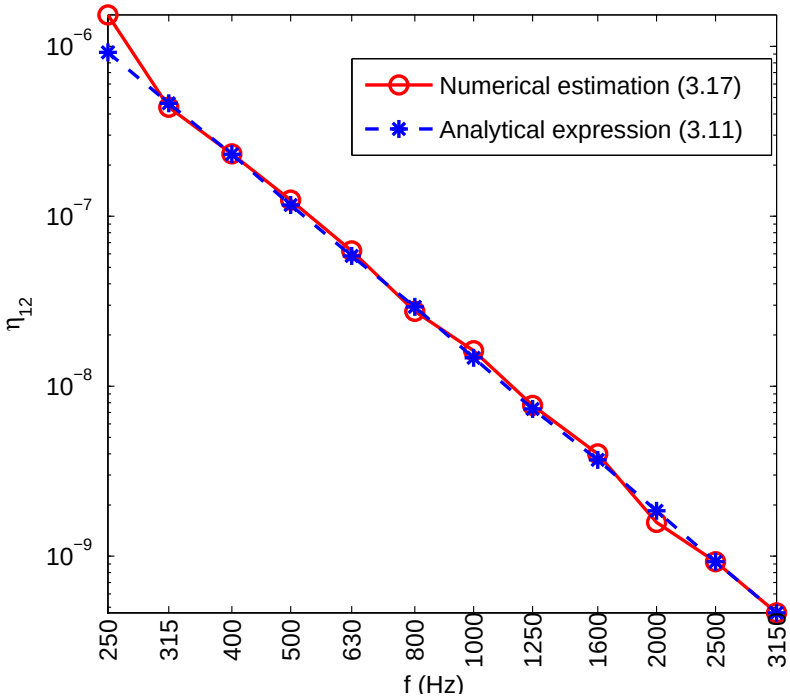

Fig. 3.5: Validation of the estimation of the CCLF η_{12} for a mechanical connection.

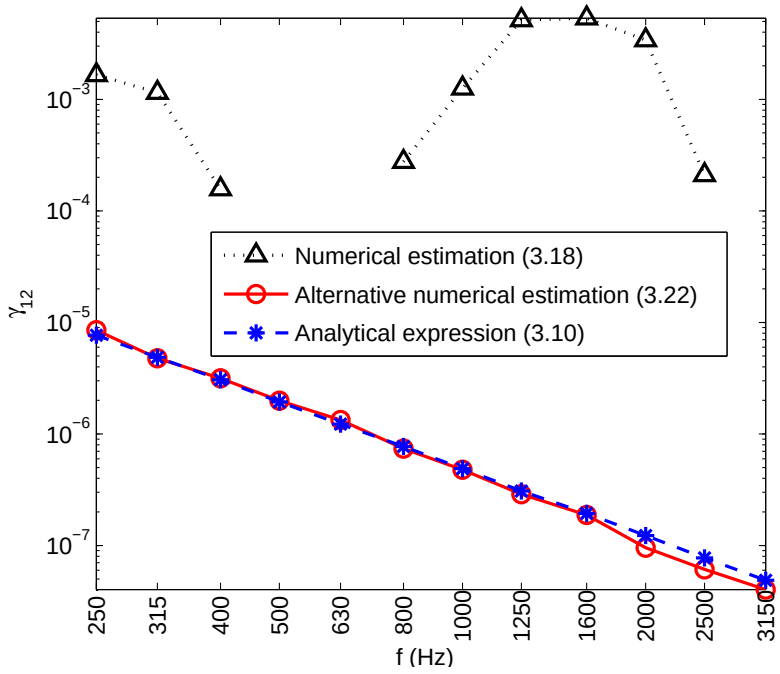

Fig. 3.6: Validation of the estimation of the NCLF γ_{12} for a mechanical connection.

More complex examples of the estimation of CCLF and NCLF are presented in Chapter 7 (Part II). In particular, absorbing layers in double walls are modelled as non-conservative couplings. The estimated parameters are then applied for modelling larger problems combining conservative and non-conservative couplings with SEA.

3.6 Concluding remarks

- This chapter shows an SEA-like formulation accounting for non-conservative connections. These connections are characterised by means of two types of coupling loss factors: the conservative η_{ij} and the non-conservative γ_{ij} coupling loss factors, related to the transmitted and dissipated energy respectively.

- Factors η_{ij} and γ_{ij} can be computed with numerical simulations of a system consisting of 2 subsystems with a non-conservative connection. Attention must be paid to the error propagation in these computations. Once these factors are obtained, they can be used to solve larger problems with SEA, as in Chapter 7.

3.7 Future directions

The next steps in the modelling of non-conservative couplings with SEA should be the following:

- A comparison between the effect of treating absorbing materials as SEA subsystems or as non-conservative couplings should be done. Experimental data could be used to validate both approaches.

- The proposed SEA-like approach should be validated for different types of absorbing material.

- Simplified expressions for the CCLFs and NCLFs associated to different dissipative elements, such as absorbing layers, should be developed. These expressions would provide the coupling loss factors in terms of the properties of the connection and the subsystems surrounding it.

Chapter 4

Subsystem identification

In this chapter a new strategy for decomposing a vibroacoustic domain into SEA subsystems is proposed. It consists in performing a cluster analysis based on the problem eigenmodes and incorporates the mutual inertia ratio between subsystems as a decision variable. This analysis is combined with a classification of the eigenmodes to allow the identification of SEA subsystems, even if they share the same physical region.

4.1 Preliminaries

The statistical energy analysis framework is based on the power flow between subsystems. Therefore, the proper subdivision of the domain into subsystems is crucial for the good performance of SEA. These subsystems are defined by Lyon (1975) as "groups of 'similar' energy storage modes. These modes are usually modes of the same type (flexural, torsional, etc.) that exist in some section of the system". For classifying a certain set of modes as a subsystem, they must fulfil two main criteria:

1. Similarity: all the modes must have a similar energetic response in front of any possible excitation.

2. Significance: they must play an important role in the transmission, dissipation or storage of energy of the problem.

In many typical applications, subsystem identification is straightforward. Common building elements like beams or thin plates clearly fulfil the requirements previously discussed. However, SEA may also be a powerful tool for dealing with vibroacoustic problems with complex shapes and non-conventional configurations. Examples of this kind of problems might be found, for instance, in the automotive or aerospace industries, or even in some new architectonic designs. In these cases the domain subdivision is not so clear and often the decomposition is done following material or geometrical criteria, see Chen et al. (2012) or Forssén et al. (2012).

Different authors have worked on domain substructuring for energy models. For instance, Kassem et al. (2011) propose an strategy for their local vibroacoustic energy model based on searching the validity frequencies for a certain substructuring. In the particular case of the identification of SEA subsystems, relevant works are those by Fahy (2004), Gagliardini et al. (2005) and Totaro and Guyader (2006).

Fahy (2004) studies qualitatively the effect of subdividing the cavity inside a car into different subsystems. He concludes that this can be done, in particular at the region below the seats, but recommends the use of experimental information for checking the robustness of the approach.

Gagliardini et al. (2005) propose a strategy for identifying SEA subsystems. It is based on the energetic transfer functions obtained between points of the domain for different excitations. This analysis involves solving the vibratory problem for every excitation in a particular frequency band.

The strategy proposed by Totaro and Guyader (2006) also requires the numerical simulation of the vibratory problem for a representative set of excitations and provides an spatial division of the domain into subsystems. They discretise the domain with finite elements and perform a cluster analysis of these elements. The analysis is based on a set of energy transfer functions obtained for different excitations, and a principal component analysis of these functions is performed before the cluster analysis, to reduce the data size.

The main limitation of these methods is that they perform a purely spatial subdivision into subsystems. This means that a certain point of the domain cannot belong to two different subsystems at the same time. However, a certain region of the domain may present two types of modes with very different energetic responses to excitations, as commented by Lyon (1975) or Maidanik (1977). For example, a structure consisting of thin shells may present both flexural and in-plane modes for

the frequency range of interest.

The new strategy proposed here is based on a modal analysis of the problem. The domain is decomposed in small cells, and these cells are classified with a cluster analysis as Totaro and Guyader (2006) do, but in this case the analysis is based on the energies for a set of eigenmodes of the problem. This approach is intimately related to the definition of subsystem proposed by Lyon, and allows as a novelty the possibility of preprocessing the modes for defining more than one subsystem at a certain spatial region. Even if this research is on an early stage, the obtained results are very promising. Two added advantages of this strategy are that no excitations are required for the analysis (there are no issues of excitation selection), and its low computational cost (it only requires the computation of a few eigenmodes). This last advantage is particularly important because the identification of subsystems is a preprocessing step in SEA calculation, and one of the main features of SEA is its low computational cost.

4.2 Methodology for one type of significant modes

In this section, the case where only one type of modes fulfils the significance criterion is analysed. Hence, the goal is to obtain a geometrical decomposition of the domain into subsystems. If there are different types of significant modes in the domain, further considerations need to be done. That case is discussed in Section 4.3.

4.2.1 Cluster analysis based on the system eigenmodes

The idea of cluster analysis was first introduced by Tryon (1939). It consists in grouping a set of elements in such a way that elements in the same group (called cluster) are more similar (in some sense or another) to each other than to those in other groups, Everitt et al. (2009). The similarity between elements is measured as the distance between them in the sample space. The dimensions of this space coincide with the number of samples used for the analysis. The main ingredients for the hierarchical cluster analysis performed here are the following:

- **The cluster elements:**

  In the work by Totaro and Guyader (2006), the cluster elements are the finite elements. However, a fine mesh that can capture properly the wave behaviour of the vibration and pressure fields, presents huge differences between the averaged energies of the elements. This may lead to a wrong subdivision, where elements coinciding with nodes or anti-nodes of the waves, or strongly influenced by the boundary conditions, might be identified as different subsystems. The averaged behaviour of the waves is better captured if cells with a size equal or larger than half a wavelength are considered. Therefore, the maximum wavelength (for the lowest frequency considered) of the problem is computed, and the domain is divided into **cells of side equal or greater than half the maximum wavelength**. These are the cluster elements to classify.

- **The sample space:**

  This space is formed by the normalised energetic contributions to different eigenmodes of the problem. Therefore, the dimension of the space is equal to the number of eigenmodes considered. These modes are computed with Cast3M (2003) from a finite element model of the physical problem. The eigenmodes of the problem are good samples for the cluster analysis, because each of them provides an independent and significant case to analyse.

  This contrasts with the approach of Totaro and Guyader (2006). They obtain their samples by computing the energy transfer functions for different positions of the excitation and at every Hz within a third octave band of interest. Two variables are combined to generate a representative set of samples. Then, they project the results of the simulations in their principal components, in order to extract the most representative information and reduce the number of dimensions of their space.

  The approach based on a set of eigenmodes of the problem reduces the computational cost in the sense that the most representative frequencies within a certain range are obtained directly, and independently of the possible excitations to the system.

  To obtain the normalised energetic contribution to each mode of a certain cluster element i, first its averaged energy density (the total energy divided by the area of the cell) is calculated, and a map of energy densities e_{ij} is created for every mode j. This total energy is obtained as the result of adding the kinetic and the strain

energy. The analysis could have also been done in terms of the kinetic or the strain energy separately, see Lyon (1975), but the total energy has been chosen following the criterion suggested by Totaro and Guyader (2006). A further discussion on this topic is provided in Section 4.3.

The analysis, however, is not performed directly on the energy densities. The most important variable is not the energy itself but the normalised difference between the energy at each cell and the averaged energy of the system. Therefore, a new map is produced, computing for each mode j and each cell i the value of $\tilde{e}_{ij}$ as

$$\tilde{e}_{ij} = \frac{e_{ij} - \bar{E}_j}{S_j\sqrt{N}}, \tag{4.1}$$

where

$$\bar{E}_j = \frac{1}{N}\sum_{i=1}^{N} e_{ij} \tag{4.2}$$

is the mean energy density in the domain for mode j,

$$S_j^2 = \frac{1}{N}\sum_{i=1}^{N} \left(e_{ij} - \bar{E}_j\right)^2 \tag{4.3}$$

is the variance of e_{ij} for mode j and N is the number of cells. A vector belonging to the sample space is associated to a certain cluster element, and has as j-th component the normalised energy density of that element for mode j.

The magnitude used for defining the sample space is also different in the approach of Totaro and Guyader (2006). Since they obtain the values of the energies associated to particular excitations, they choose to perform the cluster analysis based on the energy transfer functions, in order to consider the effect of the excitation on the energies. In the strategy presented here, the lack of excitation has led to the decision of defining the sample space in terms of the energies.

- **The distance function:**

  Once the energy maps are known, the energy vector $\mathbf{x}_i$ associated to a cell (cluster element) i is defined as the vector whose j-th component is the normalised energy density of that cell for mode j, $\tilde{e}_{ij}$.

Then, **the distance between two cluster elements m and n is computed as the Euclidean distance between their energy vectors**

$$d(\mathbf{x}_m, \mathbf{x}_n) = \sqrt{\sum_{j=1}^{n_{\text{modes}}} (\tilde{e}_{mj} - \tilde{e}_{nj})^2}. \tag{4.4}$$

- **The number of clusters:**

  The cluster analysis performed here requires the previous definition of the number of clusters desired. Therefore, **several analyses are performed, fixing a different amount of subsystems for each case.** Hence, the cells are arranged first in two clusters, then in three, four and so on. In typical SEA applications, no more than ten or twenty clusters should be considered. The remaining step is to decide which of these subdivisions is more representative of the real problem.

4.2.2 The mutual inertia ratio as the decision variable

As described in Table 1.1, one of the SEA hypothesis is the weak coupling between subsystems. Once the cluster distribution is known for every fixed number of subsystems, the choice of the best one is done in terms of the coupling strength between subsystems. In this sense, the mutual inertia ratio (mir) is used as an indicator of this strength. It is defined by Totaro and Guyader (2006) as the ratio of intra-cluster and inter-clusters inertia of two groups of elements of a given partition. For a couple of clusters $\{k, l\}$ it is computed as

$$\text{mir}\,(k,l) = \frac{\sum_{p=1}^{N_k} d(\mathbf{x}_p, \mathbf{g}_k) + \sum_{q=1}^{N_l} d(\mathbf{x}_q, \mathbf{g}_l)}{N_k d(\mathbf{g}_k, \mathbf{g}_{kl}) + N_l d(\mathbf{g}_l, \mathbf{g}_{kl})} \tag{4.5}$$

where N_k is the number of elements in cluster k, $d(\mathbf{x}_i, \mathbf{g}_k)$ is the distance between the energy vector $\mathbf{x}_i$ and the energy centroid $\mathbf{g}_k$ of cluster k, $\mathbf{g}_k$ is computed by averaging the energy vectors of all the elements in cluster k and $\mathbf{g}_{kl}$ is the average of the energy vectors of all the elements of clusters k and l.

The distance between the cluster elements is computed as in Section 4.2.1. That means that, for a given couple of clusters, the value of the mir between them can be increased in two ways. On the one hand, if the energetic responses of the elements within a cluster become more dissimilar to each other for every mode, their intra-cluster inertia becomes higher, and therefore the numerator of Eq. (4.5) increases,

leading to an increment of the mir. On the other hand, if the global energetic behaviour of the clusters becomes more similar to each other for the different modes, the denominator of Eq. (4.5) (inter-clusters inertia) decreases, leading as well to an increment of the mir.

As an example, in Fig. 4.1 a simplified analysis with two modes (2D plot) and two clusters, with nine elements each, is performed. The effect on the mir of making the behaviour of the clusters more and more similar (reducing the inter-clusters inertia keeping the intra-cluster inertia constant) is shown from left to right.

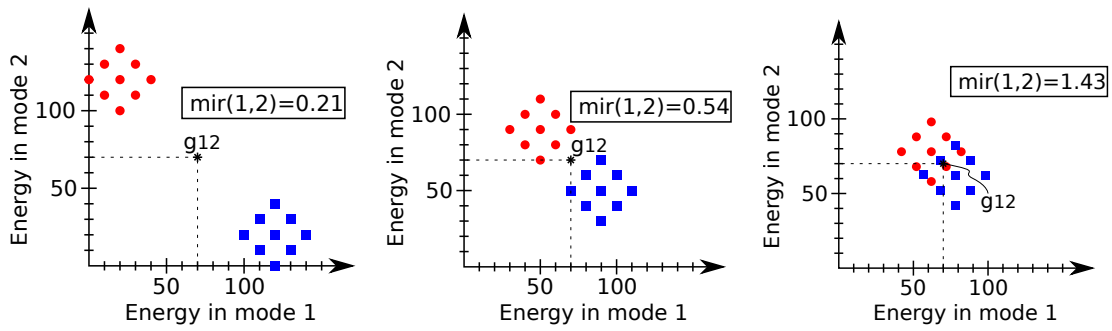

(a) (b) (c)

Fig. 4.1: Evolution of the mir with the distance between clusters

Totaro and Guyader (2006) use the MIR (maximum value of the mir) as the decision variable for picking the optimal division into subsystems and an analogous process is followed here. For a given decomposition, the mutual inertia ratio is computed between each pair of subsystems $\{k, l\}$. Then, the maximum of all the mir values for that subdivision

$$\text{MIR} = \max(\text{mir}(k, l)) \tag{4.6}$$

is computed. This process is repeated for all the possible decompositions of the system (with different amounts of clusters), obtaining a value of the MIR for each one. The optimal decomposition is the one with the minimum value of MIR, that is, the one in which subsystems are more dissimilar to each other. In the example of Fig. 4.2, a simplified analysis with two modes is shown. Two possible decompositions are analysed: division into two or three clusters. In this case, the optimal subdivision is the one with only two clusters, because of its lower MIR.

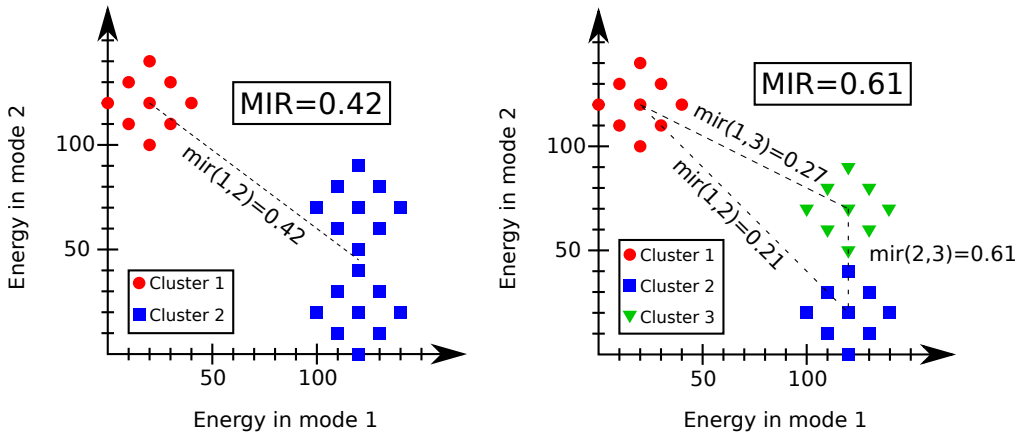

(a) (b)

Fig. 4.2: Computation of the MIR for two different decompositions of the same system.

4.2.3 Robustness of the decompositions

An important element in the subsystem identification is the robustness of the method when changing the cluster elements. If the division into subsystems is clear for a certain problem, a cluster analysis performed with slightly different cells should lead to the same subdivision. If it does not, it seems logical to conclude that this subdivision should not be chosen.

The choice of the number of subsystems forming a certain system can be improved following this idea: if the cluster analysis is repeated with larger cells and the optimal subdivision obtained is the same, then its optimality is confirmed. Otherwise, the system may have an intermediate behaviour between two options. To deal with this case, more cluster analyses should be performed changing the cell size, and the most probable decomposition should be identified. For this subdivision, the coupling loss factors between each pair of subsystems should be estimated and compared with their internal loss factors. If the coupling loss factor between two possible subsystems k and l is larger than their internal loss factors, the SEA hypothesis of weak coupling (Table 1.1) is not fulfilled and, therefore, they should be grouped as a single subsystem.

4.2.4 Step-by-step summary of the methodology

The step-by-step strategy proposed here to identify the subsystems within a certain system is the following:

1. Obtain a representative set of the eigenmodes of the problem.
2. Compute the total energy density in the cells for each mode. These cells should have a side equal or greater than half the largest wavelength.
3. Compute the normalised energies $\tilde{e}_{ij}$ at the cells.
4. Do the cluster analysis for different amounts of clusters.
5. Compute the MIR associated to each analysis and choose the subdivision with a lower value.
6. Repeat the analysis with larger cells and check if the optimal subdivision is still the same.
7. If the optimal subdivision coincides, the problem is finished. Otherwise, compute the coupling loss factors and base the decision on the fulfilment of the weak coupling hypothesis.

4.2.5 Other aspects of the analysis

The systematic methodology summarised in Section 4.2.4 provides reasonable results for the examples in Section 4.2.6. However, when applying it to more complex configurations, other aspects may have to be considered. A brief summary of these issues, and the recommended approach for dealing with them, is presented here:

- The proposed methodology assumes that a unique subdivision of the system holds for the whole frequency range of analysis. If a particular system is suspected to have a different behaviour (and therefore should have a different distribution of subsystems) depending on the frequency range, this analysis might be performed for different groups of modes, corresponding to different frequency ranges, leading to a new division into subsystems for each range.
- The modal analysis of the problem has been performed without considering any loss factor in the structures. In general, statistical energy analysis cannot be

performed if the damping levels are too high because it would violate the diffuse field assumption, but real-life problems usually have some damping. If the subsystem identification is robust and clear, the addition of some damping should not affect the final result. If, on the contrary, the subsystem identification is not clear (due to the lack of robustness of the analysis or to high values of the MIR), the choice of the subdivision should be done as described in Section 4.2.3.

- In case the strategy leads to an optimal subdivision involving disjoint subsystems, which are non-physical, they must be divided providing a new subdivision with physical meaning. This is a very exceptional case, only likely in problems with periodic geometries or consisting of disjoint components with identical features.

- The proposed method is based on a comparative meaning of the MIR parameter. The absolute value of this index is not as important as its relative value for different subdivisions. Therefore, this approach is not appropriate for detecting the case where the whole system acts as a single subsystem. For this very specific case, the MIR cannot be computed and thus cannot be compared with other decompositions.

  Totaro and Guyader (2006) provide a relation between the value of $\mathrm{mir}(k,l)$ and the coupling of the subsystems for the case of an L-shaped plate. They say that values lower than 1.3 correspond to different (weakly coupled) subsystems, and values higher than 2.0 correspond to coupled regions, which should be treated together as a single subsystem. Values in-between are inconclusive. The definition of the mir is slightly modified in this work, and therefore this rule cannot be assumed directly. However an example consisting of a rectangular homogeneous plate has been analysed. The eigenmodes of the plate have been obtained and the mir associated to dividing the plate into two identical halves has been computed, following the expressions of Section 4.2.2. The obtained value of the mir is 2.4. This value is somehow coherent with Totaro's indications and gives a reference value for understanding the meaning of the MIR absolute value. However, both Totaro's reference values and this one have been computed for very specific cases and cannot be extrapolated directly to other configurations.

The best option for detecting a system consisting of a single subsystem is following the procedure recommended in Section 4.2.3.

4.2.6 Examples

The methodology summarised in Section 4.2.4 is validated here with the help of some examples. All of them consist of thin plates connected in different ways. Therefore, the only significant modes correspond to the flexural waves. These examples have been chosen for testing the method, because the subsystem distribution is easier to interpret than in more complex configurations. However, any device consisting of thin elements such as casings or shells with complex shapes could be approached in the same way.

In the examples considered here, around thirty eigenmodes associated to frequencies located between 1100 and 1500 Hz are considered. Preliminary numerical tests indicate that this amount provides a good compromise between computational cost and representativity of the set of modes. The material properties are the same for all the examples, and are summarised in Table 4.1.

Variable	**Symbol**	**Value**
Young's modulus	E	$3 \times 10^{10}\,\mathrm{N\ m^{-2}}$
Density	ρ	$2400\,\mathrm{kg\ m^{-3}}$
Poisson's ratio	ν	0.2
Thickness	h	50 mm

Table 4.1: Properties of the adjacent plates.

4.2.6.1 Two adjacent plates

The first set of examples consists of two adjacent plates of different thickness made of the same material, see Fig. 4.3. The displacement of the plates is blocked at the boundaries Γ_D. The thickness of the plate on the left h is always the same, and three different values of the thickness of the plate on the right δh are considered. The influence of δ on the optimal subdivision is studied.

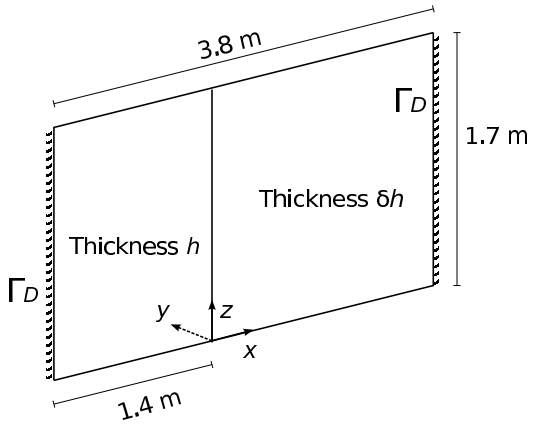

Fig. 4.3: Sketch of the two adjacent plates.

Thickness ratio $\delta = 0.1$

A thickness ratio $\delta = 0.1$ is considered first. Three different clusters (with two, three and four subsystems respectively) are proposed both for cells of side λ_{plate} and $\lambda_{\text{plate}}/2$, where λ_{plate} is the wavelength of the first mode used in the analysis. The values of the MIR for each case are shown in Table 4.2. The optimal subdivision consists of the same two subsystems for both cell sizes, as shown in Fig. 4.4.

	MIR		
	2 subsystems	**3 subsystems**	**4 subsystems**
Cell size: $\lambda_{\text{plate}}/2$	**0.15**	0.59	0.57
Cell size: λ_{plate}	**0.26**	1.01	0.75

Table 4.2: Value of the MIR for different subdivisions. Two adjacent plates of thickness ratio $\delta = 0.1$

The subdivision proposed is robust and, therefore, the conclusion reached by the method is that the system should be decomposed into two subsystems: one for each plate.

If other subdivisions are computed for the example of $\delta = 0.1$, fixing larger amounts of clusters, the value of the MIR either stays constant or keeps increasing, see Fig. 4.5. Therefore, computing only divisions into two, three and four clusters is enough.

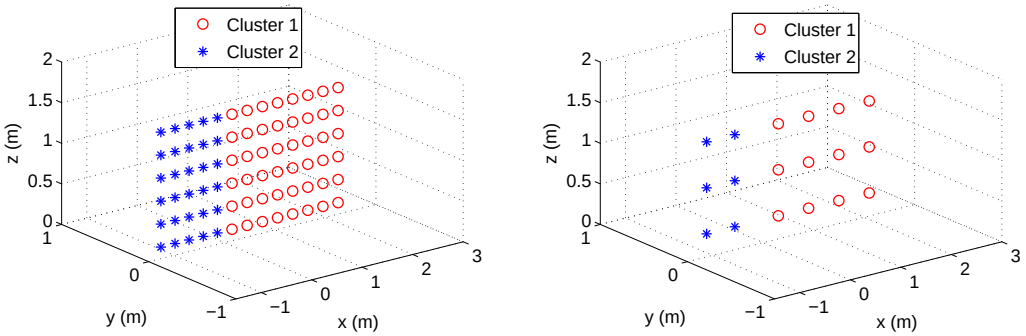

(a) Cell size: $\lambda_{\text{plate}}/2$ (b) Cell size: λ_{plate}

Fig. 4.4: Optimal subsystem distribution for two adjacent plates of thickness ratio $\delta = 0.1$

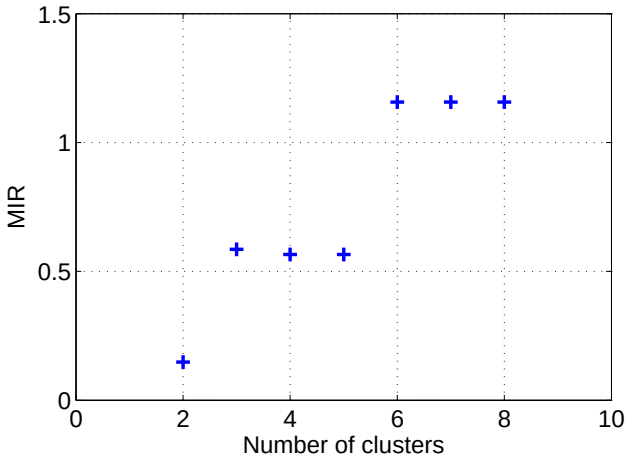

Fig. 4.5: Evolution of the MIR with the number of clusters. Example of two adjacent plates of thickness ratio $\delta = 0.1$

Thickness ratio $\delta = 0.5$

In the second example, the thickness of one plate is half the thickness of the other one. In this case, the optimal subdivision consists always of 2 subsystems (see Table 4.3), but the proposed subdivision is not the same for the two cell sizes, see Fig. 4.6. Therefore, this subdivision should not be considered as optimal, and the result of the analysis is inconclusive.

In this case, further analyses (with different cell sizes) should be performed and the coupling loss factor between the two most probable subsystems should be compared

	MIR		
	2 subsystems	**3 subsystems**	**4 subsystems**
Cell size: $\lambda_{\text{plate}}/2$	**0.23**	0.39	0.39
Cell size: λ_{plate}	**0.37**	0.78	0.82

Table 4.3: Value of the MIR for different subdivisions. Two adjacent plates of thickness ratio $\delta = 0.5$

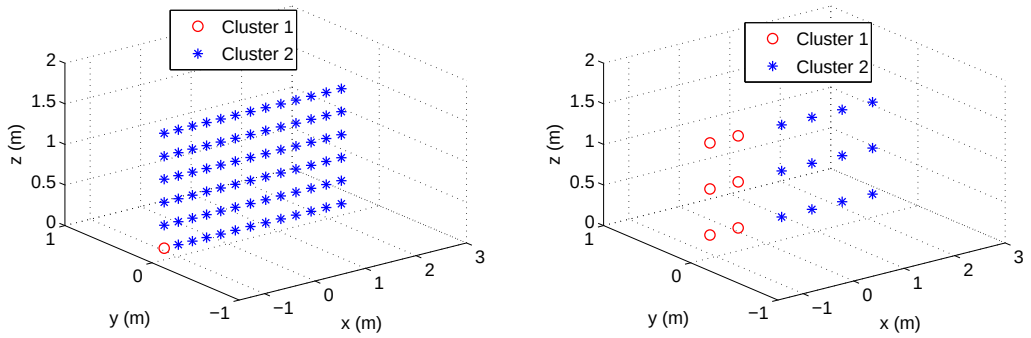

(a) Cell size: $\lambda_{\text{plate}}/2$ (b) Cell size: λ_{plate}

Fig. 4.6: Optimal subsystem distribution for two adjacent plates of thickness ratio $\delta = 0.5$

with their internal loss factors. This measure of the strength of the coupling would help to decide if the system must be treated as a single subsystem or as two, as described in Section 4.2.3.

Equal thickness $\delta = 1$

Finally, the case of two plates with the same thickness is analysed. The values of the MIR for each case are shown on Table 4.4 and the optimal subdivision (with the lowest value of MIR) is depicted for each cell size in Fig. 4.7.

	MIR		
	2 subsystems	**3 subsystems**	**4 subsystems**
Cell size: $\lambda_{\text{plate}}/2$	**0.45**	0.49	0.68
Cell size: λ_{plate}	0.77	0.73	**0.49**

Table 4.4: Value of the MIR for different subdivisions. Two adjacent plates of equal thickness, $\delta = 1$

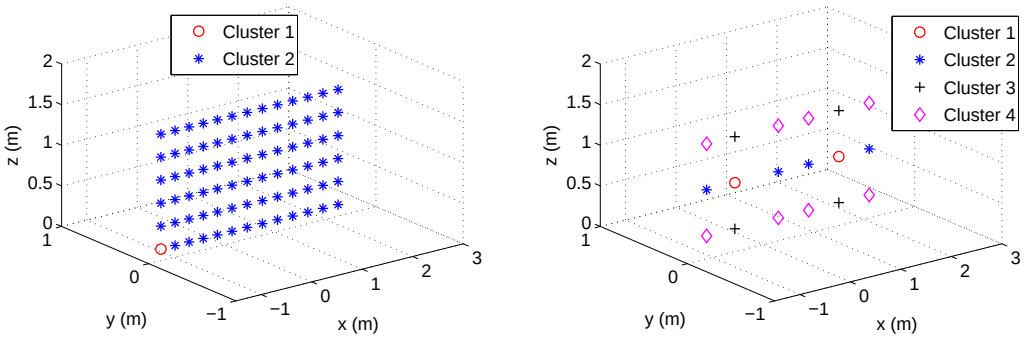

(a) Cell size: $\lambda_{\text{plate}}/2$

(b) Cell size: λ_{plate}

Fig. 4.7: Optimal subsystem distribution for two adjacent plates of equal thickness, $\delta = 1$

The main conclusion is that the subdivision proposed is not robust at all. Changing the cell size leads to the identification of different subsystems. As commented in Section 4.2.5, this most probably happens because this system consists of a single subsystem, as the physical properties of the problem suggest.

Conclusions

The main conclusion extracted here is that two adjacent plates of the same material can behave as a single subsystem or as two subsystems depending on their relative thickness. If they are different enough (for instance $\delta = 0.1$), the two plates behave differently and should be considered as separated subsystems. If the thicknesses are similar, the associated coupling loss factors should be compared with the internal loss factors in order to determine the strength of the coupling. In the limit case of equal thicknesses, the two plates form a single subsystem.

4.2.6.2 L-shaped structure

The second set of examples is based on an L-shaped structure with dimensions defined in Fig. 4.8. The displacement on the plates is blocked at the boundaries Γ_D and the material properties are the same of Table 4.1. For this case, again three possible values of δ are analysed, in order to study the influence of this ratio in the subsystem identification.

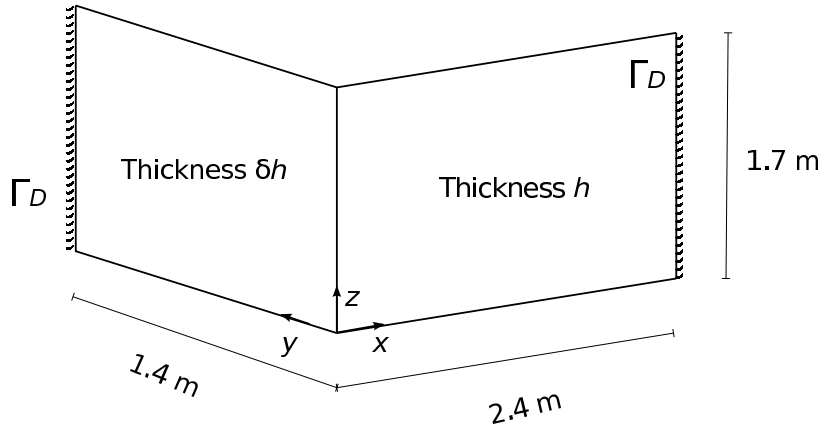

Fig. 4.8: Sketch of the L-shaped structure.

Thickness ratio $\delta = 0.1$

If $\delta = 0.1$, both cell sizes lead to an optimal subdivision into two subsystems, Table 4.5. Moreover, these subdivisions are equivalent, as shown in Fig. 4.9. Therefore, a subdivision into two subsystems, coinciding with the two plates of the L-shaped structure, is recommended by the proposed strategy.

	MIR		
	2 subsystems	**3 subsystems**	**4 subsystems**
Cell size: $\lambda_{\text{plate}}/2$	**0.13**	0.67	0.62
Cell size: λ_{plate}	**0.18**	2.44	2.44

Table 4.5: Value of the MIR for different subdivisions. L-shaped structure with plates of thickness ratio $\delta = 0.1$

Thickness ratio $\delta = 0.5$

For the case of $\delta = 0.5$, the conclusions reached are similar as for the case of $\delta = 0.1$. A division into two subsystems coincident with the two plates is proposed by the method, as shown in Table 4.6 and Fig. 4.10. In this case, the values of the MIR obtained are higher than those for $\delta = 0.1$, which means that the coupling is stronger in this case. These results are coherent with the idea that a larger difference between the subsystems leads to a weaker coupling between them.

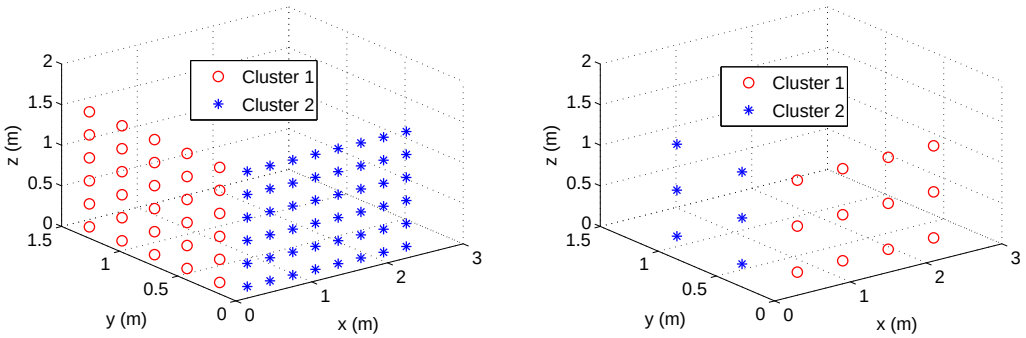

(a) Cell size: $\lambda_{\text{plate}}/2$ (b) Cell size: λ_{plate}

Fig. 4.9: Optimal subsystem distribution for an L-shaped structure with plates of thickness ratio $\delta = 0.1$

	MIR		
	2 subsystems	**3 subsystems**	**4 subsystems**
Cell size: $\lambda_{\text{plate}}/2$	**0.29**	0.59	0.91
Cell size: λ_{plate}	**0.41**	0.96	1.11

Table 4.6: Value of the MIR for different subdivisions. L-shaped structure with plates of thickness ratio $\delta = 0.5$

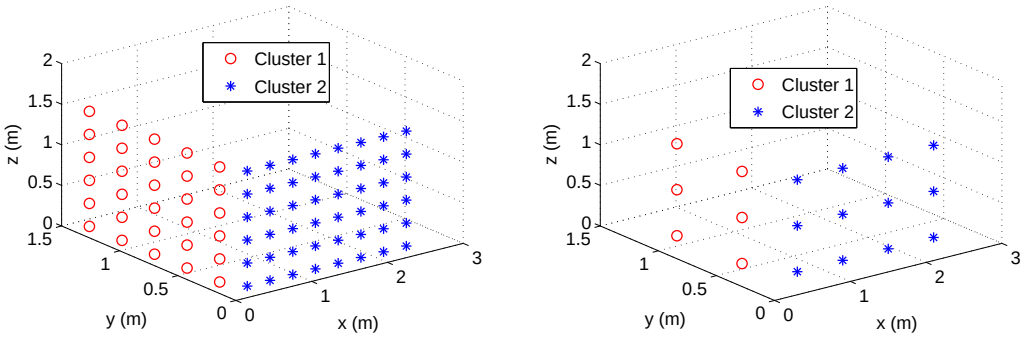

(a) Cell size: $\lambda_{\text{plate}}/2$ (b) Cell size: λ_{plate}

Fig. 4.10: Optimal subsystem distribution for an L-shaped structure with plates of thickness ratio $\delta = 0.5$

Equal thickness $\delta = 1$

For the case of two plates with the same thickness, different divisions are proposed for different cell sizes, see Table 4.7 and Fig. 4.11. The strategy is not robust for this

case. Therefore, the associated coupling loss factors should be compared with the internal loss factors in order to decide if the system consists of a single subsystem or has to be divided into more subsystems.

	MIR		
	2 subsystems	**3 subsystems**	**4 subsystems**
Cell size: $\lambda_{\text{plate}}/2$	**0.64**	0.86	0.86
Cell size: λ_{plate}	0.93	**0.77**	1.59

Table 4.7: Value of the MIR for different subdivisions. L-shaped structure with plates of equal thickness, $\delta = 1$

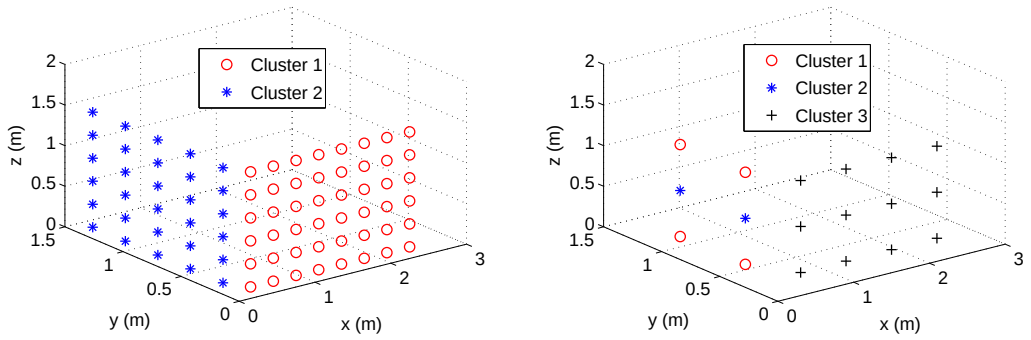

(a) Cell size: $\lambda_{\text{plate}}/2$ (b) Cell size: λ_{plate}

Fig. 4.11: Optimal subsystem distribution for an L-shaped structure with plates of equal thickness, $\delta = 1$

Conclusions

Perpendicular plates have a more uncoupled behaviour than adjacent plates. The particular case of equal thickness for both plates is still inconclusive in terms of the subsystem identification, but larger differences between the thicknesses lead to a clear division into two subsystems coinciding with the two plates.

4.2.6.3 T-shaped structure

The last set of examples is based on a T-shaped structure like the one in Fig. 4.12. Again, the displacement on the plates is blocked at the boundaries Γ_D and the mate-

rial properties are the same of Table 4.1. Two different combinations of thicknesses are presented.

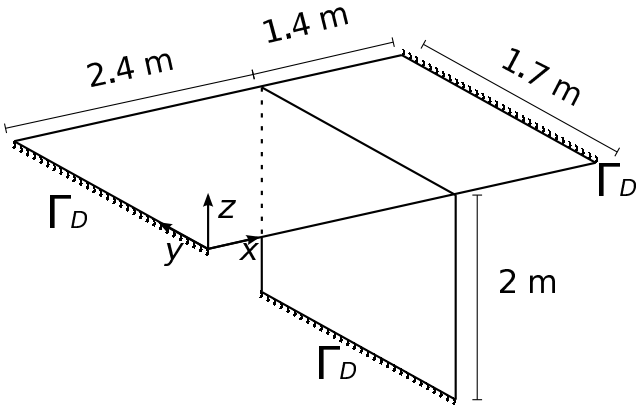

Fig. 4.12: Sketch of the T-shaped structure.

Equal thickness

The first case considers equal values of the thickness for all the plates of the T-shaped structure: $h = 50$ mm for all of them. As shown in Table 4.8, the optimal subdivision according to the MIR is three subsystems. This subdivision coincides for the two cell sizes considered, as can be seen in Fig. 4.13, and therefore can be considered as the optimal subdivision. However, the similarity between the MIR indexes of the different subdivisions leads to the conclusion that the coupling may be strong if the internal loss factor is low, and its effect should be considered in order to guarantee better results.

	MIR		
	2 subsystems	**3 subsystems**	**4 subsystems**
Cell size: $\lambda_{\text{plate}}/2$	0.70	**0.69**	0.87
Cell size: λ_{plate}	1.74	**0.96**	0.97

Table 4.8: Value of the MIR for different subdivisions. T-shaped structure with plates of equal thickness

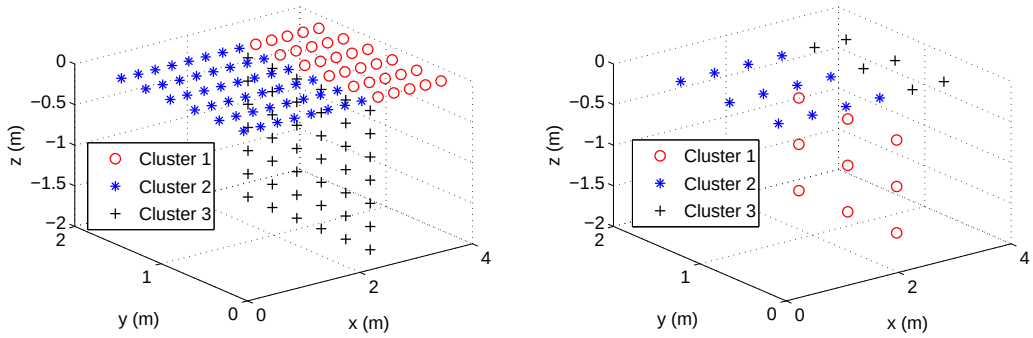

(a) Cell size: $\lambda_{\text{plate}}/2$ (b) Cell size: λ_{plate}

Fig. 4.13: Optimal subsystem distribution for a T-shaped structure with plates of equal thickness

Different thickness

The case of three different thicknesses in the T-shaped structure is considered now. The horizontal plate on the left has thickness $h = 50$ mm, the thickness of the one on the right is $0.2h$, and for the vertical plate is $0.5h$.

In this case, the decomposition into three subsystems is even clearer than for the one with constant thickness along the plates. The optimal MIR corresponds to the case of 3 clusters, Table 4.9, and the proposed subdivision is the same for both cell sizes, Fig. 4.14. Moreover, the difference between the MIR for 3 subsystems and for other options is larger than in the previous case and the absolute value of the optimal MIR is lower (weaker coupling).

	MIR		
	2 subsystems	**3 subsystems**	**4 subsystems**
Cell size: $\lambda_{\text{plate}}/2$	0.63	**0.34**	0.57
Cell size: λ_{plate}	1.21	**0.44**	0.60

Table 4.9: Value of the MIR for different subdivisions. T-shaped structure with plates of different thickness

Conclusions

The proposed methodology leads to the conclusion that a T-shaped structure made of an homogeneous material must be divided into three subsystems. However, if all the

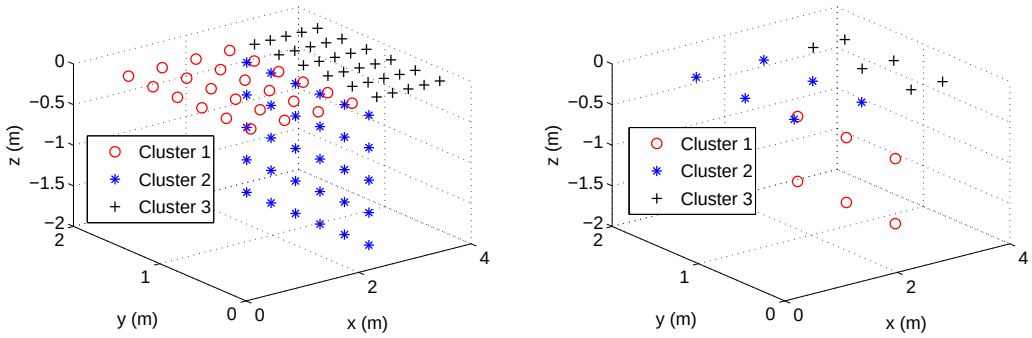

(a) (b)

Fig. 4.14: Optimal subsystem distribution for a T-shaped structure with plates of different thickness

plates have the same thickness, attention must be paid to the strength of the coupling, because the MIR associated to the three-subsystem division is not so different from those of other subdivisions.

4.3 Global strategy: different types of modes

The case of having dissimilar and significant groups of modes coexisting in the same physical region is considered here. One of the most typical cases in building acoustics is the presence of in-plane and transverse waves together in the same area (for instance in plates or shells). A methodology for identifying SEA subsystems, accounting for this two types of modes is presented here.

4.3.1 Methodology

To account for the effect of in-plane and transverse modes separately, the analysis is done in terms of the kinetic energy of the problem eigenmodes. In this sense, two magnitudes are computed for each eigenmode at every point: the kinetic energy associated to the normal velocity and the kinetic energy associated to the in-plane velocity. To do so, the vector normal to the plate or shell is computed at each point and, for each mode, the vibration velocity is decomposed into its normal and in-plane components. With them, the normal and in-plane kinetic energies can be computed.

Once the two kinetic energy maps are known for each eigenmode, every mode is classified as a *normal mode* or an *in-plane mode*. To do so, the averaged value of each type of energy along the whole domain is computed for every mode. If the averaged normal energy is larger than the in-plane one, the mode is classified as normal. Otherwise, it is classified as an in-plane mode.

After classifying the modes in two sets, the size of each set is computed. If one set is much larger than the other, the modes of the small one do not fulfil the principle of significance. Therefore they should not be taken into account and the analysis described in Section 4.2 must be applied only to the largest group of modes.

If, on the contrary, the two sets have a non-negligible size, both of them should be taken into account, and the analysis described in Section 4.2 should be done separately for each group of modes. Therefore, two geometric decompositions of the domain are obtained, one for each set of modes. The global amount of subsystems is obtained as the sum of the in-plane and transverse subsystems. For these analyses, the same considerations done in Section 4.2.3 regarding the robustness and the strength of the coupling still apply.

Since taking a set of modes into account depends on the amount of modes of each type within the frequency range analysed, it is important to remark that the lack of modes of a certain type within a particular frequency range does not guarantee that they will not appear at higher frequencies. If the amount of modes of a certain set within the frequency range considered is too small (or non-existent), more modes should be checked for a range of higher frequencies to confirm this fact, before deciding to ignore the set of modes definitely.

The procedure described here is restricted to systems consisting of plates or shells. Systems of this kind are very common in vibroacoustic problems. Therefore, it is interesting to develop a methodology for identifying their SEA subsystems. However, analogous analyses can be performed for other types of elements, if the directions governing the main types of waves are known in advance. For instance, for the case of a system of beams, energies associated to its flexural, axial, and even torsional waves can be computed separately in order to detect which of these phenomena are significant within the frequency range considered. Once the significant sets of modes are identified, the analysis of Section 4.2 is applied to each of them.

Finally, an interesting remark must be done. Even if in Section 4.2 the analysis is performed in terms of the total energy, and here in terms of the kinetic en-

ergy, this difference should not affect the global result, as discussed by Lyon (1975). Totaro and Guyader (2006) report that they do not obtain the same results with the kinetic and the total energy, specially for low frequencies and curved shapes. A possible reason for this phenomenon is the different response provided by different types of modes coexisting in the same spatial region. In this work, this effect is eliminated by classifying the modes before the cluster analysis.

4.3.2 Example

The performance of the methodology presented in Section 4.3.1 is tested here for the example of the L-shaped structure shown in Fig. 4.15. This example corresponds to a structure like the one in Section 4.2.6.2, with $\delta = 1$ and the same material properties and boundary conditions, but twice as thick.

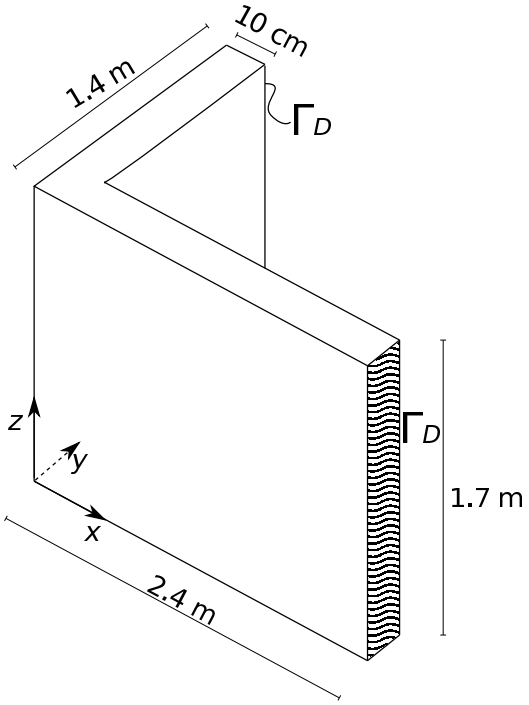

Fig. 4.15: Sketch of the thick L-shaped structure.

For this case, 25 modes are found between 1100 and 2000 Hz. The normal and in-plane kinetic energy maps are obtained for each of them. After comparing the two types of energies for every mode, 19 of them are classified as normal modes and 6 as in-plane modes (24%).

Once the two types of modes are differentiated, the analysis described in Section 4.2 is performed with the 19 normal modes. The optimal number of subsystems for the normal modes is 2, as can be seen in Table 4.10 and Fig. 4.16.

	MIR	
	2 subsystems	**3 subsystems**
Cell size: $\lambda_{\text{plate}}/2$	**0.56**	1.40
Cell size: λ_{plate}	**0.17**	0.27

Table 4.10: Value of the MIR for different subdivisions. Thick L-shaped structure. Normal modes.

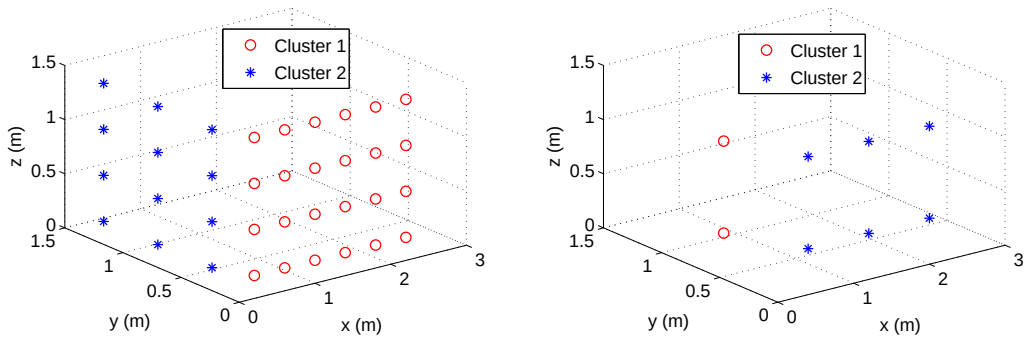

(a) Cell size: $\lambda_{\text{plate}}/2$ (b) Cell size: λ_{plate}

Fig. 4.16: Optimal subsystem distribution for the transverse modes of the thick L-shaped structure

The analysis of Section 4.2 is also done for the 6 in-plane modes. In this case, again the division into 2 subsystems has a lower MIR than the case with 3, as shown in Table 4.11, but the identified regions are not the same, see Fig. 4.17. The result is not robust. Thus, more simulations with different cell sizes should be performed and the decision of considering one or two in-plane subsystems will be based on the strength of the coupling.

Therefore, the global system consists of, at least, three subsystems: two for the normal (flexural) modes of the two plates, and another one (or two) for the in-plane modes of the system.

	MIR	
	2 subsystems	**3 subsystems**
Cell size: $\lambda_{\text{plate}}/2$	**0.24**	0.59
Cell size: λ_{plate}	**0.31**	0.91

Table 4.11: Value of the MIR for different subdivisions. Thick L-shaped structure. In-plane modes.

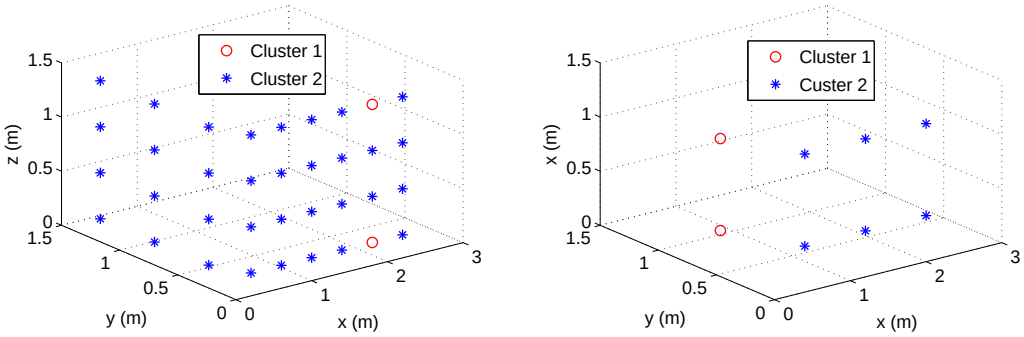

(a) Cell size: $\lambda_{\text{plate}}/2$ (b) Cell size: λ_{plate}

Fig. 4.17: Optimal subsystem distribution for the in-plane modes of the thick L-shaped structure

4.4 Concluding remarks

- A strategy for identifying SEA subsystems is presented. It consists in performing different cluster analyses based on the system eigenmodes and uses the mutual inertia ratio as a decision variable. It provides reasonable results for systems consisting of plates of different thickness.

- The information provided by the modal analysis gives the possibility of classifying the modes of the system before doing the cluster analysis. In this way, modes associated to different types of waves can be treated separately. This preprocessing of the modes allows the detection of different subsystems sharing the same physical region.

- The use of a set of eigenmodes as samples for the cluster analysis avoids the need of projecting the results in their principal components. This leads to a lower amount of calculations and, therefore, a lower computational cost.

4.5 Future directions

Preliminary results of this research are very promising. However, there are still several aspects to be considered in order to get a better and more systematic technique:

- An expression relating the mir between two subsystems and their coupling loss factor is necessary for clarifying those cases where the analysis is not robust.
- The effect of the damping should be incorporated in the analysis, since it may become important when the coupling between two subsystems is not weak enough.
- The detection of different types of modes shown in Section 4.3 should be validated for other types of examples.
- A study on the influence of the set of modes considered on the optimal subdivision should be done. Two main aspects should be discussed: the importance of the amount of modes analysed and the possibility of considering random subsets of modes within a certain frequency range.
- The method should be combined with the strategy proposed in Chapter 2, in order to verify that the coupling loss factors between the proposed subsystems are weak.
- An application of this strategy for vibroacoustic problems is planned. For such a case, the amount of eigenmodes within a certain frequency range will increase dramatically and a methodology for selecting a random sample of modes within the desired range should be proposed.

Part II

Double walls: one problem with many approaches

Chapter 5

Introduction: review of methods for double walls

5.1 Introduction

Lightweight structures are increasingly used in construction, in order to cheaply provide load-bearing configurations with good acoustic properties and a minimal mass. One of the most important structural elements in lightweight structures are double walls, Fig. 5.1: they consist of two thin leaves, a few centimetres thick each, with a cavity (which might be totally or partially filled with absorbing material) between them, see sketch of Fig. 5.2. This cavity is typically around 10 cm thick. The leaves are usually made of light materials such as timber or plasterboard, and the absorbing filling of the cavity is typically made with a very porous material such as mineral wool, Arenas and Crocker (2010). Double walls usually consist also of stiffening elements between the leaves, called studs. They are usually wooden or metallic beams and can have different cross-sections.

Due to the increasing use of these elements, there is interest in reliable models of their sound insulation. These models should reproduce the acoustic behaviour of double walls both for impact and airborne noise.

The analysis of sound transmission through double walls is also interesting because it is a representative example of the problems that arise when dealing with vibroacoustic systems. Due to this, an extensive analysis of the different approaches to this problem is performed along this part of the thesis. Both deterministic and

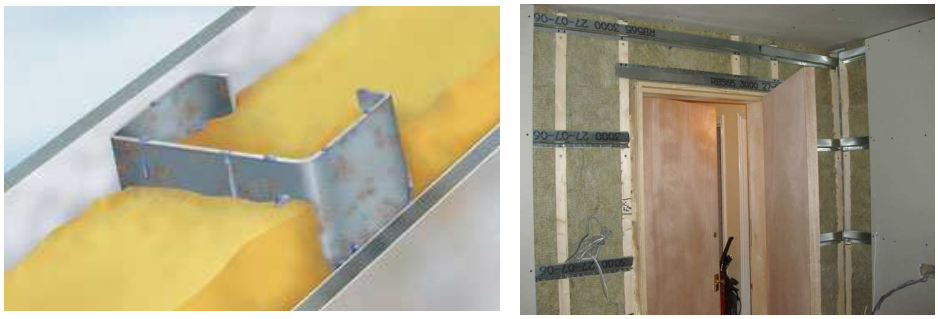

(a) (b)

Fig. 5.1: Double walls images. (a) Sketch of the basic elements of a double wall, source: http://continuingeducation.construction.com. (b) Construction of a double wall, source: http://www.keepitquiet.co.uk. Both of them retrieved on 2013-08-01.

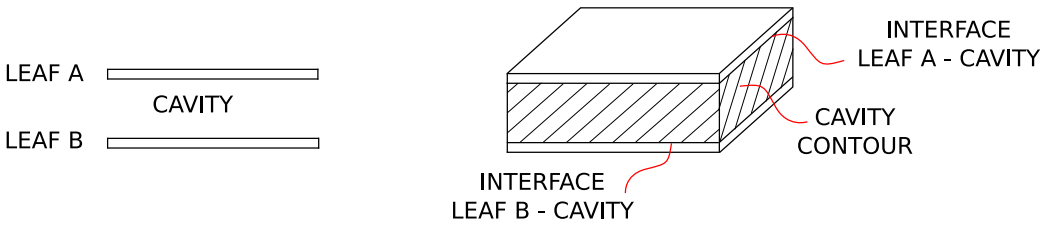

Fig. 5.2: Sketches of the double wall and its parts.

statistical techniques are shown and compared. In particular, a new numerical approach is presented and compared with more traditional models in Chapter 6. This approach combines the finite layer method (FLM) for discretising the acoustic domain and modal analysis for the solid domain. Moreover, all the aspects discussed in Part I are recovered in Chapter 7 to model a realistic double wall with a combination of SEA and numerical simulations.

Due to its representativity, many authors have dealt with the problem of sound transmission through double walls. In fact, an extensive review on models for double walls was done by Hongisto (2006). Most of these models assume the structure as infinite and use the impedance approach for the propagation of sound in the cavity. Some examples are the works of Beranek and Work (1949), London (1950) and Fahy (1985).

Another type of models, more complex than the previous ones, are the wave models. Kropp and Rebillard (1999) use a wave approach to the problem, with different behaviours depending on the frequency: when the double wall resonance frequency is

much lower than the critical frequency, the double wall acts as a single plate; when it is much higher than the critical frequency, the wall leaves act as independent plates; and for resonance frequencies close to the critical frequency, the wall has an intermediate behaviour. Guigou-Carter and Villot (2003) show a wave model that also takes into account the structural flanking paths with the help of statistical energy analysis (SEA). Wang et al. (2005) express the incident waves, the pressure field inside the cavity and the radiated waves in terms of their velocity potentials.

Some authors have developed impedance models for multilayered structures. They also assume an infinite size for the leaves, and express the transmission of pressure and vibrations with the help of transfer matrices. Brouard et al. (1995) combine transfer matrices with interface matrices in order to take into account the interfaces between layers. Geebelen et al. (2006) consider layers of poroelastic materials inside and Dijckmans et al. (2010) compare the results of the transfer matrix method with those of a wave-based model.

Other authors solve a one-dimensional version of the problem with the help of numerical techniques. Trochidis and Kalaroutis (1986) use Fourier transforms and Alba et al. (2004) refine this technique using an iterative method.

To account for the wall size and boundary conditions, different techniques are employed. Numerical methods can be used for solving the thin plate equation at the wall leaves and the Helmholtz equation at the cavity. Beyond the use of FEM, whose cost happens to be extremely high as shown by Panneton and Atalla (1996), other discretisation techniques can be applied.

One of them is the use of modal bases for solving the differential equations, as done by Brunskog (2005), Sjökvist et al. (2008) and Chung and Emms (2008). It consists in expressing the vibration and acoustic fields in terms of the eigenfunctions of the problem. This approach has less computational cost than FEM but is restricted to simple geometries, since the eigenfunctions of complex domains cannot be obtained analytically. However, the typical shapes of leaves and cavities fulfil this requirement.

To simplify the numerical approach, some assumptions on the pressure or vibration field can be done. Villot et al. (2001) present a technique that relies on the wave approach and introduces the diffraction effect associated to the finite size of a structure, using spatial windowing. Kernen and Hassan (2005) express the velocity field as a function of forced waves (bending nearfields) and free (propagating) waves. Xin et al. (2010) describe the behaviour of the pressure field with the sound velocity

potential method instead of solving the Helmholtz equation numerically.

Another simplified numerical approach is the waveguide finite element method (WFEM). This technique, used by Aalami (1973), Orrenius and Finnveden (1996) or Brunskog and Davidsson (2004), is particularly suitable for structures where one dimension is clearly larger than the others. It is based on the FEM discretisation of the cross-section of the structure, combined with a wave description of the vibration and pressure fields in the third dimension. It is particularly useful for long structures with complex cross-sections. The wave length of the solution is imposed along the extrusion direction in most of the cases. This is not the case of the double wall cavity where the finite layer method (FLM) is better adapted to the geometry of the problem.

An approach similar to the WFEM is the finite strip method (FSM). It also combines the finite element discretisation of the cross-section of the structure with a wave-like description in the third dimension. The main difference with the WFEM is that the FSM considers a finite size of the structure in the third dimension, accounting for the corresponding boundary conditions, see Cheung and Tham (1997) and Friedrich (2000).

In Chapter 6, the finite layer method is proposed as an alternative way of discretising the pressure field in the cavity inside double walls. This method, used by Cheung and Chakrabarti (1972) and Smith et al. (1992), combines a FEM-like discretisation in the direction perpendicular to the wall with trigonometric functions in the two in-plane directions. To the best of the author's knowledge, this is the first time a finite layer method is proposed for solving the Helmholtz equation. The idea is similar to that of the finite strip method but this one is particularly suitable for multilayered structures because it allows the resolution of the Helmholtz equation at each layer, taking into account the continuity of the normal velocity at their interfaces. Moreover, due to the use of trigonometric functions in the in-plane directions, its computational cost is significantly lower than that of pure finite element analysis, see Poblet-Puig and Rodríguez-Ferran (2011).

This approach is verified in Section 6.4 by comparing it with experimental data. It is also compared with existing prediction models in order to check the influence of common simplifications. Some of these simplifications are: assuming infinite size of the wall, using interpolation functions with null derivative in the boundary, or considering the problem as one-dimensional.

Finally, in Chapter 7 the combination of deterministic and statistical methods is presented as a possible solution for dealing with vibroacoustic problems consisting of double walls and other elements.

5.2 Four methods with different level of complexity

Four different models for the sound transmission through double walls are compiled in this chapter. They have been chosen as a representative set of the approaches to this problem, with different level of complexity. The two first models, developed by Fahy (1985) and Au and Byrne (1987) respectively, are two simple impedance models. The third approach is a technique based on the model of Xin et al. (2010). This technique does less assumptions than the impedance models but still has less degrees of freedom than the purely numerical approaches of Section 5.2.3 and Chapter 6. It uses the same interpolation functions for the velocity potential and the plate displacement. Finally an approach based on the discretisation of the wall leaves and cavity in terms of their separate eigenfunctions is analysed. This description is more realistic than the others. However, the functions used for discretising the pressure field have a null value of the normal derivative at the fluid-structure interface. This simplification may affect the continuity of the normal velocity at the interfaces.

5.2.1 Simple impedance equations

The first two techniques are impedance models that assume infinite size of the wall. They provide explicit expressions for the transmission coefficient of the double walls for a certain incidence angle, $\tau(\varphi)$. These approaches have almost no computational cost but include a large amount of simplifications. They are based on the 2D sketch of Fig. 5.3.

In order to obtain regulated outputs such as the sound reduction index R, the transmission coefficient is computed for several incidence angles and averaged. In this way a field incidence is simulated

$$\tau_{\text{diff}} = \frac{\int_0^{\varphi_{\text{lim}}} \tau(\varphi)\cos(\varphi)\sin(\varphi)\,\mathrm{d}\varphi}{\int_0^{\varphi_{\text{lim}}} \cos(\varphi)\sin(\varphi)\,\mathrm{d}\varphi}. \tag{5.1}$$

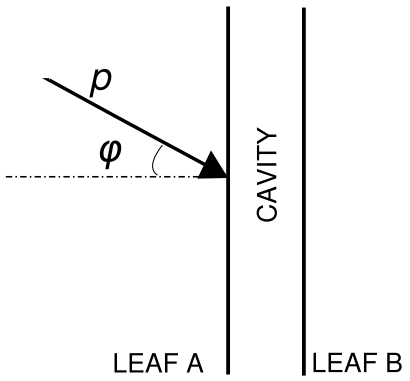

Fig. 5.3: Angle of incidence of the pressure.

In these examples the value of φ_{lim} is chosen equal to 78° following the recommendations of Beranek (1988) for a diffuse field.

The sound reduction index is computed as

$$R = 10 \log_{10} \left(\frac{1}{\tau_{\text{diff}}} \right). \tag{5.2}$$

5.2.1.1 Fahy (1985)

Fahy (1985) presents a model for empty cavity and diffuse sound incidence angle. In this model, the transmission coefficient is computed in terms of the mechanical impedances of the leaves and cavity, following a one-dimensional analysis of the problem and taking the lowest eigenfrequency of the leaves into account:

$$\tau(\varphi) = \left| \frac{\overline{p}_{\text{trans}}}{\overline{p}_{\text{inc}}} \right|^2 = \left| - \frac{2\mathrm{i} Z_0^2 \sin(kH\cos\varphi)/\cos^2\varphi}{\overline{z_1' z_2'} \sin^2(kH\cos\varphi) + Z_0^2/\cos\varphi} \right|^2, \tag{5.3}$$

where p_{trans} is the pressure of transmitted sound, p_{inc} is the pressure of the incident sound, $Z_0 = \rho_{\text{air}} c$ is the characteristic impedance of the air, $k = \omega/c$ is the wavenumber in the air, η_i is the loss factor of layer i,

$$\overline{z_i'} = \overline{z_i} + Z_0 \frac{1 - \mathrm{i}/\tan(kH\cos\varphi)}{\cos\varphi} \quad \text{and} \quad \overline{z_i} = \mathrm{i}\omega\rho_{s,i} + \eta_i \omega_0 \rho_{s,i} - \mathrm{i}\frac{\omega_{0,i}^2}{\rho_{s,i}\omega}.$$

Here ω_0 is the first eigenfrequency of the leaves.

The main limitation of this model is that it does not consider the resonant transmission.

5.2.1.2 Au and Byrne (1987)

The second impedance model is the one presented by Au and Byrne (1987). This model assumes that the wavenumber component parallel to the leaf surface is the same in all the layers. It also enforces the continuity of the acoustical pressure and particle velocity at the interfaces. It distinguishes between the input impedance Z_I, the terminal impedance Z_T and the specific impedance Z_i of each material layer i, and the calculation starts from the receiving room side, Fig. 5.4.

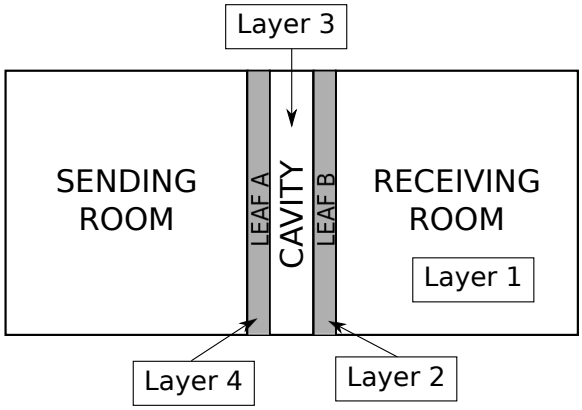

Fig. 5.4: Sketch of the mode of Au and Byrne (1987).

In this model the input impedance of the receiving room is defined as $Z_I = Z_0/\cos\varphi$. This term is the terminal impedance of the excited leaf. The impedances of leaves B and A (layers 2 and 4 respectively) are:

$$\begin{aligned} Z_2 &= Z_1 + \eta_2 B_2 k_x^4/\omega + \mathrm{i}\left(\omega\rho_{s,2} - B_2 k_x^4/\omega\right) \\ Z_4 &= Z_3 + \eta_1 B_1 k_x^4/\omega + \mathrm{i}\left(\omega\rho_{s,1} - B_1 k_x^4/\omega\right). \end{aligned} \tag{5.4}$$

The impedance of the cavity is

$$Z_3 = Z_c \frac{\Gamma_c}{\Gamma_{cy}} \frac{\left(1+\frac{Z_c\Gamma_c}{Z_2\Gamma_{cy}}\right)\exp\left(\mathrm{i}\Gamma_{cy}H\right) + \left(1-\frac{Z_c\Gamma_c}{Z_2\Gamma_{cy}}\right)\exp\left(-\mathrm{i}\Gamma_{cy}H\right)}{\left(1+\frac{Z_c\Gamma_c}{Z_2\Gamma_{cy}}\right)\exp\left(\mathrm{i}\Gamma_{cy}H\right) - \left(1-\frac{Z_c\Gamma_c}{Z_2\Gamma_{cy}}\right)\exp\left(-\mathrm{i}\Gamma_{cy}H\right)} \tag{5.5}$$

where $\Gamma_{cy}^2 = \Gamma_c^2 - k_x^2$, $k_x = k\sin\varphi$, $Z_c = Z_0\sqrt{1-\mathrm{i}\sigma/\rho_{\mathrm{air}}\omega}$, $\Gamma_c = k\sqrt{1-\mathrm{i}\sigma/\rho_{\mathrm{air}}\omega}$ and σ is the resistivity of the cavity absorbent ($\sigma = 0$ for air cavities).

$p_4 = p_i\, 2A_z/(A_z{+}1)$ is the input pressure for layer 3 (cavity) and $A_z = Z_4\cos\varphi/Z_0$. The transmitted pressure over an impervious leaf is: $p_2 = p_1 Z_2/Z_1$ (leaf B), $p_4 =$

$p_3 Z_4/Z_3$ (leaf A), and the transmitted pressure over the cavity absorbent is calculated by

$$p_2 = \frac{p_3}{2}\left[\left(1+\frac{Z_c\Gamma_c}{Z_3\Gamma_{cy}}\right)\exp\left(-\mathrm{i}\Gamma_{cy}H\right)+\left(1-\frac{Z_c\Gamma_c}{Z_3\Gamma_{cy}}\right)\exp\left(\mathrm{i}\Gamma_{cy}H\right)\right]. \tag{5.6}$$

Therefore, the transmission coefficient is computed as

$$\tau(\varphi)=\left|\frac{p_1}{p_i}\right|^2=\frac{Z_1Z_3}{Z_2Z_4}\,\frac{A_z}{A_z+1}\left[\left(1+\frac{Z_c\Gamma_c}{Z_3\Gamma_{cy}}\right)\exp\left(-\mathrm{i}\Gamma_{cy}H\right)+\right.$$
$$\left.+\left(1-\frac{Z_c\Gamma_c}{Z_3\Gamma_{cy}}\right)\exp\left(\mathrm{i}\Gamma_{cy}H\right)\right]. \tag{5.7}$$

5.2.2 Adaptation of model of Xin et al. (2010)

A more complex approach is presented in the paper by Xin et al. (2010). This technique consists in solving the thin plate equation for the leaves and describing the pressure field in the cavity with the sound velocity potential method.

The thin plate equation

$$B\nabla^4 u(x,y)-\omega^2\rho_s u(x,y)=q(x,y)+p^{\mathrm{int}}(x,y), \tag{5.8}$$

is solved with the boundary conditions of a simply supported plate

$$\begin{aligned} u(0,y)=u(L_x,y)=u(x,0)=u(x,L_y)=0\\ M(0,y)=M(L_x,y)=M(x,0)=M(x,L_y)=0. \end{aligned} \tag{5.9}$$

In Eq. (5.8), $u(x,y)$ the displacement of the leaf. The term $q(x,y)$ is the applied excitation pressure and $p^{\mathrm{int}}(x,y)$ is the pressure of the cavity fluid at the leaf-cavity interface. In Eq. (5.9), $M(x,y)$ is the bending moment and L_x and L_y are the dimensions of the leaf, see Fig. 5.5.

The vibration field solution of Eq. (5.8) is expressed in terms of the eigenfunctions $\phi_r(x,y)$ of a simply supported plate as

$$u(x,y)=\sum_{r=1}^{n_{\mathrm{modes}}} a_r\,\phi_r(x,y) \tag{5.10}$$

where n_{modes} is the number of modal functions used in the interpolation, a_r is the phasor modal contribution of mode ϕ_r and

$$\phi_r(x,y)=\sin\left(\frac{r_x\pi x}{L_x}\right)\sin\left(\frac{r_y\pi y}{L_y}\right), \qquad r_x,r_y=1,2,\ldots \tag{5.11}$$

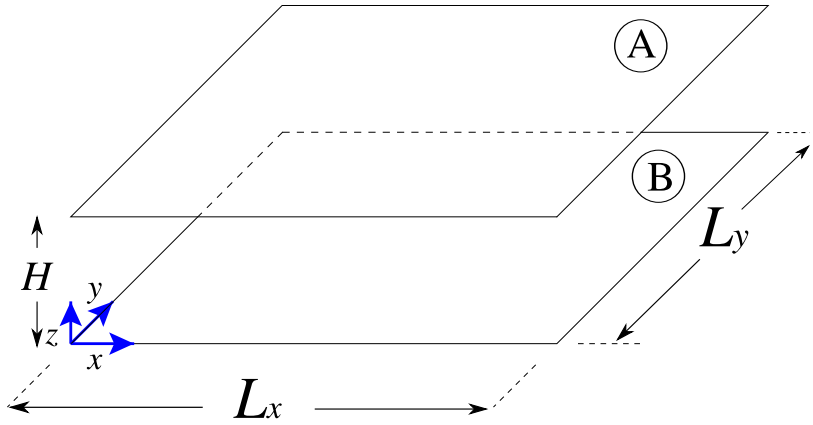

Fig. 5.5: Double wall dimensions.

The pressure field inside the cavity is expressed in terms of the velocity potential $\Psi(\boldsymbol{x})$ as

$$p(\boldsymbol{x}) = \mathrm{i}\omega\rho_{\mathrm{air}}\,\Psi(\boldsymbol{x}) \tag{5.12}$$

so there is no need to solve the Helmholtz equation. In Eq. (5.12), $\boldsymbol{x} = (x, y, z)$ and

$$\Psi(\boldsymbol{x}) = \sum_{r=1}^{n_{\mathrm{modes}}} \epsilon_r\,\phi_r(x,y)\exp\left(-\mathrm{i}k_z z\right) + \sum_{r=1}^{n_{\mathrm{modes}}} \zeta_r\,\phi_r(x,y)\exp\left(\mathrm{i}k_z z\right), \tag{5.13}$$

where, $k_z = k\cos\varphi$.

Xin et al. (2010) use this description of the pressure field both for the pressure inside the cavity and for the incident and radiated pressures. However, in this work the velocity potential is only used for the pressure field inside the cavity. The computation of the incident and radiated pressures is performed as described in Appendix B, allowing a better comparison with the other techniques.

For each frequency and couple of modes $\{r_x, r_y\}$, ϵ_r and ζ_r are expressed in terms of the vibration of the plates by means of the leaf-cavity interface conditions

$$\begin{aligned} \tfrac{\partial\Psi}{\partial z} &= \mathrm{i}\omega u_A \quad \text{at } z = H \\ \tfrac{\partial\Psi}{\partial z} &= \mathrm{i}\omega u_B \quad \text{at } z = 0. \end{aligned} \tag{5.14}$$

In Eq. (5.14) $u_A(x,y) = \sum_{r=1}^{n_{\mathrm{modes}}} a_r\,\phi_r(x,y)$ is the vibration field in the excited leaf of the wall, $u_B(x,y) = \sum_{r=1}^{n_{\mathrm{modes}}} b_r\,\phi_r(x,y)$ is the vibration field in the other one and H is the thickness of the cavity.

Hence, after replacing expression (5.12) of the pressure field $p(\boldsymbol{x})$ in the differential equations of the leaves (5.8), for each frequency and couple of modes $\{r_x, r_y\}$ a 2 degree-of-freedom system has to be solved with a_r and b_r as unknowns.

The main drawback of this approach is that the description of the pressure field implies a null value of the pressure at the cavity contour. This condition is somehow restrictive, since the contour of finite-dimension cavities is usually purely reflecting with boundary condition

$$\nabla p \cdot \boldsymbol{n} = 0, \tag{5.15}$$

or absorbing with low values of absorption. In both cases a cosine description of the pressure field in the cavity is more adequate than the sine based description of Eq. (5.11). In Eq. (5.15), $\boldsymbol{n}$ is the outward unit normal. The effect of these conditions is discussed in Section 6.4.

5.2.3 Discretisation with modal bases

The boundary conditions (5.9) and (5.15) can be taken into account if the thin plate equation (5.8) for each leaf and the Helmholtz equation

$$\nabla^2 p(\boldsymbol{x}) + k^2 p(\boldsymbol{x}) = 0 \tag{5.16}$$

for the acoustic domain are solved numerically with the help of a discretisation of the domain.

This discretisation can be performed in different ways. Here, the separate eigenfunctions of the acoustic and structural equations are used as interpolation bases for the pressure and vibration fields respectively. Similar ideas have been proposed by Brunskog (2005) or Chung and Emms (2008).

In this model, the discretisation of the vibration field in the leaves is the same as in Section 5.2.2. The integral form of the thin plate equation is used for each leaf

$$\int_{\Omega_{xy}} \left(B k_r^4 - \omega^2 \rho_s\right) u\, v \,\mathrm{d}x\,\mathrm{d}y = \int_{\Omega_{xy}} \left(q + p^{\mathrm{int}}\right)\, v \,\mathrm{d}x\,\mathrm{d}y \qquad \forall v, \tag{5.17}$$

where v is the test function, $\Omega_{xy} = [0,\, L_x] \times [0,\, L_y]$ is the leaf domain and

$$k_r^2 = \left(\frac{r_x \pi}{L_x}\right)^2 + \left(\frac{r_y \pi}{L_y}\right)^2. \tag{5.18}$$

The pressure field is expressed through a modal expansion

$$p(\boldsymbol{x}) = \sum_{s=1}^{n_{\mathrm{modes}}} p_s \psi_s(\boldsymbol{x}). \tag{5.19}$$

The cavity eigenfunctions are

$$\psi_s(\boldsymbol{x}) = \cos\left(\frac{s_x \pi x}{L_x}\right) \cos\left(\frac{s_y \pi y}{L_y}\right) \cos\left(\frac{s_z \pi z}{H}\right) \qquad s_x,\, s_y,\, s_z = 0,\, 1,\, 2... \tag{5.20}$$

as if the whole cavity boundary was reflecting, see Vigran (2008).

This modal expansion is replaced in the integral version of the Helmholtz equation

$$\int_{\Omega_c} p\, \nabla^2 v \, \mathrm{d}\Omega \,+\, k^2 \int_{\Omega_c} p\, v \, \mathrm{d}\Omega \,+ \int_{\Omega_{xy}} \rho_{\text{air}}\, \omega^2 v\,(x, y, H)\,(\boldsymbol{u_A} \cdot \boldsymbol{n})\, \mathrm{d}x\, \mathrm{d}y + \\ + \int_{\Omega_{xy}} \rho_{\text{air}}\, \omega^2 v\,(x, y, 0)\,(\boldsymbol{u_B} \cdot \boldsymbol{n})\, \mathrm{d}x\, \mathrm{d}y = 0 \qquad \forall v, \tag{5.21}$$

where $\Omega_c = [0,\, L_x] \times [0,\, L_y] \times [0,\, H]$ is the cavity domain, $\boldsymbol{u_A} = (0,\, 0,\, u_A)$ and $\boldsymbol{u_B} = (0,\, 0,\, u_B)$ are the vibration fields in leaves A and B respectively.

All the eigenfunctions of the cavity used in the interpolation are also used as test functions. The coupling with the leaves is imposed in the third and fourth terms of Eq. (5.21), connecting the modal contributions of the pressure field with those of the vibration fields of the leaves.

If the only external excitation is applied to leaf A, the resulting block tridiagonal linear system is

$$\begin{pmatrix} \mathbf{A} & \mathbf{A_C} & \mathbf{0} \\ \mathbf{C_A} & \mathbf{C} & \mathbf{C_B} \\ \mathbf{0} & \mathbf{B_C} & \mathbf{B} \end{pmatrix} \begin{Bmatrix} \mathbf{a} \\ \mathbf{p} \\ \mathbf{b} \end{Bmatrix} = \begin{Bmatrix} \mathbf{f} \\ \mathbf{0} \\ \mathbf{0} \end{Bmatrix} \tag{5.22}$$

where $\mathbf{a}$ and $\mathbf{b}$ are the vectors of modal contributions for the vibration field of leaves A and B respectively, $\mathbf{p}$ is the vector of modal contributions for the pressure field in the cavity and $[\mathrm{f}]_r = \int_{\Omega_{xy}} q\, \phi_r \, \mathrm{d}x\, \mathrm{d}y$.

$\mathbf{A}$ and $\mathbf{B}$ are diagonal matrices, whose components are

$$[\mathrm{A}]_{rr}\,, [\mathrm{B}]_{rr} = (B k_r^4 - \omega^2 \rho_s) \int_{\Omega_{xy}} \phi_r\,(x, y)\; \phi_r\,(x, y)\; \mathrm{d}x\, \mathrm{d}y. \tag{5.23}$$

These matrices are associated to the independent behaviour of each leaf.

Due to the orthogonality of the cavity eigenfunctions, $\mathbf{C}$ is also a diagonal matrix, associated to the behaviour of the cavity alone, whose components are

$$[\mathrm{C}]_{ss} = (k^2 - k_s^2) \int_{\Omega_c} \psi_s\,(\boldsymbol{x})\, \psi_s\,(\boldsymbol{x})\; \mathrm{d}\Omega, \tag{5.24}$$

where

$$k_s^2 = \left(\frac{s_x \pi}{L_x}\right)^2 + \left(\frac{s_y \pi}{L_y}\right)^2 + \left(\frac{s_z \pi}{H}\right)^2. \tag{5.25}$$

The fluid-structure coupling matrices for the leaves are $\mathbf{A_C}$ and $\mathbf{B_C}$, where

$$[\mathrm{A_C}]_{rs} = -\int_{\Omega_{xy}} \phi_r(x,y)\,\psi_s(x,y,H)\,\mathrm{d}x\,\mathrm{d}y \tag{5.26}$$

$$[\mathrm{B_C}]_{rs} = \int_{\Omega_{xy}} \phi_r(x,y)\,\psi_s(x,y,0)\,\mathrm{d}x\,\mathrm{d}y. \tag{5.27}$$

The fluid-structure coupling matrices for the cavity are $\mathbf{C_A}$ and $\mathbf{C_B}$, where

$$[\mathrm{C_A}]_{sr} = -\rho_{\mathrm{air}}\omega^2 \int_{\Omega_{xy}} \psi_s(x,y,H)\ \phi_r(x,y)\,\mathrm{d}x\,\mathrm{d}y \tag{5.28}$$

$$[\mathrm{C_B}]_{sr} = \rho_{\mathrm{air}}\omega^2 \int_{\Omega_{xy}} \psi_s(x,y,0)\ \phi_r(x,y)\,\mathrm{d}x\,\mathrm{d}y. \tag{5.29}$$

This approach takes into account the boundary conditions of the leaves (5.9) and the cavity contour (5.15), but has a disadvantage: the eigenfunctions of the cavity have null normal derivative at the boundaries. Therefore, the continuity of the normal velocity at the fluid-structure interface can only be enforced weakly.

5.2.4 Summary

In this section four different models of the sound transmission through double walls have been presented. In Chapter 6 they are compared with the finite layer method. A summary of the main hypotheses of each method is shown in Table 5.1 .

	Fahy	**Au and Byrne**	**Adapt. of Xin et al.**	**Modal bases**
Finite size of the leaves	No	No	Yes	Yes
Continuity of normal velocity at interfaces	No	No	Yes	No
Reflecting boundary conditions for the cavity	No	No	No	Yes
Thin plate equation for the leaves	No	No	Yes	Yes
Helmholtz equation for the cavity	No	No	No	Yes
Dimensionality of the pressure field	1D	1D	3D	3D

Table 5.1: Hypotheses of four models of the sound insulation of double walls

Chapter 6

A new deterministic approach: the finite layer method[3]

In this chapter the finite layer method (FLM) is presented as a discretisation technique for the computation of noise transmission through double walls. It combines a FEM discretisation in the direction perpendicular to the wall with trigonometric functions in the two in-plane directions. It is used for solving the Helmholtz equation at the cavity inside the double wall, while the wall leaves are modelled with the thin plate equation and solved with modal analysis. The main advantage of FLM over other discretisation techniques is the possibility of extending it to multilayered structures without changing the interpolation functions and with an affordable computational cost.

6.1 Bases of the method

The finite layer method is a technique with less computational cost than FEM but still detailed enough to enforce the interface conditions between fluid and structure. Thus, it is specially suitable for solving the noise transmission through layered configurations of finite dimensions.

The finite layer method is used as a discretisation technique for the pressure field when solving the vibroacoustic problem in the double wall. For the structural part

[3]Based on reference: Díaz-Cereceda et al. (2012)

of the problem, the same modal formulation described in Section 5.2.3 is used.

The weak form of the acoustic problem is

$$\int_{\Omega_c} \nabla p \cdot \nabla v \, \mathrm{d}\Omega \; - \; k^2 \int_{\Omega_c} p \, v \, \mathrm{d}\Omega \; - \int_{\Omega_{xy}} \rho_{\mathrm{air}} \, \omega^2 v \, (x, y, H) \, (\boldsymbol{u_A} \cdot \boldsymbol{n}) \, \mathrm{d}x \, \mathrm{d}y - \\ - \int_{\Omega_{xy}} \rho_{\mathrm{air}} \, \omega^2 v \, (x, y, H) \, (\boldsymbol{u_B} \cdot \boldsymbol{n}) \, \mathrm{d}x \, \mathrm{d}y = 0 \qquad \forall v. \quad (6.1)$$

The pressure field is interpolated by means of layer functions. These can be understood as standard FEM interpolation functions in the z direction $N_j(z)$, see Zienkiewicz and Taylor (2000), multiplied by appropriate interpolation functions $\Phi_s(x, y)$ in the xy plane

$$p(\boldsymbol{x}) = \sum_{s=1}^{n_{xy}} \sum_{j=1}^{n_z} p_{js} \, N_j(z) \, \Phi_s(x, y) \, . \quad (6.2)$$

In Eq. (6.2), n_z is the number of nodes in the z direction as shown in Fig. 6.1, n_{xy} is the number of interpolation functions considered in the xy plane and p_{js} is the pressure phasor value at node j for the interpolation function $\Phi_s(x, y)$. In this work, $\Phi_s(x, y)$ is chosen such as to provide the same description in the xy plane as in Section 5.2.3

$$\Phi_s(x, y) = \cos\left(\frac{s_x \pi x}{L_x}\right) \cos\left(\frac{s_y \pi y}{L_y}\right) \qquad s_x, s_y = 0, 1, 2, \ldots \quad (6.3)$$

Therefore, the set of functions $\Phi_s(x, y)$ satisfies orthogonality and also the condition (5.15) at the cavity contour.

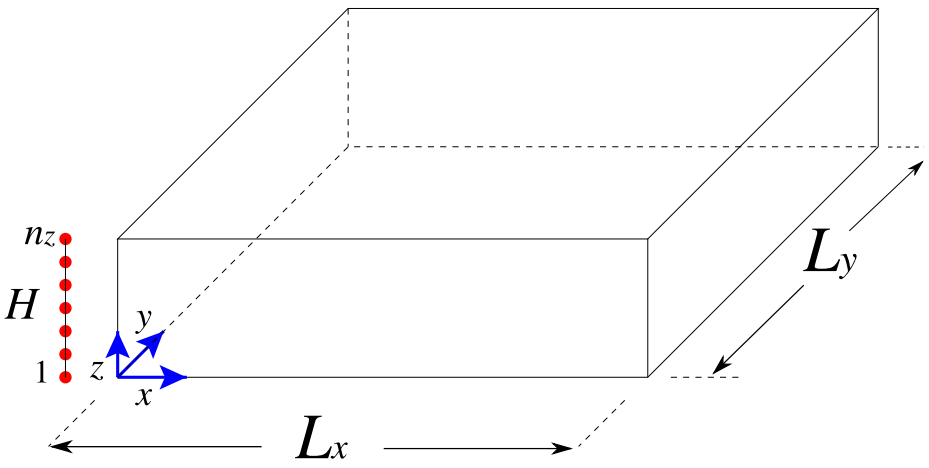

Fig. 6.1: Sketch and notation used in the finite layer method.

The test functions v are chosen of the same type as the interpolation functions of Eq. (6.2)

$$v(\boldsymbol{x}) = \sum_{t=1}^{n_{xy}} \sum_{i=1}^{n_z} v_{it}\, N_i\,(z)\, \Phi_t\,(x, y)\,. \tag{6.4}$$

Eq. (6.1) must be satisfied for any set of values v_{it}.

With these functions, the operations in Eq. (6.1) can be split among those in the xy cross-section and those in the z direction. The xy cross-section is treated analytically in order to reduce the problem to a one-dimensional FEM type calculation in the z direction. Thus, n_{xy} sets of n_z linear equations are obtained.

As an example, the first term of the weak form (6.1) and the test function $v = N_i\,(z)\, \Phi_t\,(x, y)$ are considered. The contribution to the $\{i, j\}$ matrix coefficient corresponding to the layer functions t and s can be written as

$$\begin{aligned}\left[\int_{\Omega_c} \nabla p \cdot \nabla v \,\mathrm{d}\Omega\right]_{ts,ij} &= \int_0^H N_i' N_j' \,\mathrm{d}z \int_{\Omega_{xy}} \Phi_t\, \Phi_s \,\mathrm{d}x\,\mathrm{d}y + \\ &+ \int_0^H N_i N_j \,\mathrm{d}z \int_{\Omega_{xy}} \nabla_{xy}\Phi_t \cdot \nabla_{xy}\Phi_s \,\mathrm{d}x\,\mathrm{d}y \\ &\qquad i, j = 1, 2, \ldots, n_z \qquad t, s = 1, 2, \ldots, n_{xy}\end{aligned} \tag{6.5}$$

where $N_i' = \frac{\mathrm{d}N_i}{\mathrm{d}z}$ and $\nabla_{xy} = (\partial/\partial x, \partial/\partial y)^T$ is the gradient in the xy plane. A similar substitution can be done for the other terms of Eq. (6.1).

Combining the discretised weak form for the cavity pressure with those of the leaf equations, the resulting linear system has the same structure as that of Eq. (5.22):

$$\begin{pmatrix} \mathbf{A} & \mathbf{A_C} & \mathbf{0} \\ \mathbf{C_A} & \mathbf{C} & \mathbf{C_B} \\ \mathbf{0} & \mathbf{B_C} & \mathbf{B} \end{pmatrix} \begin{Bmatrix} \mathbf{a} \\ \mathbf{p} \\ \mathbf{b} \end{Bmatrix} = \begin{Bmatrix} \mathbf{f} \\ \mathbf{0} \\ \mathbf{0} \end{Bmatrix} \tag{6.6}$$

where $\mathbf{p}$ is the vector with the contributions p_{js} and $\mathbf{a}$, $\mathbf{b}$ and $\mathbf{f}$ have already been defined in Section 5.2.3.

$\mathbf{A}$ and $\mathbf{B}$ are the same matrices of Eq. (5.23) and $\mathbf{C}$ is the FLM discretisation matrix of the cavity, which is a block-diagonal matrix. Each block $\{s, s\}$ is

$$\mathbf{C}_{ss} = \mathbf{K}\, I_1\,(s, s) + \mathbf{M}\, I_2\,(s, s) - k^2 \mathbf{M}\, I_1\,(s, s)\,, \tag{6.7}$$

has $n_z \times n_z$ size and a tridiagonal structure. The number of non-zero blocks in the matrix is n_{xy}. In Eq. (6.7),

$$I_1(s,s) = \int_{\Omega_{xy}} \Phi_s \, \Phi_s \, \mathrm{d}x \, \mathrm{d}y = \\ = \int_0^{L_x} \left[\cos\left(\frac{s_x \pi x}{L_x}\right)\right]^2 \mathrm{d}x \int_0^{L_y} \left[\cos\left(\frac{s_y \pi y}{L_y}\right)\right]^2 \mathrm{d}y, \quad (6.8)$$

$$I_2(s,s) = \int_{\Omega_{xy}} \nabla_{xy}\Phi_s \cdot \nabla_{xy}\Phi_s \, \mathrm{d}x \, \mathrm{d}y = \\ = \int_0^{L_x} \left[-\frac{s_x \pi}{L_x} \sin\left(\frac{s_x \pi x}{L_x}\right)\right]^2 \mathrm{d}x \int_0^{L_y} \left[\cos\left(\frac{s_y \pi y}{L_y}\right)\right]^2 \mathrm{d}y + \\ + \int_0^{L_x} \left[\cos\left(\frac{s_x \pi x}{L_x}\right)\right]^2 \mathrm{d}x \int_0^{L_y} \left[-\frac{s_y \pi}{L_y} \sin\left(\frac{s_y \pi y}{L_y}\right)\right]^2 \mathrm{d}y \quad (6.9)$$

and $\mathbf{M}$, $\mathbf{K}$ are the one-dimensional mass and stiffness matrices defined as

$$[\mathrm{K}]_{ij} = \int_0^H N_i' N_j' \, \mathrm{d}z \quad (6.10)$$

$$[\mathrm{M}]_{ij} = \int_0^H N_i N_j \, \mathrm{d}z. \quad (6.11)$$

The fluid-structure coupling matrices for the leaves are $\mathbf{A_C}$ and $\mathbf{B_C}$. They are also block matrices and each block has $1 \times n_z$ size. The j component of block $\{r,s\}$ is $[\mathrm{A}_{\mathrm{C}rs}]_j = -N_j(H)\, I_3(r,s)$ and $[\mathrm{B}_{\mathrm{C}rs}]_j = N_j(0)\, I_3(r,s)$, where $I_3(r,s) = \int_{\Omega_{xy}} \phi_r \, \Phi_s \, \mathrm{d}x \, \mathrm{d}y$.

The fluid-structure coupling matrices for the cavity are $\mathbf{C_A}$ and $\mathbf{C_B}$. They are also block matrices and in this case the size of the blocks is $n_z \times 1$. The j component of block $\{s,r\}$ is $[\mathrm{C}_{\mathrm{A}sr}]_j = -\rho_{\mathrm{air}}\omega^2 \, N_j(H)\, I_3(s,r)$ and $[\mathrm{C}_{\mathrm{B}sr}]_j = \rho_{\mathrm{air}}\omega^2 \, N_j(0)\, I_3(s,r)$.

6.2 Modelling of multilayered double walls

The finite layer method can be applied for dealing with multilayered double walls. A particular case of this is a double wall partially filled with absorbing material (with a filling ratio β) as depicted in Fig. 6.2.

The absorbing material is modelled in this work with the equivalent fluid model suggested by Delany and Bazley (1970) and improved by Miki (1990): it is considered

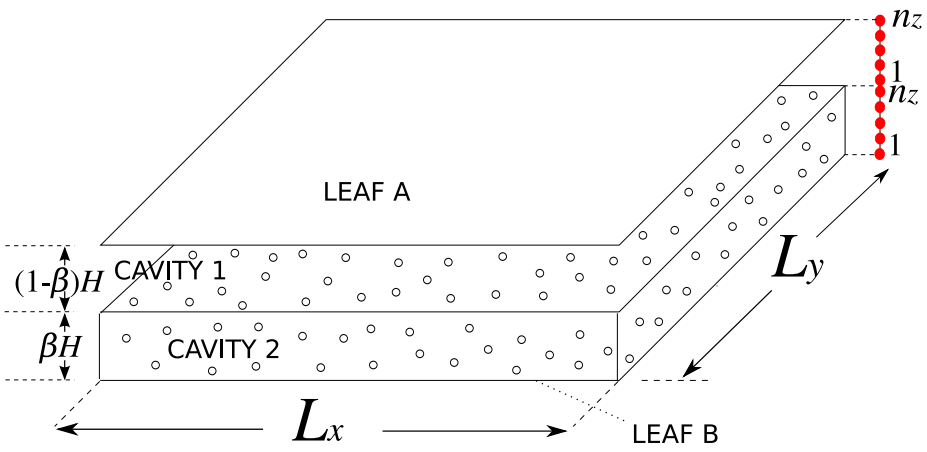

Fig. 6.2: Sketch of the multilayer double wall.

as a fluid with complex and frequency-dependent wavenumber and density. This model is specially suitable for fibrous materials with porosity near 1. For dealing with other types of absorbing materials, more complex models such as those described by Allard and Atalla (2009) should be used.

The two fluid phases (air cavity and absorbing material) can be modelled with the finite layer method just by defining two different fluid media (cavity 1 and cavity 2) with the appropriate interface conditions: balance of forces (continuity of the pressure)

$$\begin{aligned} \int_{\Omega_{xy}} \left[p_1\left(x,y,\beta H\right) - p_2\left(x,y,\beta H\right)\right] v_1 \,\mathrm{d}\Omega = 0 \\ \int_{\Omega_{xy}} \left[p_1\left(x,y,\beta H\right) - p_2\left(x,y,\beta H\right)\right] v_2 \,\mathrm{d}\Omega = 0 \end{aligned} \tag{6.12}$$

and permanent contact between phases (continuity of the normal velocity)

$$\begin{aligned} \mathrm{v}_{n,1} &= -\mathrm{v}_{n,2} \\ &\downarrow \\ -\tfrac{1}{\mathrm{i}\omega\rho_1}\nabla_n p_1(z=\beta H) &= \tfrac{1}{\mathrm{i}\omega\rho_2}\nabla_n p_2(z=\beta H). \end{aligned} \tag{6.13}$$

In Eq. (6.13), ρ_1 and ρ_2 are the densities of the air and absorbing material respectively (see Fig. 6.2). In that sense, FLM shows an advantage compared to the modal bases of Section 5.2.3, since the bases of functions allow the enforcement of the interface conditions.

Combining these conditions with the discretised weak forms of the leaf and cavity equations (one for each leaf and one for each cavity), the linear system to solve if the

only external excitation is applied to leaf A is

$$\begin{pmatrix} \mathbf{A} & \mathbf{A_C} & \mathbf{0} & \mathbf{0} \\ \mathbf{C_A} & \mathbf{C_{11}} & \mathbf{C_{12}} & \mathbf{0} \\ \mathbf{0} & \mathbf{C_{21}} & \mathbf{C_{22}} & \mathbf{C_B} \\ \mathbf{0} & \mathbf{0} & \mathbf{B_C} & \mathbf{B} \end{pmatrix} \begin{Bmatrix} \mathbf{a} \\ \mathbf{p_1} \\ \mathbf{p_2} \\ \mathbf{b} \end{Bmatrix} = \begin{Bmatrix} \mathbf{f} \\ \mathbf{0} \\ \mathbf{0} \\ \mathbf{0} \end{Bmatrix}. \tag{6.14}$$

Matrices $\mathbf{C_{11}}$ and $\mathbf{C_{22}}$ have the structure of matrix $\mathbf{C}$ of Eq. (5.24) plus some extra terms due to the interface conditions (6.12) and (6.13). Matrices $\mathbf{C_{12}}$ and $\mathbf{C_{21}}$ are sparse and carry the rest of the information of Equations (6.12) and (6.13). See Appendix C for more details.

6.3 Truncating the trigonometric series

A key issue in the modal expansions is to decide which and how many functions are taken into account, see the paper of Gagliardini et al. (1991). This question also arises regarding the trigonometric functions used in finite layer methods.

In these techniques, the trigonometric series must be truncated at some point. For simple problems, such as the vibration analysis of a single plate, the modes located in a range around the frequency of the excitation are enough. However, for the case of a double wall other considerations must be done. Since the wave speed is different in the leaves and in the cavity, when considering the pressure field in the cavity, selected modes are:

- Resonant modes of the cavity: those whose eigenfrequency is around the frequency of the excitation.
- Geometrically coincident modes or critical frequency modes of the cavity: those with a wavelength in the xy plane similar to the resonant vibration wavelengths caused in the leaf by the external excitation. These modes are required in order to reproduce the transmission of sound caused at the critical frequency (joint acceptance).

For instance, when exciting at a certain frequency f_0, the modes considered in the cavity will be those around f_0 and those around $\hat{f}_i$, where $\hat{f}_i$ are such that $\lambda_{\text{plate}} = c_{\text{plate}}/f_0 = c/\hat{f}_i = \lambda^{xy}_{\text{cav}}$. As an example, in Fig. 6.3 the modal contributions for the cavity at $f_0 = 3000$ Hz are shown. The figure reflects that in this case $\hat{f}_i = 1469$ Hz.

The same discussion applies when choosing the modes considered for the vibration field in the leaves.

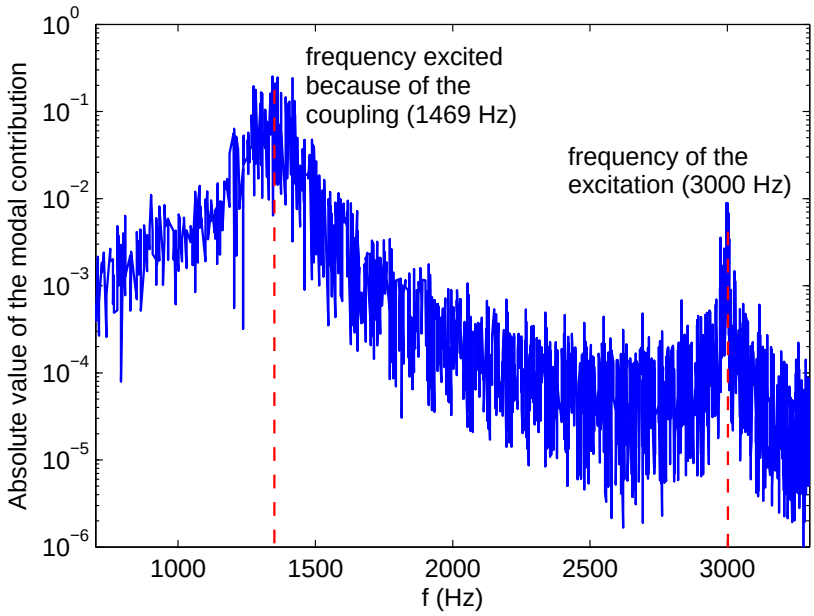

Fig. 6.3: Modal contributions for the cavity at f=3000 Hz.

6.4 Simulations and comparisons

In this section, FLM is compared both with experimental data and with the other models described in Chapter 5.2. An example of the possible applications of the finite layer method is also shown: a double wall with the cavity partially filled with absorbent material.

The two impedance models provide directly the transmission coefficient for every frequency. However, the other models only provide the vibration field for the leaves and the pressure field for the cavity. The computation of the impact noise level and the sound reduction index for these cases is detailed in Appendix B.

6.4.1 Comparison of the FLM with experimental data

The use of FLM for modelling the sound transmission in double walls is tested by comparing it with available experimental data. Tadeu et al. (2004) show the sound

reduction index measured in the lab for a double glazing. In Table 6.1 the properties of the glass leaves are shown. The cavity between them is 12 mm thick.

Variable	**Symbol**	**Value**
Leaf size, x direction	L_x	1.2 m
Leaf size, y direction	L_y	1.2 m
Thickness	h	4 mm
Young's modulus	E	7.2×10^{10} N m^{-2}
Density	ρ	2500 kg m^{-3}
Poisson's ratio	ν	0.22
Loss factor	η	4%

Table 6.1: Properties of the double glazing.

The experimental results shown by Tadeu et al. (2004) are depicted averaged in 1/10 octave bands. For the comparison, their sound energies have been averaged in order to provide the sound reduction index law in one-third octave bands

$$\langle R \rangle = 10 \log_{10} \left[\frac{1}{n} \sum_{i=1}^{n} 10^{0.1 R_i} \right]. \tag{6.15}$$

In Fig. 6.4 the comparison between the simulation with FLM and the experimental results is shown. The good performance of the numerical method is verified, since the trend of the numerical results coincides with that of the experimental values.

6.4.2 Comparison with other models

All the methods described in Chapter 5.2 are compared here with the finite layer method. Both the impact noise and the airborne sound are calculated for a wood double wall with an empty cavity.

In Table 6.2 the main features of the finite layer method have been added to those of the other four techniques used for the comparison, already shown in Table 5.1.

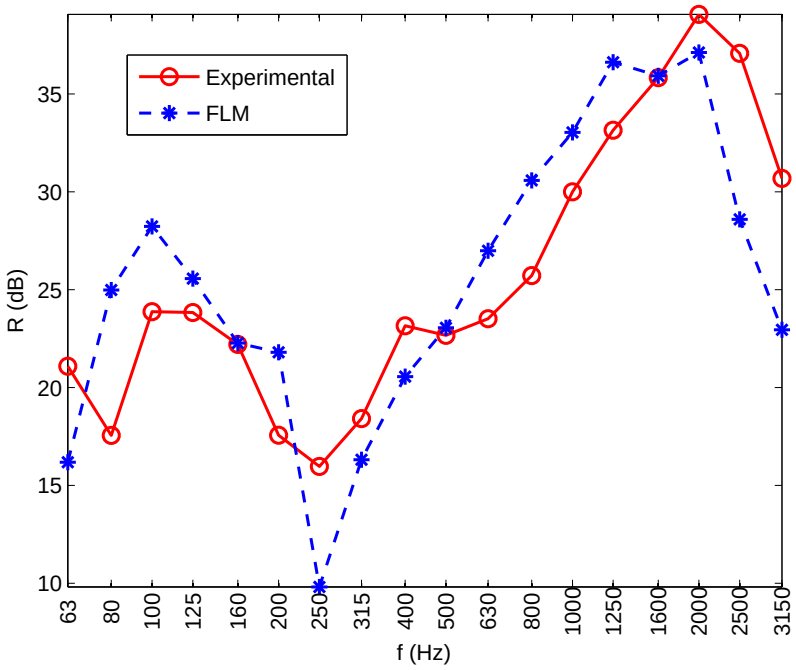

Fig. 6.4: Comparison with experimental measurements.

	Fahy	**Au and Byrne**	**Adapt. of Xin et al.**	**Modal bases**	**FLM**
Finite size of the leaves	No	No	Yes	Yes	**Yes**
Continuity of normal velocity at interfaces	No	No	Yes	No	**Yes**
Reflecting boundary conditions for the cavity	No	No	No	Yes	**Yes**
Thin plate equation for the leaves	No	No	Yes	Yes	**Yes**
Helmholtz equation for the cavity	No	No	No	Yes	**Yes**
Dimensionality of the pressure field	1D	1D	3D	3D	**3D**

Table 6.2: Hypotheses of the five models of the sound insulation of double walls

For all the comparisons, the properties of the leaves are defined in Table 6.3. The cavity is 70 mm thick.

Variable	**Symbol**	**Value**
Leaf size, x direction	L_x	2.4 m
Leaf size, y direction	L_y	2.4 m
Thickness	h	20 mm
Young's modulus	E	10^{10} N m^{-2}
Density	ρ	400 kg m^{-3}
Poisson's ratio	ν	0.25
Loss factor	η	5%

Table 6.3: The assumed properties for a wood leaf, used for all the analysis.

6.4.2.1 Comparison for the impact noise

First, the impact noise associated to the wood double wall is computed and shown in Fig. 6.5. In this case only the models presented in Sections 5.2.2 and 5.2.3 are compared with the finite layer method. The simple impedance models of Section 5.2.1 are not considered because they only provide the transmission coefficient and, therefore, only model the transmission of airborne sound.

In Fig. 6.5, the results provided by the FLM and the discretisation with modal bases are essentially the same. However, the adaptation of the model of Xin et al. (2010) provides slightly different results.

The main conclusion to be drawn here is that using interpolation functions with zero derivative at the fluid-structure interface for the air cavity (modal bases) is not a problem for this example. Not imposing strongly the continuity of the normal velocity does not affect the result.

Fig. 6.5 also shows that the description of the pressure field of Xin et al. (2010) provides a slightly different impact noise law. In particular, at the band of 125 Hz, the effect of the mass-spring-mass resonance is more pronounced due to the use of the same in-plane functions in leaves and cavity. The conclusion here is that the boundary conditions at the cavity contour are the main responsibles of the different performance of the model of Xin et al. (2010). The influence of the boundary conditions at the cavity contour is larger than that of the interface conditions at the fluid-structure contact.

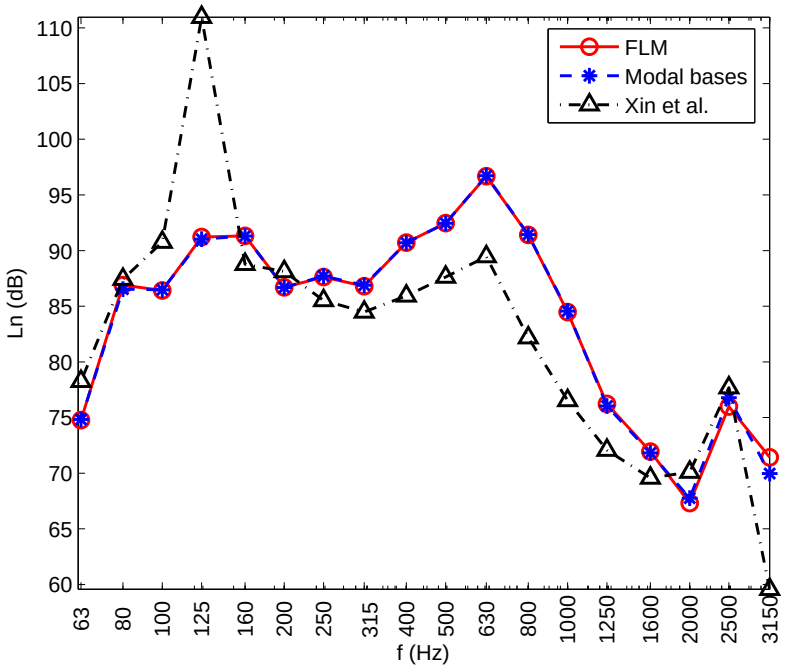

Fig. 6.5: Comparisons of models for the impact noise of the double wall.

A remark must be done here in terms of the computational cost. The number of degrees of freedom inside the air cavity for the analysis with modal bases at 3400 Hz (one of the highest frequencies considered) is 4340. If the discretisation is done with FLM the system has 22 934 degrees of freedom. This value is about six times larger than that of the modal analysis. This is due to the wave behaviour of the sound: for that cavity size, at a frequency of 3400 Hz, the wavelength of the pressure field is of the same size of the thickness of the cavity. Hence, it is reproducible with only one trigonometric function in the z direction. However, for the same wave, six nodes are required in that direction in the FEM-like approach of FLM (six times more degrees of freedom). Finally, if the computation was done with pure finite elements along the cavity, respecting the rule of six elements per wavelength, the required number of degrees of freedom would be around 200 000. The quantitative reduction due to the use of trigonometric functions is significant.

The optimal approach for the acoustic behaviour of double walls with empty cavities would be the analysis with modal bases.

6.4.2.2 Comparison for the airborne sound

In Fig. 6.6 the sound reduction index provided by the wood double wall is shown, computed with all the models described in Section 5.2 and the finite layer method, and averaged in one-third octave bands.

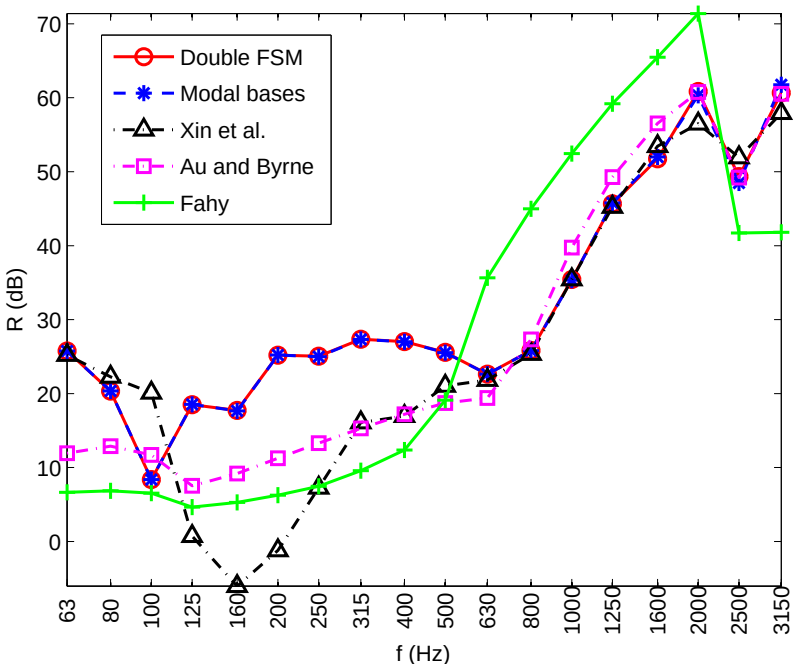

Fig. 6.6: Comparisons of models for the sound reduction index of the double wall.

For frequencies larger than the coincidence frequency of the leaves ($f_c = 616.5$ Hz), the two discretisation-driven techniques, the adaptation of the method of Xin et al. (2010) and the impedance model of Au and Byrne (1987) provide the same trend in the results. The impedance model provided by Fahy (1985) captures the shape of the sound reduction index law but not the values provided by the other models. For frequencies lower than f_c, the discretisation-driven techniques provide different values than the others. This shows that the assumptions of the other methods, shown in Table 6.2, are not satisfied at low frequencies. In particular, modelling the fluid with the Helmholtz equation and respecting the size and boundary conditions of the wall is more important than enforcing the continuity of the normal velocity at the fluid-structure interface.

6.4.3 Modelling of multilayered double walls

The sound reduction index caused by a double wall with different filling ratios of absorbing material is computed. The properties of the leaves are the same as those of Section 6.4.2. The resistivity of the absorbing material is $\sigma = 10\,000$ N s m^{-4}, the distance between the two leaves is 70 mm and different values of β are simulated: 0, 0.25, 0.5 and 1. Since the equivalent fluid model is not recommended for $f < 0.01\sigma$, in Fig. 6.7 the sound reduction index is only shown for frequencies larger than 100 Hz.

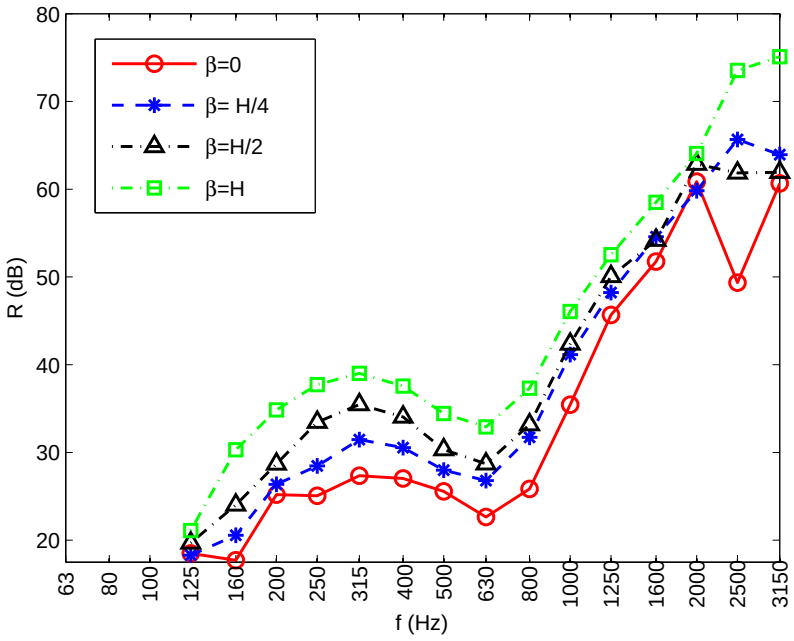

Fig. 6.7: Effect of the absorbing ratio inside the cavity.

Fig. 6.7 illustrates the insulating effect of the absorbing material. Higher ratios of absorbing material inside the cavity cause an increase in the sound reduction index, specially at low frequencies. However, between 1000 and 2000 Hz, the variations in the sound reduction index caused by the absorbing material are not larger than 10 dB.

The influence of the position of the absorbing layer has also been analysed: the simulations with the upper half of the cavity filled with absorbing material provide the same results as those with the absorbing material in the lower part. The position of the absorbing layer has no influence at all in the sound reduction index. The FLM

can be used in the same way for any filling ratio and material, just by changing the size and properties of the cavities. Thus, it is especially suitable for this type of analyses.

6.5 Concluding remarks

The finite layer method has been presented in this chapter as a discretisation technique for modelling the sound transmission through double walls. The main conclusions of the research are:

- The finite layer method is a reliable technique to model the sound transmission through double walls, specially when dealing with multilayer walls with different fluid-like materials.
- Accounting for the size and boundary conditions of the wall becomes a relevant aspect when modelling the sound transmission at low frequencies.
- Capturing well the continuity of the normal velocity is not relevant for modelling the sound transmission through double walls with empty air cavity.

Chapter 7

A model of double walls combining SEA and numerical simulations[4]

In this chapter, an efficient approach for modelling the sound insulation of double walls is presented. It is based on statistical energy analysis, but uses deterministic simulations for obtaining SEA parameters. This technique is presented here for the simplified case of two rooms separated by a double wall, but can be extended to more complex vibroacoustic problems, with more subsystems or different types of connections. First, the case of a double wall with an air cavity is simulated with this technique and compared with a fully deterministic approach. For this case, the effect on the global result of the excitation used for the estimation of coupling loss factors (CLF) is analysed. Then, the effect of adding steel studs or absorbing layers between the leaves of the double wall is studied.

7.1 Basic example: double wall with an air cavity

The sound reduction index between two rooms separated by a double wall (Fig. 7.1) is computed with SEA in this chapter. To do so, the coupling loss factors required for the analysis are estimated from numerical simulations, as described in Chapter 2. In a first stage, the sound reduction index is compared with the one obtained from the deterministic approach to the same problem.

[4]Based on references: Díaz-Cereceda et al. (2013a) and Díaz-Cereceda et al. (2013b)

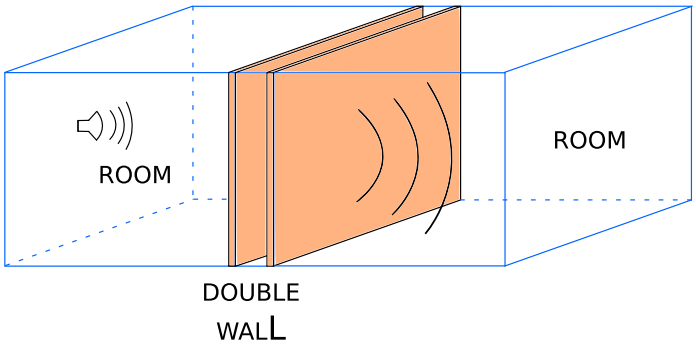

Fig. 7.1: Sketch of the sound transmission through a double wall.

The sound reduction index is obtained from the mean square pressures at the source $\langle p^2_{\mathrm{rms}_1} \rangle$ and receiving $\langle p^2_{\mathrm{rms}_2} \rangle$ rooms as

$$R = 10 \log_{10} \frac{\langle p^2_{\mathrm{rms}_1} \rangle}{\langle p^2_{\mathrm{rms}_2} \rangle} + 10 \log_{10} \frac{S}{A}. \tag{7.1}$$

where S is the surface of the wall and $A = \sum \alpha_j S_j$ is the absorption area in the receiving room.

The deterministic approach is based on solving numerically the Helmholtz equation for the rooms and using the analysis described in Section 5.2.3 for the double wall.

The SEA approach consists of 4 subsystems: sending room, leaf A, leaf B and receiving room. The internal loss factors of subsystems 2 and 3 are the loss factors of the leaves ($\eta_{ii} = \eta = 0.03$) and the internal loss factors of subsystems 1 and 4 are computed as

$$\eta_{ii} = \frac{c S_{\mathrm{room}} \alpha}{8 \pi f V_{\mathrm{room}}}, \tag{7.2}$$

where S_{room} is the surface of the room boundary and α is the absorption coefficient at that boundary. The excitation is a sound source in one of the rooms (subsystem 1).

The coupling loss factors between the two leaves η_{23} and η_{32} are obtained from the results of the deterministic computation described in Section 2.4.2. The coupling loss factors between each leaf and the adjacent room have been computed with numerical simulations too, because the expressions provided by Maidanik (1962) for the radiation efficiency are only suitable for mechanical excitations. Therefore, they un-

derestimate the sound transmission when the excitation consists of a diffuse pressure field, as shown by Vigran (2008).

The leaf-room CLF is obtained with Eq. (2.3), computing the averaged energies from the numerical simulation of a system consisting of a room in contact with a leaf (see Fig. 7.2). Since the first SEA subsystem is the sending room and the last one is the receiving room, the influence of applying the correct excitation when estimating the coupling loss factor between the room and the leaf is studied.

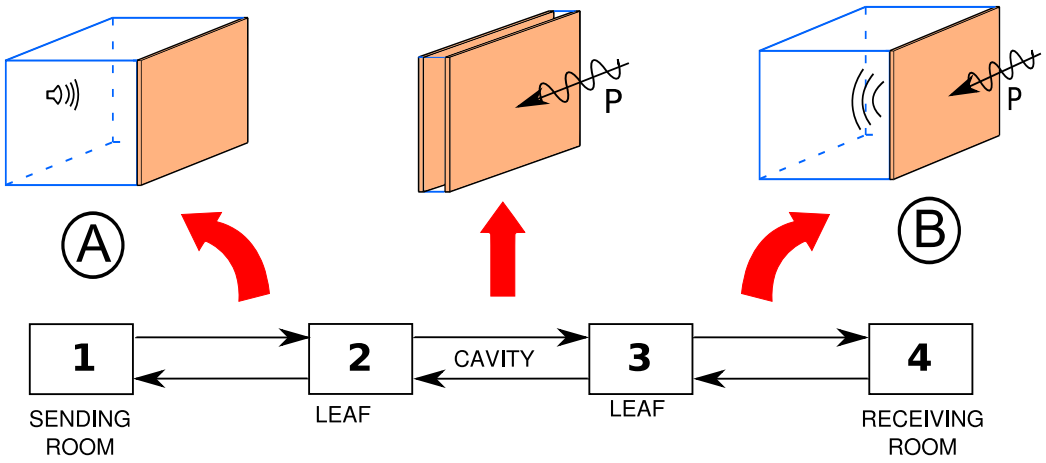

Fig. 7.2: Sketch of the 2-subsystem vibroacoustic problems solved to obtain the coupling loss factors.

Two vibroacoustic problems have been solved, with the only difference of the excitation applied to the system. In problem A, the excitation is a sound source in the room (left part of Fig. 7.2). In problem B, the excitation is a pressure wave impinging on the leaf (right part of Fig. 7.2). A natural approach would be to estimate η_{12} and η_{21} from problem A and η_{34} and η_{43} from problem B. However, the influence of this choice is analysed here.

In Fig. 7.3 the sound reduction index between the two rooms is shown from three different approaches. Two of them correspond to solving the problem with SEA. On the first one, η_{12} and η_{21} are estimated from problem A, and η_{34} and η_{43} from problem B. On the second one, the four coupling loss factors between the rooms and leaves are obtained from problem B. The third one is the result of a numerical calculation of the sound reduction index with the full deterministic approach.

In this example, the two rooms are identical, as well as the two GN plasterboard leaves. Their material properties are enumerated in Table 2.1 and the rest of the

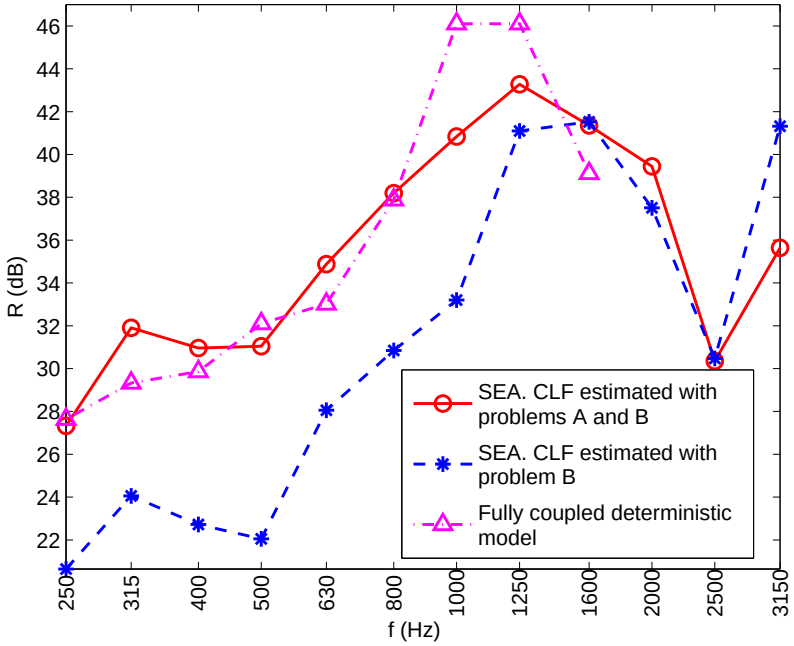

Fig. 7.3: Comparison of the sound reduction index between two rooms separated by a double wall.

problem data are described in Table 7.1.

Variable	**Symbol**	**Value**
Plate size, x direction	L_x	2 m
Plate size, y direction	L_y	3 m
Plate thickness	h	13 mm
Cavity thickness	H	70 mm
Room dimensions	$L_x \times L_y \times L_z$	2 m × 3 m × 5 m
Room absorption	α	10 %
Cavity absorption	α_{cav}	0 %

Table 7.1: Sound reduction index through the double plasterboard wall. Problem data.

Results in Fig. 7.3 are not shown for the lowest frequencies because SEA hypotheses are not satisfied there. The sound reduction index law computed numerically, or with SEA and the CLFs obtained from problems A and B, present the same trend. However, the trend of the results computed only with the CLFs estimated

from problem B is much different than the other two. This illustrates the importance of estimating the coupling loss factors from problems with the same excitation at which the subsystems will be subjected afterwards.

The computation of the sound reduction index with the deterministic approach could not be performed for the highest frequencies, due to the large number of degrees of freedom (more than 65 000) involved in the numerical computation at each frequency. The improvement of the proposed approach in terms of the computational cost is remarkable, since the SEA approach only requires solving a 4×4 linear system at each frequency, and the numerical simulations required for estimating the coupling loss factors are much smaller than the full coupled approach. Furthermore, once the coupling loss factors are computed, they can be used in the SEA resolution of any other problem consisting of repetitions of the same elements (rooms and walls), such as a whole building.

7.2 Effect of the studs in the sound transmission through double walls

The acoustic effect of steel studs located between the two leaves of the double wall is studied with SEA, Fig. 7.4. To do so, the coupling loss factor associated to the stud connections is computed and added to that of the air cavity to reproduce the global behaviour of the double wall.

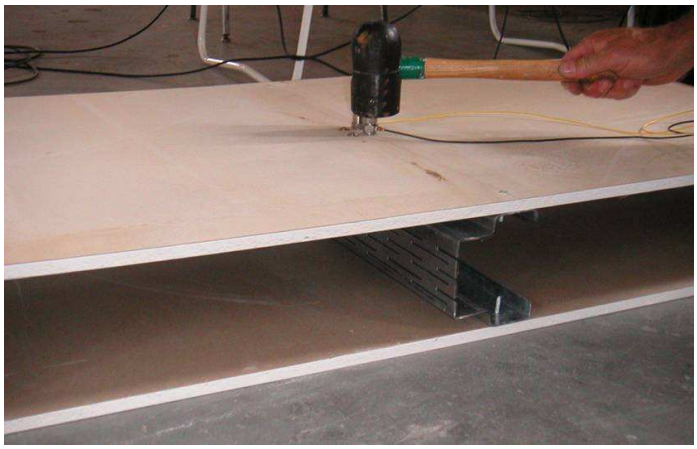

Fig. 7.4: Location of a stud between the leaves, see Poblet-Puig et al. (2009).

The computation of the coupling loss factor associated to the studs is performed assuming them to be line springs with frequency-dependent stiffnesses. These stiffness laws were computed from numerical simulations by Poblet-Puig et al. (2009). If the connections were more complex and could not be approximated by line springs, a finite element analysis would have to be performed, see Fig. 7.5, and the CLF would be computed with one of the expressions described in Section 2.2.

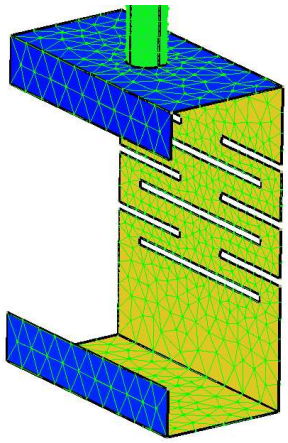

Fig. 7.5: Finite element mesh of a stud.

Given the equivalent stiffness of the stud, the associated coupling loss factor can be derived as done by Poblet-Puig et al. (2009)

$$\eta_{12} = \frac{n_L \mathrm{Re}\left\{Y_2^L/L_y\right\}}{\omega M_1 |Y_1^L/L_y + Y_2^L/L_y + Y_c^L/L_y|^2}\,, \tag{7.3}$$

where n_L is the number of studs.

The line mobilities of the leaves, modelled as thin plates, are obtained with the expression provided by Sharp (1978)

$$Y^L = \frac{1}{2(1+\mathrm{i})\rho_s c_{\mathrm{plate}} \left(f/f_c\right)^{1/2}}\,, \tag{7.4}$$

and the line mobility of the spring is $Y_c^L = \mathrm{i}\omega/K_L$, where K_L is its line stiffness.

The coupling loss factor computed with Eq. (7.3) is added to that of the air cavity in the SEA system. In Fig. 7.6 the sound reduction index of the same example described in Section 7.1 is shown, both for the simple leaf-cavity-leaf system and for the same wall with four studs inside. Two types of studs are considered: on the one

hand a conventional S-section stud and on the other hand an acoustic stud (LR), with the shapes shown in Fig. 7.7. The dimensions of the studs are $d1 = 70$ mm, $d2 = 40$ mm, $d3 = 10$ mm, $d4 = 14$ mm, $d5 = 14$ mm and $d6 = 28$ mm.

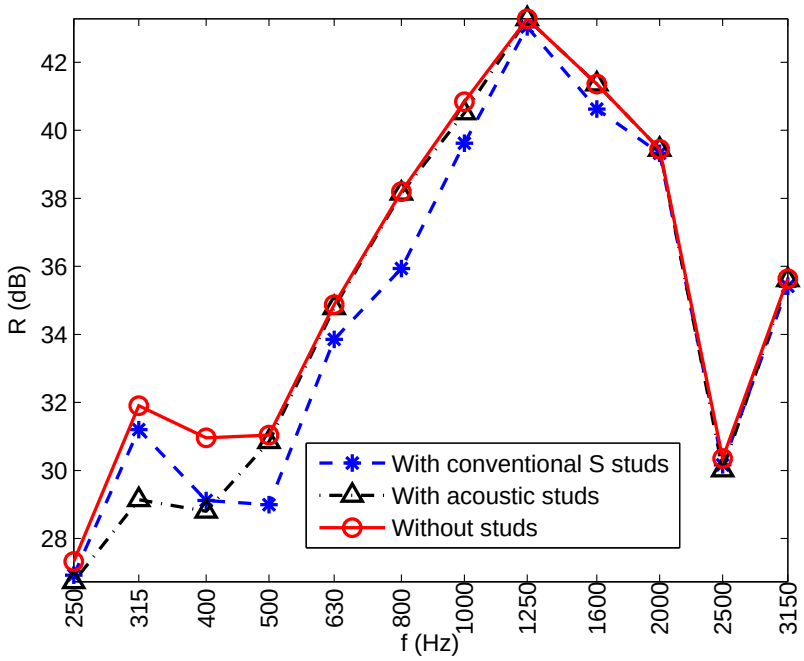

Fig. 7.6: Effect of the studs in the sound reduction index through the double wall.

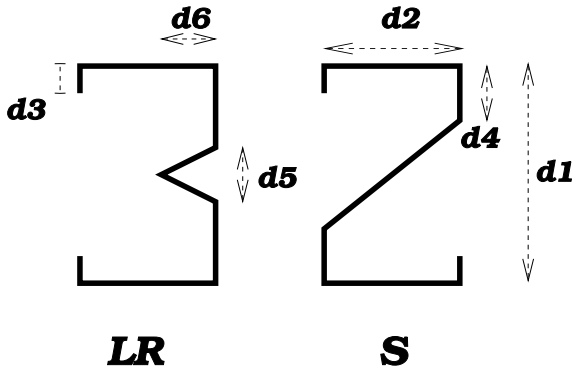

Fig. 7.7: Cross-section of the studs.

For the highest frequencies the increment in the sound transmission due to the extra path added by the studs is negligible. This happens because the transmission

through the air cavity for these frequencies is already large compared to the one added by the studs. For the mid-frequency range, however, the presence of the studs reduces the sound insulation of the double wall. The improvement of the performance with the acoustic stud in front of the conventional one happens, as expected, for the mid and high frequencies. As explained by Poblet-Puig et al. (2009), the increase of flexibility due to stud shape is more relevant around the eigenfrequencies where the central part of the stud acts as a spring. These eigenfrequencies do not happen in the low-frequency range.

7.3 Effect of the cavity filling

7.3.1 Single absorbing layer

In order to study the effect of an absorbing filling for the double wall on a real-life problem, the SEA-like approach suggested in Chapter 3 is used to simulate the sound reduction index between two rooms separated by a double wall filled with absorbing material. Four double walls filled with absorbing materials of different resistivities are compared with one without absorbing material inside. The rooms have dimensions 2 m $\times$ 3 m $\times$ 5 m. The plate properties are summarised in Tables 2.1 and 2.2.

For the simulation, the system is divided again into four SEA subsystems: sending room, leaf 1, leaf 2 and receiving room, and the absorbing material is considered as a non-conservative connection between subsystems 2 and 3. Therefore, the SEA-like system to be solved is

$$\omega \begin{bmatrix} \eta_{11}+\eta_{12} & -\eta_{21} & 0 & 0 \\ -\eta_{12} & \eta_{21}+\eta_{22}+\eta_{23}+\gamma_{23} & -\eta_{32} & 0 \\ 0 & -\eta_{23} & \eta_{32}+\eta_{33}+\eta_{34}+\gamma_{32} & -\eta_{43} \\ 0 & 0 & -\eta_{34} & \eta_{43}+\eta_{44} \end{bmatrix} \begin{Bmatrix} \langle E_1 \rangle \\ \langle E_2 \rangle \\ \langle E_3 \rangle \\ \langle E_4 \rangle \end{Bmatrix} = \begin{Bmatrix} \Pi_1^{\text{in}} \\ 0 \\ 0 \\ 0 \end{Bmatrix}. \tag{7.5}$$

The internal loss factors and the excitation are the same as in Section 7.1. To obtain all the parameters η_{ij} and γ_{ij} required by the SEA-like approach, again three small deterministic problems have been solved. On the one hand, the coupling loss factors between each leaf and its adjacent room have been computed as described in Section 7.1. On the other hand, the double wall itself has been simulated, in order to obtain factors η_{ij} and γ_{ij} between the two leaves as described in Section 3.3. The simulation is done combining modal analysis for the leaves and FLM for the cavity,

as described in Chapter 6. The absorbing material is modelled with the equivalent fluid model suggested by Delany and Bazley (1970) and improved by Miki (1990), as in Section 6.2.

In Fig. 7.8 the effect of the flow resistivity on the sound reduction index between the two rooms is analysed. The insulating effect of filling the cavity with an absorbing material is remarkable. However, different values of the flow resistivity only provide different values of the sound reduction index for high frequencies. This behaviour was also reported by Stani et al. (2005) and can be explained as a competition between two opposite effects.

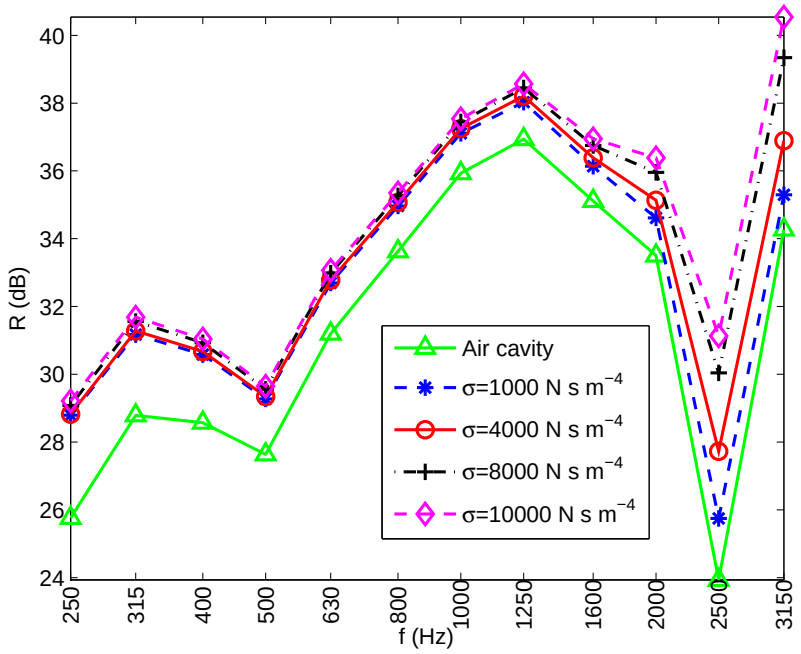

Fig. 7.8: Effect of the flow resistivity on the sound reduction index.

First, the wavenumber of the equivalent fluid grows with the flow resistivity, leading to smaller transmissions. Second, the fluid density also increases with the flow resistivity, causing in this case an increment of the transmission. At low frequencies the increase of the wavenumber compensates the increase of the density and the sound insulation does not change with the resistivity. However, at high frequencies the effect of the wavenumber dominates that of the density, and larger resistivities cause more insulating behaviours.

7.3.2 Effect of a second absorbing layer

The potential of the technique presented here is further illustrated by computing the sound reduction index through a triple wall. This wall consists of a leaf-cavity-leaf-cavity-leaf configuration, where the leaves are identical to those in Section 7.3.1, and the cavities are 70 mm thick and completely filled with an absorbing material of resistivity $\sigma = 8000$ N s m^{-4}. A 5×5 SEA-like system is solved at each frequency, using the same internal and coupling loss factors of the double wall. The sound reduction index through this triple wall is compared with that of the classical double wall on Fig. 7.9.

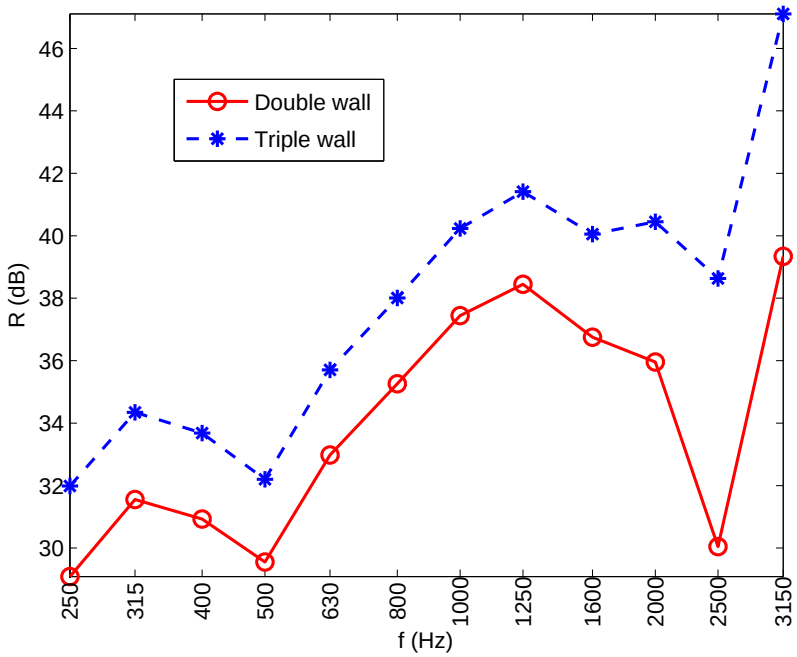

Fig. 7.9: Effect of a second absorbing layer on the sound reduction index.

As expected, the sound insulation increases by adding new layers to the wall. Moreover, the drop in the insulation at 2500 Hz associated to the coincidence frequency of the leaves is considerably reduced by the addition of the extra layers.

7.4 Concluding remarks

The main conclusions extracted from this chapter are the following:

- The application of the CLF estimated from systems consisting of only two subsystems for the simulation of larger problems with SEA shows a good agreement with the deterministic analysis. However, its computational cost is much lower.
- The CLF estimation must be performed with the same type of excitation of the problem where it will be applied.
- The effect of studs can be easily considered with SEA if they are treated as line springs with frequency-dependent stiffness.
- The coupling loss factors associated to the studs do not always involve a significant increment of the sound transmission. However, the use of acoustic studs improves the insulation of the double wall in front of the conventional ones for mid and high frequencies.
- The influence of the flow resistivity of the absorbing material filling a plasterboard double wall is only relevant for high frequencies. At low frequencies, the behaviour is different if the cavity is empty or filled with absorbing material, but the resistivity of the material does not affect the sound insulation.
- The addition of new layers of plasterboard and absorbing material reduces considerably the sound transmission through the wall and dampens the effect of the coincidence frequency of the plasterboards.

7.5 Future directions

The future lines to be followed in the field of the combination of SEA and deterministic simulations are the following:

- The combined effect of studs and absorbing materials in a double wall should be analysed with SEA.
- A combined approach between the strategies proposed in Chapter 4 and this chapter should be performed. First, the subsystem identification would be done according to the strategy of Chapter 4, then the coupling loss factor between

each couple of identified subsystems would be computed with the technique shown in Chapter 2 and, if the weak coupling hypothesis is satisfied for every couple, the global problem would be solved with SEA.

- The analysis proposed in Chapter 4 might me used to detect those configurations, or those frequencies, at whom the whole double wall acts as a single subsystem.

Conclusions, contributions and future work

Conclusions and contributions

In this dissertation two main topics in the field of computational building acoustics have been addressed. For each topic, different conclusions have been reached, as detailed at the end of the chapters of this thesis. Therefore, in this section only the main contributions are summarised.

The first part of the document deals with the extension of the applicability of statistical energy analysis (SEA) by means of numerical simulations. The main contributions made in this field are:

1. **A methodology is proposed for estimating SEA coupling loss factors from small deterministic simulations.** In Chapter 2 a study on the optimal procedure for obtaining SEA coupling loss factors (CLF) numerically is presented. These factors are obtained from a small simulation and can be further used to solve larger problems with SEA. The way of computing the CLF once the deterministic problem is solved is very important in order to perform a good estimation. The values from which the CLF is computed already have a certain error, and therefore a study of the error propagation is required. Expressions where two similar quantities are subtracted must be avoided. The best option is to obtain the CLF from the power balance of the unexcited subsystem.

   Chapter 2 corresponds to the work presented in Díaz-Cereceda et al. (2013a).

2. **An SEA-like method that accounts for non-conservative connections is presented.** In Chapter 3 an equivalent circuit analogy is used to relate

the power dissipation at non-conservative couplings with the energies of the subsystems. The coupling is characterised by means of two factors: the conservative coupling loss factor (CCLF) and the non-conservative coupling loss factor (NCLF), related to the transmitted and dissipated energy respectively. A methodology for obtaining these parameters from small numerical simulations is presented. Once these factors are obtained, they can be used to solve larger problems with SEA where both conservative and non-conservative couplings are combined.

Chapter 3 corresponds to the work presented in Díaz-Cereceda et al. (2013b) and Díaz-Cereceda et al. (2013c).

3. **A strategy for decomposing a vibroacoustic domain into SEA subsystems is proposed.** In Chapter 4 a methodology involving a cluster analysis based on the problem eigenmodes is presented for identifying SEA subsystems within a given vibroacoustic system. This technique incorporates the mutual inertia ratio between subsystems as a decision variable, and allows the identification of SEA subsystems, even if some of them are associated to sets of modes sharing the same physical region. This is done decomposing the kinetic energy of the modes in components and classifying the modes according to their dominant component before performing the cluster analysis.

The second part of the document deals with different approaches for modelling the sound transmission through double walls. The main contributions made in this part are:

4. **The finite layer method is introduced as a discretisation technique for modelling the sound transmission through double walls.** In Chapter 6 this method is presented and compared with other approaches to model the sound insulation of double walls. The finite layer method (FLM) combines a FEM discretisation in the direction perpendicular to the wall with trigonometric functions in the two in-plane directions. It is used for solving the Helmholtz equation at the cavity inside the double wall, while the wall leaves are modelled with the thin plate equation and solved with modal analysis. The main advantage of FLM over the other discretisation techniques is the possibility of extending it to multilayered structures without changing the interpolation functions and with an affordable computational cost.

Chapter 6 corresponds to the work presented in Díaz-Cereceda et al. (2012).

5. **An efficient approach for modelling the sound insulation of double walls, based on the combination of statistical energy analysis and deterministic simulations, is developed.** In Chapter 7 this technique is presented for the simplified case of two rooms divided by a double wall. The application of the coupling loss factors estimated from systems consisting of only two subsystems for the simulation of larger problems with SEA shows a good agreement with deterministic analyses and a much lower computational cost. The possibility of adding the effect of studs or absorbing layers inside the double wall is also shown. This can be easily done with SEA if their associated parameters are obtained from numerical simulations.

   Chapter 7 corresponds to the work presented in Díaz-Cereceda et al. (2013a) and Díaz-Cereceda et al. (2013b).

Future developments

The research developed in this thesis leaves several topics to be further investigated in the future:

1. **Extending statistical energy analysis with numerical simulations.** Different topics have been studied in Part I, in order to extend the SEA applicability. However, there are still many aspects to be improved in this field.

   - The combination of deterministic simulations with SEA could be used to study quasi-SEA systems. Cases of strong coupling or subsystems with low modal densities might be analysed numerically and an SEA-like approach could be proposed for modelling them.
   - A comparison between the treatment of absorbing materials as SEA subsystems or as non-conservative couplings could be done, exploring different types of absorbing material.
   - Simplified expressions for the CCLFs and NCLFs associated to different dissipative elements, such as absorbing layers, should be developed. These expressions must provide the coupling loss factors in terms of the properties of the connection and the subsystems surrounding it.

- The strategy for identifying SEA subsystems of Chapter 4 could be improved: the influence of the set of modes used for the analysis should be analysed, an expression relating the mutual inertia ratio (mir) between two subsystems and their coupling loss factor is necessary, and the effect of the damping could be incorporated to the analysis. Moreover, it should be applied to vibroacoustic problems.
- The strategy for the identification of SEA subsystems could be combined with the methods for the estimation of coupling loss factors from numerical simulations to provide a full systematic method for analysing vibroacoustic systems. Besides, the information of the coupling loss factors would help in the identification of subsystems.

2. **Models for double walls.** The discussion of the different approaches for modelling double walls in Part II has left some issues to be further investigated in the future.

   - The advantages of the finite layer method for modelling the acoustic behaviour of multilayered structures should be exploited for models of multilayered walls alternating cavities, absorbing materials and thin plates. These simulations could be used to estimate the coupling loss factors (either conservative or non-conservative) associated to these configurations as described in Chapter 2.
   - The combined effect of studs and absorbing materials in a double wall could be analysed with SEA.
   - The possibility of using the analysis proposed in Chapter 4 for detecting those configurations, or those frequencies, at which the double wall acts as a single subsystem should be studied.

Appendix A

Deterministic approach for vibroacoustic problems

A.1 Vibroacoustic problem

The energies and powers required for the estimation of coupling loss factors in Chapters 2 and 3 are obtained from numerical simulations of the vibroacoustic problems. Most of them consist of floors or walls connected by different devices. They are modelled with the thin plate equation in the frequency domain

$$B\nabla^4 u\,(x,y) - \omega^2 \rho_s u\,(x,y) = q\,(x,y), \tag{A.1}$$

expressing the vibration field in the plates in terms of the eigenfunctions of simply supported plates.

If the plates are connected with a mechanical device, its effect is modelled as an extra force or moment, connecting the vibrations of both plates as explained in Díaz-Cereceda et al. (2011).

If the plates are separated by an air cavity forming a double wall, the coupled vibroacoustic problem is solved, namely the thin plate equation (A.1) for the plates and the Helmholtz equation

$$\nabla^2 p\,(\boldsymbol{x}) + k^2 p\,(\boldsymbol{x}) = 0 \tag{A.2}$$

for the acoustic domain, where $p\,(\boldsymbol{x})$ is the pressure field and k is the wavenumber in the air. Modal analysis is used for solving the acoustic part of the problem, enforcing

weakly the continuity and equilibrium at the vibroacoustic interface, as described in Section 5.2.3. This technique exploits the simple geometry of the problem to achieve an accurate result with less computational cost than a finite element discretisation. However, a more complex problem might be solved with other discretisation techniques, such as the finite element method, see Panneton and Atalla (1996). In particular, the case of two leaves divided by a cavity filled with absorbing material is modelled with the finite layer method described in Chapter 6.

A.2 Energy calculation

The coupling loss factor (CLF) estimations require the computation of the averaged energy of each plate and also the power exchanged between the connection and the plates.

Once the displacement field $u(x, y)$ in a plate is known, its velocity is obtained as $v(x, y) = \mathrm{i}\,\omega\, u(x, y)$. Then, the averaged energy of the plate is computed as described by Hopkins (2007)

$$\langle E \rangle = M \left\langle v_{\mathrm{rms}}^2 \right\rangle \tag{A.3}$$

where M is the mass of the plate and $\langle v_{\mathrm{rms}}^2 \rangle$ is the spatial mean square value of its velocity.

According to SEA hypotheses, the incident field must be diffuse. For instance, if the excitation is an impact on one of the plates, the spatially distributed and uncorrelated excitation required by SEA is achieved by solving twenty different problems, each one with the force applied in a different (random) excitation point. The resulting energies and powers are averaged to provide the diffuse output. The decision to use twenty different excitations was motivated by the works of Maxit and Guyader (2003) and Totaro et al. (2009). Moreover, a convergence study has been performed, showing that the differences between using 20, 30 or 40 points are barely noticeable.

The computation of the power $\mathit{\Pi}_{12}$ transmitted between plates 1 and 2 through a connection depends on the connection characteristics. Its general expression is

$$\mathit{\Pi}_{12} = \frac{1}{2}\mathrm{Re}\left(\int_{\Omega} q(x, y)\, v^*(x, y)\, \mathrm{d}\Omega\right) \tag{A.4}$$

for a translational connection, or

$$\mathit{\Pi}_{12} = \frac{1}{2}\mathrm{Re}\left(\int_{\Omega} m(x, y)\, w^*(x, y)\, \mathrm{d}\Omega\right) \tag{A.5}$$

for a rotational connection; $m(x, y)$ is the moment per unit surface and $w(x, y)$ the rotational speed, both of them at the connection. The superscript $*$ means the conjugate of a complex number. This surface integral reduces to a line integral or a point evaluation for a line or point connection respectively. In case the connection is conservative, computing this integral on one plate or the other provides the same result. However, if there is a non-conservative coupling, $\Pi_{12}^{(1)} \neq \Pi_{12}^{(2)}$.

The computation of the incoming power to the system is also necessary. If the excitation is a point force on one of the plates, the associated power is computed as

$$\Pi^{\text{in}} = \frac{1}{2}\text{Re}\left\{F_p v_p^*\right\} \tag{A.6}$$

where the subscript p means evaluated at the point where the impact is exerted and F_p is the value of the applied force.

However, if the excitation is a pressure wave impinging on one of the plates, the associated power is computed as

$$\Pi^{\text{in}} = \frac{\langle p_{\text{rms}}^2 \rangle_{\text{plate}} L_x L_y \cos\varphi}{\rho_{\text{air}} c}, \tag{A.7}$$

where $\langle p_{\text{rms}}^2 \rangle_{\text{plate}}$ is the mean square pressure exciting the leaf. This value is also averaged for different incident angles, ranging from 0^{o} to 90^{o} in order to reproduce the diffuse field excitation.

In some examples of this work, the CLF between a room and an adjacent wall is also required. It has been computed numerically in order to capture as much information as possible. For the calculation, the energy of the room is computed assuming diffuse field as

$$\langle E \rangle = \frac{V_{\text{room}} \langle p_{\text{rms}}^2 \rangle_{\text{room}}}{\rho_{\text{air}} c^2}. \tag{A.8}$$

This expression is also used to obtain the value of $\langle p_{\text{rms}}^2 \rangle$ required to compute the sound reduction index with Eq. (7.1) from the averaged energies obtained with SEA.

Appendix B

Definition of acoustical outputs[5]

The magnitudes used to compute the airborne sound and the impact noise in Section 6.4 are defined here in terms of the system excitation and the outputs provided by the discretisation methods defined in Sections 5.2.2, 5.2.3 and Chapter 6.

B.1 Impact noise pressure level

The impact noise is measured with the normalised impact noise pressure level L_{n}, averaged in one-third octave bands as defined in ISO 140-6 (1998). For obtaining this value, the excitation must be exerted by the normalised tapping machine. In this work, it is modelled with the expressions provided by Brunskog and Hammer (2003). They suggest that the behaviour of the machine depends on the properties of the contact surface. There are two limit situations in this behaviour. One of them is the case of the hammers rebounding with the same velocity of the impact (elastic behaviour). In the other limit situation the hammers do not rebound at all (damped behaviour). The formulation takes into account the fact that the floor may have an intermediate behaviour between these two limits. It provides the spectrum of the force exerted by the tapping machine $F_0(f)$ for a floor of known properties, with

$$F_0(f) = \sum_{n=-\infty}^{\infty} F_n \delta(f - n f_r), \tag{B.1}$$

[5]The meaning of some symbols in this appendix is different from that in the List of Symbols. For those symbols whose meaning changes, the definition is provided here.

$F_n = F_1(nf_r)f_r$, $f_r = 10\,\mathrm{Hz}$ and

$$F_1 = \begin{cases} \frac{v_0 KM}{K-\omega^2 M+\mathrm{i}\omega KM/R_r} & \text{for } KM \geq 4R_r^2 \\ \frac{v_0 KM(1+\exp(-t_{\mathrm{cut}}(\mathrm{i}\omega+K/2R_r)))}{K-\omega^2 M+\mathrm{i}\omega KM/R_r} & \text{for } KM < 4R_r^2 \end{cases} \tag{B.2}$$

where:

- v_0 is the speed with which the hammer hits the plate and its value is $v_0 = (2gh_0)^{1/2} = 0.866\,\mathrm{m\,s^{-1}}$ as the hammer is dropped from a height of 0.04 m.
- $K = ED_h/\left(1-\nu^2\right)$ is the stiffness of the local deformation.
- D_h and M are the diameter and the mass of each hammer respectively.
- $R_r = 8\sqrt{\rho_s B}$ is the input impedance of an infinite plate
- $t_{\mathrm{cut}} = \pi\sqrt{\frac{M}{K}}$ is the time of zero-crossing.

The force is located in four different positions and the resulting radiated power, averaged in each case before computing the impact noise pressure level. With the (0,0) located at a corner of the plate, these positions are: (0.57 L_x, 0.57 L_y), (0.19 L_x, 0.19 L_y), (0.19 L_x, 0.57 L_y), (0.35 L_x, 0.35 L_y). The noise level is computed in terms of the power radiated by the unexcited leaf as defined in Eq. (I.3).

As proposed by Williams (1983), the power radiated by the unexcited leaf is expressed in terms of the leaf surface velocity as

$$\mathit{\Pi}^{\mathrm{rad}} = \frac{\omega\rho_{\mathrm{air}}}{4\pi}\int_{\Omega'_{xy}}\int_{\Omega_{xy}} \hat{v}(x',y')\,\hat{v}^*(x,y)\,\frac{\sin(kr)}{r}\,\mathrm{d}x\,\mathrm{d}y\,\mathrm{d}x'\,\mathrm{d}y' \tag{B.3}$$

where $\hat{v}$ is the velocity field, $r = \left[(x-x')^2+(y-y')^2\right]^{1/2}$ and Ω_{xy}, Ω'_{xy} are used to denote the double integral over the leaf.

This integral is calculated numerically with the trapezoidal composite rule, using six nodes per wavelength. However, at large frequencies (f greater than 708 Hz in the examples of Section 6.4.2), the computation of the power is simplified by means of the expressions shown by Renji et al. (1998). In them, the radiation efficiency σ_{rad} depends on the excitation frequency, the properties of the structure and the medium into which sound is radiated. With these expressions, the radiated power is computed as

$$\mathit{\Pi}^{\mathrm{rad}} = R_{\mathrm{rad}}\left\langle v_{\mathrm{rms}}^2\right\rangle, \tag{B.4}$$

where $\langle v_{\text{rms}}^2 \rangle$ is the spatial mean square value of the leaf vibration velocity and $R_{\text{rad}} = \sigma_{\text{rad}} \rho_{\text{air}}\, c\, S$ is the radiation resistance (with S the surface of the leaf). This combination of techniques was used by Díaz-Cereceda et al. (2011) and reduces significantly the computational cost of the calculation.

B.2 Sound reduction index

The airborne sound is measured with the sound reduction index R. Models of Section 5.2.1 provide directly the transmission loss and, with Eq. (5.2), R can be obtained. In the rest of the approaches, this value is computed in terms of the incident and radiated powers, Π^{in} and Π^{rad}, of the structure.

The computation of this value requires a pressure wave impinging on one of the leaves, modelled as

$$p(\boldsymbol{x}) = |p| \exp\left(-\mathrm{i}\left(k_x x + k_y y + k_z z\right)\right) \tag{B.5}$$

where $k_x = k \sin\varphi \cos\theta$, $k_y = k \sin\varphi \sin\theta$ and $k_z = k \cos\varphi$.

This wave may have several orientations, defined by angles θ and φ as shown in Fig. B.1. Four different values of θ, equispaced between $\theta = 0$ and $\theta = 45^{\text{o}}$ due to the symmetry of the problem, are considered. If the leaf was rectangular instead of square, this limit would be 90^{o}. Also ten different values of φ have been considered, equispaced between $\varphi = 0$ and $\varphi_{\text{lim}} = 90^{\text{o}}$ for the finite size models, and $\varphi_{\text{lim}} = 78^{\text{o}}$ for the two impedance models, in order to reproduce a diffuse incident field.

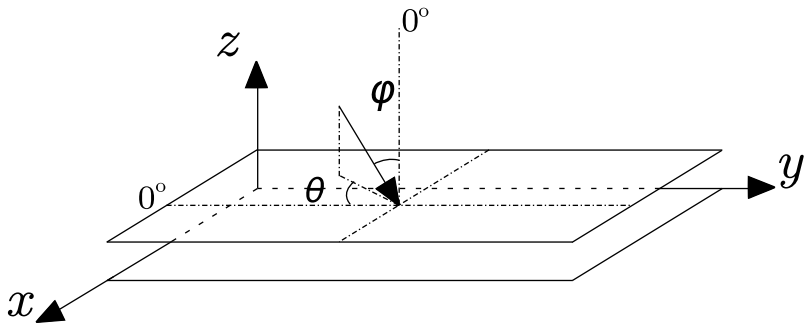

Fig. B.1: Incident angles.

The final value of the sound reduction index is computed with Eq. (5.2), where

$$\tau_{\text{diff}} = \frac{\int_0^{\theta=45^{\text{o}}} \int_0^{\varphi_{\text{lim}}} \tau(\theta,\varphi)\, \cos(\theta)\sin(\theta)\, \cos(\varphi)\sin(\varphi)\, \mathrm{d}\varphi\, \mathrm{d}\theta}{\int_0^{\theta=45^{\text{o}}} \int_0^{\varphi_{\text{lim}}} \cos(\theta)\sin(\theta)\, \cos(\varphi)\sin(\varphi)\, \mathrm{d}\varphi\, \mathrm{d}\theta} \tag{B.6}$$

and

$$\tau(\theta,\varphi) = \frac{\Pi^{\mathrm{rad}}(\theta,\varphi)}{\Pi^{\mathrm{in}}(\theta,\varphi)}. \tag{B.7}$$

In Eq. (B.7), $\Pi^{\mathrm{rad}}(\theta,\varphi)$ is obtained with the same technique described in Section B.1 and

$$\Pi^{\mathrm{in}}(\theta,\varphi) = \frac{\langle p^2_{\mathrm{rms}}\rangle_{\mathrm{plate}}\, L_x L_y \cos\varphi}{\rho_{\mathrm{air}} c}. \tag{B.8}$$

Appendix C

Finite layer formulation for multilayer structures

In this appendix, a detailed explanation of the meaning of matrices defined in Section 6.2 is provided.

In system (6.14), matrices $\mathbf{C_{11}}$ and $\mathbf{C_{22}}$ are associated to the air and absorbing material layers respectively. $\mathbf{C_{11}}$ consists of two types of contributions: the same matrix $\mathbf{C}$ defined in Eq. (6.7) and a term related to Eq. (6.12) that is assembled at

$$[\mathrm{C}_{11st}]_{ij} = [\mathrm{C}_{11st}]_{ij} + N_i(\beta H)\, N_j(\beta H)\, I_1(s,t)\,, \tag{C.1}$$

where $I_1(s,t) = \int_{\Omega_{xy}} \Phi_s\, \Phi_t \,\mathrm{d}x\,\mathrm{d}y$.

Analogously, matrix $\mathbf{C_{22}}$ consists of two contributions: on the one hand, the matrix defined in Eq. (6.7) adapted with the new value of the speed of sound c_2 and, on the other hand, a term related to Eq. (6.12) that is assembled at

$$[\mathrm{C}_{22st}]_{ij} = [\mathrm{C}_{22st}]_{ij} - N_i(\beta H)\, N_j(\beta H)\, I_1(s,t)\,. \tag{C.2}$$

Matrix $\mathbf{C_{12}}$ has the information of the continuity of the normal velocity at the interface between the two layers as

$$[\mathrm{C}_{12st}]_{ij} = \frac{\rho_1}{\rho_2}\, N_i(\beta H)\, \frac{\mathrm{d}N_j}{\mathrm{d}z}\bigg|_{z=\beta H} I_1(s,t)\,, \tag{C.3}$$

and also the rest of the information of Eq. (6.12) for cavity 2

$$[\mathrm{C}_{12st}]_{ij} = [\mathrm{C}_{12st}]_{ij} - N_i(\beta H)\, N_j(\beta H)\, I_1(s,t)\,. \tag{C.4}$$

Matrix $\mathbf{C_{21}}$ has the information of Eq. (6.13) as

$$[\mathrm{C}_{21\,st}]_{ij} = -\frac{\rho_2}{\rho_1} N_i(\beta H) \left.\frac{\mathrm{d}N_j}{\mathrm{d}z}\right|_{z=\beta H} I_1(s,t), \tag{C.5}$$

and also the rest of the information of Eq. (6.12) for cavity 2

$$[\mathrm{C}_{21\,st}]_{ij} = [\mathrm{C}_{21\,st}]_{ij} + N_i(\beta H) N_j(\beta H) I_1(s,t). \tag{C.6}$$

Matrices $\mathbf{A}$, $\mathbf{B}$, $\mathbf{A_C}$, $\mathbf{B_C}$ and $\mathbf{C_A}$ are the same as defined in Eq. (6.6). Matrix $\mathbf{C_B}$ is also the same as in Eq. (6.6) but with density ρ_2 instead of ρ.

Bibliography

Aalami, B. (1973). Waves in prismatic guides of arbitrary cross section. *Journal of Applied Mechanics 40*(4), 1067–1072. doi: 10.1115/1.3423127.

Alba, J., J. Ramis, and V. J. Sánchez-Morcillo (2004). Improvement of the prediction of transmission loss of double partitions with cavity absorption by minimization techniques. *Journal of Sound and Vibration 273*(4-5), 793–804. doi: 10.1016/S0022-460X(03)00783-1.

Allard, J. and N. Atalla (2009). *Propagation of sound in porous media: modelling sound absorbing materials*. Wiley.

Arenas, J. and M. Crocker (2010). Recent trends in porous sound-absorbing materials. *Sound and Vibration 44*(7), 12–18.

Au, A. and K. Byrne (1987). On the insertion losses produced by plane acoustic lagging structures. *Journal of the Acoustical Society of America 82*(4), 1325–1333. doi: 10.1121/1.395266.

Barbagallo, M. (2013). Statistical energy analysis and variational principles for the prediction of sound transmission in multilayered structures. PhD dissertation, KTH Royal Institute of Technology.

Beranek, L. (1988). *Noise and vibration control*. Institute of Noise Control Engineering.

Beranek, L. and G. Work (1949). Sound transmission through multiple structures containing flexible blankets. *Journal of the Acoustical Society of America 21*(4), 419–428. doi: 10.1121/1.1906530.

Beshara, M. and A. Keane (1996). Statistical energy analysis of multiple non-conservatively coupled systems. *Journal of Sound and Vibration 198*(1), 95–122. doi: 10.1006/jsvi.1996.0559.

Brekke, A. (1981). Calculation methods for the transmission loss of single, double and triple partitions. *Applied Acoustics 14*(3), 225–240. doi: 10.1016/0003-682X(81)90034-7.

Brouard, B., D. Lafarge, and J. Allard (1995). A general method of modelling sound propagation in layered media. *Journal of Sound and Vibration 183*(14), 129–142. doi: 10.1006/jsvi.1995.0243.

Brunskog, J. (2005). The influence of finite cavities on the sound insulation of double-plate structures. *Journal of the Acoustical Society of America 117*(6), 3727–3739. doi: 10.1121/1.1904264.

Brunskog, J. and P. Davidsson (2004). Sound transmission of structures; a finite element approach with simplified room description. *Acta Acustica united with Acustica 90*(5), 847–857.

Brunskog, J. and P. Hammer (2003). The interaction between the ISO tapping machine and lightweight floors. *Acta Acustica united with Acustica 89*(2), 296–308.

Campolina, B., N. Atalla, N. Dauchez, and P. Neple (2012). Four-pole modelling of vibration isolators: Application to SEA of aircraft double-wall panels subjected to mechanical excitation. *Noise Control Engineering Journal 60*(2), 158–170. doi: 10.3397/1.3688316.

Cast3M (2003). Cast3M home page. http://www-cast3m.cea.fr/.

Chen, X., D. Wang, and Z. Ma (2012). Simulation on a car interior aerodynamic noise control based on statistical energy analysis. *Chinese Journal of Mechanical Engineering 25*(5), 1016–1021. doi: 10.3901/CJME.2012.05.1016.

Cheung, Y. and S. Chakrabarti (1972). Free vibration of thick, layered rectangular plates by a finite layer method. *Journal of Sound and Vibration 21*(3), 277–284. doi: 10.1016/0022-460X(72)90812-7.

Cheung, Y. and L. Tham (1997). *Finite strip method*. CRC Press.

Chow, L. and R. Pinnington (1987). Practical industrial method of increasing structural damping in machinery, I: squeeze-film damping with air. *Journal of Sound and Vibration 118*(1), 123–139. doi: 10.1016/0022-460X(87)90258-6.

Chung, H. and G. Emms (2008). Fourier series solutions to the vibration of rectangular lightweight floor / ceiling structures. *Acta Acustica united with Acustica 94*(3), 401–409. doi: 10.3813/AAA.918048.

Citizens Coalition Against Noise Pollution (2013). http://www.noiseoff.org/, retrieved on 2013-08-01.

Comité des victimes de la pollution et du bruit (2013). http://www.sos-bruit.com/, retrieved on 2013-08-01.

Cotoni, V., P. Shorter, and R. Langley (2007). Numerical and experimental validation of a hybrid finite element-statistical energy analysis method. *Journal of the Acoustical Society of America 122*(1), 259–270. doi: 10.1121/1.2739420.

Craik, R. (1996). *Sound transmission through buildings using statistical energy analysis*. Gower Publishing Ltd.

Craik, R. and R. Smith (2000). Sound transmission through double leaf lightweight partitions Part I: airborne sound. *Applied Acoustics 61*(2), 223–245. doi: 10.1016/S0003-682X(99)00070-5.

Craik, R. J. (2003). Non-resonant sound transmission through double walls using statistical energy analysis. *Applied Acoustics 64*(3), 325–341. doi: 10.1016/S0003-682X(02)00051-8.

Cremer, L., M. Heckel, and E. Ungar (1973). *Structure-borne sound*. Springer-Verlag.

Crocker, M. and A. Price (1969). Sound transmission using statistical energy analysis. *Journal of Sound and Vibration 9*(3), 469–486. doi: 10.1016/0022-460X(69)90185-0.

CTE (Update of April 2009). *Código Técnico de la Edificación. Documento básico HR: Protección frente al ruido*. Ministerio de Vivienda, España.

Culla, A. and A. Sestieri (2006). Is it possible to treat confidentially SEA the wolf in sheep's clothing? *Mechanical Systems and Signal Processing 20*(6), 1372–1399. doi: 10.1016/j.ymssp.2005.02.007.

Cuschieri, J. and J. Sun (1994). Use of statistical energy analysis for rotating machinery, Part I: Determination of dissipation and coupling loss factors using energy ratios. *Journal of Sound and Vibration 170*(2), 181–190. doi: 10.1006/jsvi.1994.1054.

De Langhe, K. and P. Sas (1996). Statistical analysis of the power injection method. *Journal of the Acoustical Society of America 100*(1), 294–303. doi: 10.1121/1.415915.

Delany, M. and E. Bazley (1970). Acoustic properties of fibrous absorbent materials. *Applied Acoustics 3*(2), 105–116. doi: 10.1016/0003-682X(70)90031-9.

Díaz-Cereceda, C., J. Hetherington, J. Poblet-Puig, and A. Rodríguez-Ferran (2011). A deterministic model of impact noise transmission through structural connections based on modal analysis. *Journal of Sound and Vibration 330*(12), 2801–2817. doi: 10.1016/j.jsv.2010.12.019.

Díaz-Cereceda, C., J. Poblet-Puig, and A. Rodríguez-Ferran (2012). The finite layer method for modelling the sound transmission through double walls. *Journal of Sound and Vibration 331*(22), 4884–4900. doi: 10.1016/j.jsv.2012.06.001.

Díaz-Cereceda, C., J. Poblet-Puig, and A. Rodríguez-Ferran (2013a). Numerical estimation of coupling loss factors in building acoustics. *Journal of Sound and Vibration 332*(21), 5433–5450. doi: 10.1016/j.jsv.2013.05.012.

Díaz-Cereceda, C., J. Poblet-Puig, and A. Rodríguez-Ferran (2013b). A model for non-conservative couplings based on statistical energy analysis. Submitted.

Díaz-Cereceda, C., J. Poblet-Puig, and A. Rodríguez-Ferran (2013c). An energy model for the acoustic insulation of absorbing materials. In *Congreso de Métodos Numéricos en Ingeniería - CMN 2013*, Bilbao (Spain).

Dijckmans, A., G. Vermeir, and W. Lauriks (2010). Sound transmission through finite lightweight multilayered structures with thin air layers. *Journal of the Acoustical Society of America 128*(6), 3513–3524. doi: 10.1121/1.3500698.

Elmallawany, A. (1978). Criticism of statistical energy analysis for the calculation of sound insulation - Part 1: Single partitions. *Applied Acoustics 11*(4), 305–312. doi: 10.1016/0003-682X(78)90006-3.

Everitt, B. S., S. Landau, and M. Leese (2009). *Cluster Analysis*. Wiley.

Fahy, F. (1985). *Sound and Structural Vibration: Radiation, Transmission and Response*. Academic Press.

Fahy, F. (1994). Statistical energy analysis: A critical overview. *Philosophical Transactions of the Royal Society of London A 346*(1681), 429–554. doi: 10.1098/rsta.1994.0027.

Fahy, F. (2004). A note on the subdivision of a volume of air in a vehicle enclosure into SEA subsystems. *Journal of Sound and Vibration 271*(3-5), 1170–1174. doi: 10.1016/S0022-460X(03)00632-1.

Finnveden, S. (2004). Evaluation of modal density and group velocity by a finite element method. *Journal of Sound and Vibration 273*(12), 51–75. doi: 10.1016/j.jsv.2003.04.004.

Forssén, J., S. Tober, A. C. Corakci, A. Frid, and W. Kropp (2012). Modelling the interior sound field of a railway vehicle using statistical energy analysis. *Applied Acoustics 73*(4), 307–311. doi: 10.1016/j.apacoust.2011.09.012.

Fredö, C. (1996). Three conservatively or two non-conservatively coupled subsystems: is a dual interpretation possible? In *Internoise 96*, Liverpool, pp. 2923–2928.

Fredö, C. (1997). A SEA-like approach for the derivation of energy flow coefficients with a finite element model. *Journal of Sound and Vibration 199*(4), 645–666. doi: 10.1006/jsvi.1996.0634.

Friedrich, R. (2000). Finite strip method: 30 years. *Engineering Computations 17*(1), 92–111. doi: 10.1108/02644400010308099.

Gagliardini, L., L. Houillon, G. Borello, and L. Petrinelli (2005). Virtual SEA – FEA-based modeling of mid-frequency structure-borne noise. *Sound and Vibration 39*(1), 22–28. doi: 10.4271/2003-01-1555.

Gagliardini, L., J. Roland, and J. Guyader (1991). The use of a functional basis to calculate acoustic transmission between rooms. *Journal of Sound and Vibration 145*(3), 457–478. doi: 10.1016/0022-460X(91)90114-Y.

Geebelen, N., L. Boeckx, G. Vermeir, and W. Lauriks (2006). A model for estimating the acoustic performances of multilayered systems based on a multiple extension of the transfer matrix method. In *Proceedings of the Sixth European Conference on Noise Control*, Tampere, Finland, 30 May - 1 June 2006.

Guasch, O. and A. Aragonès (2011). Finding the dominant energy transmission paths in statistical energy analysis. *Journal of Sound and Vibration 330*(10), 2325–2338. doi: 10.1016/j.jsv.2010.11.021.

Guigou-Carter, C. and M. Villot (2003). Modelling of sound transmission through lightweight elements with stiffeners. *Building Acoustics 10*(3), 193–209. doi: 10.1260/135101003322662005.

Henrici, P. (1964). *Elements of Numerical Analysis*. New York: Wiley.

Higham, N. (1996). *Accuracy and Stability of Numerical Algorithms*. Philadelphia: Society for Industrial and Applied Mathematics.

Hodges, C. and J. Woodhouse (1986). Theories of noise and vibration transmission in complex structures. *Reports on Progress in Physics 49*(2), 107. doi: 10.1088/0034-4885/49/2/001.

Hongisto, V. (2006). Sound insulation of double panels - comparison of existing prediction models. *Acta Acustica united with Acustica 92*(1), 61–78.

Hopkins, C. (2002). Statistical energy analysis of coupled plate systems with low modal density and low modal overlap. *Journal of Sound and Vibration 251*(2), 193–214. doi: 10.1006/jsvi.2001.4002.

Hopkins, C. (2007). *Sound insulation*. Elsevier Ltd.

ISO 140-3 (1995). *ISO 140-3:1995, Acoustics – Measurement of sound insulation in buildings and of building elements – Part 3: Laboratory measurements of airborne sound insulation of building elements*. Geneva, Switzerland.

ISO 140-6 (1998). *ISO 140-6:1998, Acoustics – Measurement of sound insulation in buildings and of building elements – Part 6: Laboratory measurements of impact sound insulation of floors*. Geneva, Switzerland.

ISO 717-1 (1997). *ISO 717-1:1997, Acoustics – Rating of sound insulation in buildings and of building elements – Part 1: Airborne sound insulation*. Geneva, Switzerland.

ISO 717-2 (1997). *ISO 717-2:1997, Acoustics – Rating of sound insulation in buildings and of building elements – Part 2: Impact sound isolation*. Geneva, Switzerland.

Juristas Contra el Ruido (2013). http://www.juristas-ruidos.org/, retrieved on 2013-08-01.

Kassem, M., C. Soize, and L. Gagliardini (2011). Structural partitioning of complex structures in the medium-frequency range. An application to an automotive vehicle. *Journal of Sound and Vibration 330*(5), 937–946. doi: 10.1016/j.jsv.2010.09.008.

Keane, A. and W. Price (1987). Statistical energy analysis of strongly coupled systems. *Journal of Sound and Vibration 117*(2), 363–386. doi: 10.1016/0022-460X(87)90545-1.

Kernen, U. and O. Hassan (2005). Airborne sound insulation of a thin plate of finite dimensions. *Acta Acustica united with Acustica 91*(4), 732–739.

Kropp, W. and E. Rebillard (1999). On the air-borne sound insulation of double wall constructions. *Acta Acustica united with Acustica 85*(5), 707–720.

Le Bot, A. and V. Cotoni (2010). Validity diagrams of statistical energy analysis. *Journal of Sound and Vibration 329*(2), 221–235. doi: 10.1016/j.jsv.2009.09.008.

London, A. (1950). Transmission of reverberant sound through double walls. *Journal of the Acoustical Society of America 22*(2), 270–279. doi: 10.1121/1.1906601.

Lyon, R. (1975). *Statistical Energy Analysis of Dynamical Systems*. M.I.T. Press.

Lyon, R. and R. DeJong (1995). *Theory and Application of Statistical Energy Analysis*. Butterworth-Heinemann.

Lyon, R. H. and G. Maidanik (1962). Power flow between linearly coupled oscillators. *Journal of the Acoustical Society of America 34*(5), 623–639. doi: 10.1121/1.1918177.

Mace, B. (2005). Statistical energy analysis: coupling loss factors, indirect coupling and system modes. *Journal of Sound and Vibration 279*(1-2), 141–170. doi: 10.1016/j.jsv.2003.10.040.

Maidanik, G. (1962). Response of ribbed panels to reverberant acoustic fields. *Journal of the Acoustical Society of America 34*(6), 809–826. doi: 10.1121/1.1918200.

Maidanik, G. (1977). Some elements in statistical energy analysis. *Journal of Sound and Vibration 52*(2), 171–191. doi: 10.1016/0022-460X(77)90638-1.

Manning, J. (1994). Formulation of SEA parameters using mobility functions. *Philosophical Transactions of the Royal Society of London A346*(1681), 477–488. doi: 10.1098/rsta.1994.0030.

Maxit, L. and J. Guyader (2001). Estimation of SEA coupling loss factors using a dual formulation and FEM modal information, Part I: theory. *Journal of Sound and Vibration 239*(5), 907–930. doi: 10.1006/jsvi.2000.3192.

Maxit, L. and J.-L. Guyader (2003). Extension of SEA model to subsystems with non-uniform modal energy distribution. *Journal of Sound and Vibration 265*(2), 337–358. doi: 10.1016/S0022-460X(02)01459-1.

Miki, Y. (1990). Acoustical properties of porous materials: modifications of Delany-Bazley models. *Journal of the Acoustical Society of Japan (E) 11*(1), 19–24.

NBE-CA (1988). *Norma Básica de la edificación NBE-CA-88 condiciones acústicas de los edificios*. Ministerio de Obras Públicas y Urbanismo.

Olson, H. (1943). *Dynamical Analogies*. D.Van Nostrand Company Inc.

Orrenius, U. and S. Finnveden (1996). Calculation of wave propagation in rib-stiffened plate structures. *Journal of Sound and Vibration 198*(2), 203–224. doi: 10.1006/jsvi.1996.0565.

Panneton, R. and N. Atalla (1996). Numerical prediction of sound transmission through finite multilayer systems with poroelastic materials. *Journal of the Acoustical Society of America 100*(1), 346–354. doi: 10.1121/1.415956.

Poblet-Puig, J. and A. Rodríguez-Ferran (2011). The finite strip method for acoustic and vibroacoustic problems. *Journal of Computational Acoustics 19*(4), 353–378. doi: 10.1142/S0218396X11004456.

Poblet-Puig, J., A. Rodríguez-Ferran, C. Guigou-Carter, and M. Villot (2009). The role of studs in the sound transmission of double walls. *Acta Acustica united with Acustica 95*(3), 555–567. doi: 10.3813/AAA.918176.

Renji, K., P. Nair, and S. Narayanan (1998). On acoustic radiation resistance of plates. *Journal of Sound and Vibration 212*(4), 583–598. doi: 10.1006/jsvi.1997.1438.

Renji, K., P. Nair, and S. Narayanan (2001). Non-resonant response using statistical energy analysis. *Journal of Sound and Vibration 241*(2), 253–270. doi: 10.1006/jsvi.2000.3270.

Semprini, G. and L. Barbaresi (2008). Acoustical proprieties of light brick walls and its effects on flanking transmission. *Journal of the Acoustical Society of America 123*(5), 3763. doi: 10.1121/1.2935355.

Sharp, B. (1978). Prediction methods for the sound transmission of building elements. *Noise Control Engineering 11*(2), 53–63. doi: 10.3397/1.2832099.

Sheng, M., M. Wang, and J. Sun (1998). Effective internal loss factors and coupling loss factors for non-conservatively coupled systems. *Journal of Sound and Vibration 209*(4), 685–694. doi: 10.1006/jsvi.1997.1291.

Sheng, M., M. Wang, J. Sun, and B. Qian (2004). Statistical energy analysis for complicated coupled system and its application in engineering. *Journal of Sound and Vibration 274*(3-5), 877–891. doi: 10.1016/j.jsv.2003.06.013.

Shorter, P. and R. Langley (2005). Vibro-acoustic analysis of complex systems. *Journal of Sound and Vibration 288*(3), 669–699. doi: 10.1016/j.jsv.2005.07.010.

Simmons, C. (1991). Structure-borne sound transmission through plate junctions and estimates of SEA coupling loss factors using the finite element method. *Journal of Sound and Vibration 144*(2), 215–227. doi: 10.1016/0022-460X(91)90745-6.

Sjökvist, L., J. Brunskog, and F. Jacobsen (2008). Parameter survey of a rib stiffened wooden floor using sinus modes model. In *Proceedings of the Acoustics'08 Conference*, Paris 2008, pp. 3011–3015.

Smith, P. W. (1962). Response and radiation of structural modes excited by sound. *Journal of the Acoustical Society of America 34*(5), 640–647. doi: 10.1121/1.1918178.

Smith, S., M. Allen, J. Puckett, and T. Edgar (1992). The finite layer method for groundwater flow models. *Water Resources Research 28*(6), 1715–1722. doi: 10.1029/92WR00425.

Stani, M., H. Muellner, I. Plotizin, and K. Zlabinger (2005). Sound insulation of plasterboard walls and airflow resistivity: an empirical examination with respect to practical applications. In *Proceedings of Forum Acusticum 2005*, Budapest, pp. 1987–1992.

Steel, J. and R. Craik (1994). Statistical energy analysis of structure-borne sound transmission by finite element methods. *Journal of Sound and Vibration 178*(4), 553–561. doi: 10.1006/jsvi.1994.1503.

Tadeu, A., J. António, and D. Mateus (2004). Sound insulation provided by single and double panel walls – a comparison of analytical solutions versus experimental results. *Applied Acoustics 65*(1), 15–29. doi: 10.1016/j.apacoust.2003.07.003.

Thite, A. and B. Mace (2007). Robust estimation of coupling loss factors from finite element analysis. *Journal of Sound and Vibration 303*(3-5), 814–831. doi: 10.1016/j.jsv.2007.02.004.

Totaro, N., C. Dodard, and J. L. Guyader (2009). SEA coupling loss factors of complex vibro-acoustic systems. *Journal of Vibration and Acoustics 131*(4), 041009. doi: 10.1115/1.3086929.

Totaro, N. and J. Guyader (2006). SEA substructuring using cluster analysis: The MIR index. *Journal of Sound and Vibration 290*(1-2), 264–289. doi: 10.1016/j.jsv.2005.03.030.

Trochidis, A. and A. Kalaroutis (1986). Sound transmission through double partitions with cavity absorption. *Journal of Sound and Vibration 107*(2), 321–327. doi: 10.1016/0022-460X(86)90241-5.

Tryon, R. (1939). *Cluster Analysis*. Edwards Bros.

Vigran, T. (2008). *Building acoustics*. Taylor and Francis.

Villot, M., C. Guigou, and L. Gagliardini (2001). Predicting the acoustical radiation of finite size multi-layered structures by applying spatial windowing on infinite structures. *Journal of Sound and Vibration 245*(3), 433–455. doi: 10.1006/jsvi.2001.3592.

Wang, J., T. Lu, J. Woodhouse, R. Langley, and J. Evans (2005). Sound transmission through lightweight double-leaf partitions: theoretical modelling. *Journal of Sound and Vibration 286*(4-5), 817–847. doi: 10.1016/j.jsv.2004.10.020.

Williams, E. (1983). A series expansion of the acoustic power radiated from planar sources. *Journal of the Acoustical Society of America 73*(5), 1520–1524. doi: 10.1121/1.389412.

Woodhouse, J. (1981). An approach to the theoretical background of statistical energy analysis applied to structural vibration. *Journal of the Acoustical Society of America 69*(6), 1695–1709. doi: 10.1121/1.385949.

Xin, F., T. Lu, and C. Chen (2010). Sound transmission through simply supported finite double-panel partitions with enclosed air cavity. *Journal of Vibration and Acoustics 132*(1), 011008. doi: 10.1115/1.4000466.

Yan, H., A. Parrett, and W. Nack (2000). Statistical energy analysis by finite elements for middle frequency vibration. *Finite Elements in Analysis and Design 35*(4), 297–304. doi: 10.1016/S0168-874X(99)00071-2.

Zienkiewicz, O. (2000). Achievements and some unsolved problems of the finite element method. *International Journal for Numerical Methods in Engineering 47*(1-3), 9–28. doi: 10.1002/(SICI)1097-0207(20000110/30)47:1/3¡9::AID-NME793¿3.0.CO;2-P.

Zienkiewicz, O. and R. Taylor (2000). *The finite element method*. Butterworth-Heinemann.